INFORMATION TO USERS

This manuscript has been reproduced from the microfilm master. UMI films the text directly from the original or copy submitted. Thus, some thesis and dissertation copies are in typewriter face, while others may be from any type of computer printer.

The quality of this reproduction is dependent upon the quality of the copy submitted. Broken or indistinct print, colored or poor quality illustrations and photographs, print bleedthrough, substandard margins, and improper alignment can adversely affect reproduction.

In the unlikely event that the author did not send UMI a complete manuscript and there are missing pages, these will be noted. Also, if unauthorized copyright material had to be removed, a note will indicate the deletion.

Oversize materials (e.g., maps, drawings, charts) are reproduced by sectioning the original, beginning at the upper left-hand corner and continuing from left to right in equal sections with small overlaps. Each original is also photographed in one exposure and is included in reduced form at the back of the book.

Photographs included in the original manuscript have been reproduced xerographically in this copy. Higher quality 6" x 9" black and white photographic prints are available for any photographs or illustrations appearing in this copy for an additional charge. Contact UMI directly to order.

UMI

A Bell & Howell Information Company
300 North Zeeb Road, Ann Arbor MI 48106-1346 USA
313/761-4700 800/521-0600

PHOTOLUMINESCENCE AND ELECTROLUMINESCENCE IN LANTHANIDE-ORGANIC COMPLEXES AND ORGANIC POLYMERS

by

ANDREW G. EDWARDS

A dissertation submitted to the Graduate Faculty in Engineering in partial fulfillment of the requirements for the Degree of Doctor of Philosophy, The City University of New York.

1997

This manuscript has been read and accepted for the Graduate Faculty in Engineering in satisfaction of the dissertation requirement for the degree of Doctor of Philosophy.

6/6/97
Date:

Prof. Roger Dorsinville (Thesis Advisor)
Department of Electrical Engineering
Chairman of the Examining Committee

6/6/97
Date:

Prof. Gerard D. Lowen
Executive Officer

Dr. Ardie Walser — Associate Professor, Dept. of Electrical Engineering, The City College of the City University of New York

Dr. Vladimir Petricevic — Assistant Professor, Department of Physics, The City College of the City University of New York

Dr. Yoshiyuki Okamoto — Professor, Department of Chemistry, Polytechnic University

Dr. Mohamed Ali — Associate Professor, Dept. of Electrical Engineering, The City College of the City University of New York

Dr. Ping Pei Ho — Professor, Department of Electrical Engineering, The City College of the City University of New York

---

Supervisory Committee

THE CITY UNIVERSITY OF NEW YORK

0.1 Abstract

PHOTOLUMINESCENCE AND ELECTROLUMINESCENCE IN LANTHANIDE-ORGANIC COMPLEXES AND ORGANIC POLYMERS

by

ANDREW G. EDWARDS

Thesis Advisor: Professor Roger Dorsinville

Recently, metal-organic compounds and organic polymers have attracted much attention for their potential applications involving organic light emitting diodes (LEDs). The visible radiation emitted by these organic LEDs can be tailored for several applications such as multicolor displays, computer backlighting, or computer display monitors. This thesis will consider the unique optical properties of the lanthanide-benzoylbenzoate complexes and use these properties to fabricate thermally stable LEDs with narrow spectral linewidths emitting in the red and green regions of the visible spectrum. These devices are constructed by combining the lanthanide-benzoylbenzoate complexes with suitable polymer matrices, compatible hole transport compounds or electron transport materials in single or multiple layer cell configurations. Organic polymers have already been synthesized for emission in the

red, orange, yellow, green, and most recently, the blue region. However, thermally stable organic emitters are also important for developing reliable light emitting devices operating in the blue region. Poly(benzoyl,1-4,phenylene) (PBP), a soluble PPP-type polymer possessing very high thermal stability, was used to fabricate LEDs emitting (with high brightness) in the blue region of the spectrum. The results show that PBP is a promising candidate material for optoelectronic applications.

Dedicated to my parents, Lloyd Edwards and Barbara Edwards, my wife, Elisabeth Edwards, and my sons, Nicholas and Brandon.

0.2 Acknowledgements

I am indebted to my mentor Dr. Roger Dorsinville for his guidance and unique insight in theoretical and experimental physics which helped to guide me towards obtaining the Ph.D. degree. I thank the members of my examining committee (Dr. Ardie Walser, Dr. Vladimir Petricevic, Dr. Yoshiyuki Okamoto, Dr. Mohamed Ali and Dr. Ping Pei Ho) for their technical support over the years. I am also thankful to Dr. Igor Sokolik who helped me to refine my approach to scientific investigation. I am appreciative of the contributions of Dr. Sylke Blumstengel who I collaborated with while investigating luminescence in organic polymers. I also appreciate the efforts of Dr. Charles Claude, Dr. T. K. Kwei, Mr. T. Y. Chu and Mr. H. C. Yun (all of Polytechnic University) for synthesizing the organic materials for my experiments.

I am deeply grateful to my wife, Elisabeth Edwards, for her support and encouragement and who, through the years, has loved me enough to believe in my quest to obtain the Ph.D. degree. To my sons Brandon and Nicholas, I am thankful to them for reminding me of the importance of maintaining balance in all areas of my life.

I am appreciative of the various teachers and mentors who I have encountered throughout my life who may have imparted wisdom and also had significant positive impacts on my life, namely: Mr. Albert Edwards, Mr. Dwight Williams, Dr. Joseph

Johnson III, Mr. Reginald Best, Dr. A. R. Bernard Sr., Dr. Edwin Louis Cole, Sensei Monte Allen and Sensei William Best.

The author is also grateful to Dr. Daniel Akins, Dr. Ronald Brown, Dr. Laurent Mars and the support team at the Center for Analysis of Structures and Interfaces for their guidance, administrative assistance and financial support over the course of my studies. I am also thankful to the New York State Center for Advanced Technology for Photonic Materials and Applications for its grant for equipment and materials to study electroluminescence in organic systems. I am also thankful to the National Science Foundation for sponsoring this project under NSF grant Nos. HRD-8802964, ECS-9212310, ECS-9520561, ECS-9311608.

TABLE OF CONTENTS

LIST OF FIGURES

0.3 Thesis Organization

This thesis will consider the techniques used to design and fabricate organic light emitting diodes using metal-organic complexes and organic polymers. The preliminary sections contain a synopsis of electroluminescence in organic materials and outlines the contents of this thesis. Chapter 1 discusses the history of electroluminescence in organics and documents the motivation for designing electroluminescent devices using novel metal organic complexes and organic polymers. Chapter 2 discusses the experimental set-up, the procedures used to fabricate these devices, the measurements used to describe the optical properties of these new materials and the characterization of the light emitting devices based on these novel materials. In particular, spectral analysis techniques will be used to select promising candidate materials for charge transport or luminescent layers. Next, the results obtained from the optical characterization studies will be used to fabricate devices using these luminophors and transport layers combined in single or multiple layer cell structures. In Chapter 3, the theoretical basis for designing multilayer EL devices will be covered.

The electroluminescent properties of the tris-(8-hydroxyquinoline)-aluminum (ALQ_3), the lanthanide(benzoylbenzoate) complexes and the poly(2,5-benzophenone) polymers will be reported in Chapters 4, 5 and 6, respectively. In particular, the

electroluminescence spectra, current versus voltage curves, brightness versus voltage curves, quantum efficiency of photoluminescence, luminous efficiency and device operating lifetimes will be discussed in these chapters. In Chapter 7, I provide conclusions based on the results of Chapters 5, 6 and 7. Finally, (in Chapter 8) experiments to be performed, improvements to enhance the device performance will be suggested for lanthanide(III)-organic– and organic polymer–based LEDs. Future device improvements and applications for these LEDs will also be discussed in the closing section.

CHAPTER ONE

1. INTRODUCTION

Chapter 1 provides a historical background of electroluminescence in lanthanide complexes and organic polymers. This chapter also discusses the experiments to be performed and measurements to be taken and reported in this thesis.

1.1 Motivation

Organic polymers and metal-organic complexes may have potential applications in optical technology such as: optical interconnects, photodetectors, light modulators, optical amplifiers or other devices such as organic light emitting diodes (OLEDs). The relatively high brightness of OLEDs makes them promising candidates for optical components that can be used in flat panel displays. These OLEDs may be useful for backlighting in liquid crystal displays, single color pixels in monochrome displays or multicolor pixels in high resolution graphics display monitors.

So far, red, orange, yellow, green, blue-green, blue, violet and white light emitting devices have already been manufactured by several research groups. To date, the most efficient devices have electroluminescence efficiencies of about 4-5 % photons per electron (with a maximum possible theoretical efficiency of 25 %), and luminous efficiencies of about 1-2 lumens per watt. The corresponding brightness

measurements for these devices have been reported to be well over 1,000 cd/m^2 for most of the brightest LEDs. Recent reports have even suggested brightness values of up to 10^6 cd/m^2.[1] Furthermore, the low currents (mA range) and operating voltages (7-20 volts) make these devices relatively efficient (low power consumption) light sources compared to cathode ray tube monitors and traditional flat panel displays.

1.2 Background

Over the past three decades, many researchers have contributed to the development of organic electroluminescent (EL) devices. In 1963, Pope and coworkers observed electroluminescence in anthracene single crystals.[23] Also H. Noarman et. al. developed EL devices based on anthracene. Unfortunately, the devices constructed from organic crystals such as anthracene need relatively high turn-on voltages (e.g., ≥ 400 Volts for a 10 μm thick organic crystal layer). These devices were visible in a dimly lit room and the corresponding electric fields were on the order of 10^6 V/cm for operation at these brightness levels. Nevertheless, research involving electroluminescence in organic crystals continued throughout the 1970's.

However, it was not until 1987 that Tang and Van Slyke fabricated the first modern day thin film organic electroluminescent diode.[4] Tang's device was based on the fluorescent metal chelate, 8-hydroxyquinoline aluminum (ALQ_3).[5,6] The device structure consisted of an indium-tin-oxide (ITO) coated glass substrate covered with a hole-transporting aromatic diamine layer (750 Å thick). The luminescent layer of ALQ_3 (600 Å) was deposited on top of the diamine layer and the cathode (deposited

on top of the ALQ_3 layer) was an alloy of magnesium and silver. The ALQ_3 layer also served as the electron transport layer because of its good electron transport properties.

When these devices were operated with the ITO electrode at positive bias and the Mg:Ag electrode at negative bias, green electroluminescence, originating from the aluminum chelate, was observed. These devices showed high brightness (> 1000 cd/m^2) with driving voltages less than 10 V dc. These LEDs also showed high external quantum efficiencies of 1 % photons/electron and luminous efficiencies of 1.5 lumens/watt (lm/W). The structure of the electroluminescent (EL) cell and the chemical structures of the organic materials are shown in Figure 1-1.

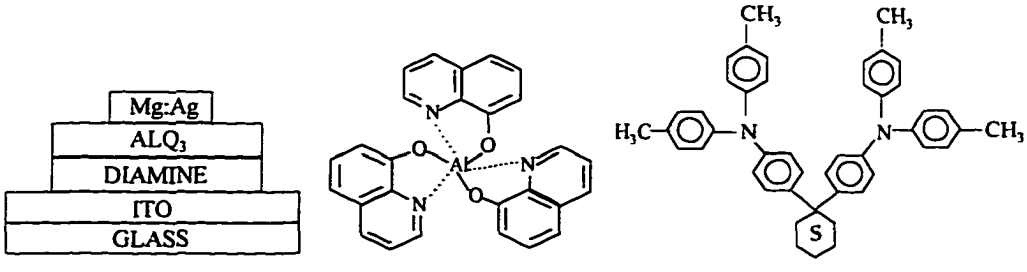

EL Cell ALQ_3 Diamine

Figure 1-1. EL Cell and Chemical Structures of Organic Materials

Later Tang and coworkers achieved increased brightness and higher EL quantum efficiency from these devices (device structure: ITO/Diamine/ALQ_3/Mg:Ag) by doping the ALQ_3 emitting layer with highly fluorescent materials such as the coumarin and DCM dyes.[7] These and other researchers also showed that the EL colors could also be tuned from the blue-green to orange-red region of the spectrum by

changing the type of dopant and the concentration of doping materials.[8] By controlling the location of the doping materials Tang and coworkers have also confirmed that the emission zone is confined to the region of the ALQ_3 layer located within 50 Å of the diamine/ALQ_3 interface.

To date, other research groups have continued research efforts involving ALQ_3. Burrows et. al. and Hamada et. al. have studied the photoluminescence and electroluminescence of the metal-quinolate systems.[9,10] Their results show that the luminescence in these complexes does not originate from the metal ions but comes from the ligands. Also, the brightness of the electroluminescent devices does not solely depend on the PL quantum efficiency of the metal chelates in solution or solid state, but the devices' light output also depends on several properties of the film including: transport properties, thermal stability and chemical stability. Other researchers have also utilized ALQ_3 as the electron transport layer in multilayer electroluminescent devices.[11]

In other instances novel light emitting device structures or optoelectronic devices have been developed. Polyaniline (PANI) and its blends are often used as a flexible substrate that may also lower the drive voltage for LEDs.[12-14] The development of flexible substrates opens the possibility of more robust device configurations as well as novel devices shapes or display monitor structures.

Narrow spectral width emitters are crucial for the development of multicolor displays. Since most organic systems produce very wide spectral emission bands,

optical design techniques are often used to narrow the devices' spectral output. In one approach, the authors have proposed the use of narrow-band optical filters to narrow the output linewidth of the devices. Another design technique adopted by Rothberg and coworkers uses optical microcavity design techniques to narrow the spectral bandpass of the coplanar optical cavity located within the organic LED. The spectral bandpass or transmissivity of these Fabry-Perot type cavities depend on the function[15]:

$$T = \frac{G_0(1-R_1)\cdot(1-R_2)}{\left(1-G_0\sqrt{R_1R_2}\right) + 4\sqrt{R_1R_2G_0}\sin\theta} \qquad \text{Equation 1-1}$$

where G_0 is the power gain of the optical medium between the cavity mirrors, R_1 and R_2 are the reflectivity of the mirrors and θ is the angle of incidence (with respect to the cavity normal) for the exiting ray.

Due to the lack of very narrow spectral width emitters, displays fabricated from currently available emitting materials may appear to have very dull spectral appearances. In addition, the range of colors and spectral resolution may be limited due to the relatively large spectral bandwidth of existing OLEDs. Microcavity design techniques can be used to reduce the optical bandwidth of these sources but this design approach is more complex and increases the total manufacturing cost for displays. If spectral filters are added to narrow the output spectrum of these devices, additional optical losses are incurred thereby limiting the overall brightness of the display. By combining the lanthanide(III) metals with different organic ligands,

device properties can be tailored for inherently narrow band emission across the visible spectrum without the use of external optical components or complex cavity designs.

The lanthanide-organic complexes differ from other metal chelates because the emission spectra of the metal complexes originate from the lanthanide ions.[16,17] The excitation energy is initially absorbed through the singlet states of the ligands which then transfer their energy to the triplet states. After intersystem crossing from the ligand to the lanthanide ion, the PL emission comes from the radiative decay of the excited lanthanide ions, producing narrow line-like spectra. See Figure 1-2 for an illustration of energy transfer in lanthanide chelates. Since the lanthanide complexes are triplet excited, they have a potential 100 % quantum efficiency of photoluminescence. For EL devices, there is a potential quadrupling of the EL quantum efficiency compared to excitation through the singlet state alone. The narrow spectral linewidths and the potential for increased energy transfer efficiency make the lanthanide complexes promising candidates for applications involving light emitting diodes.

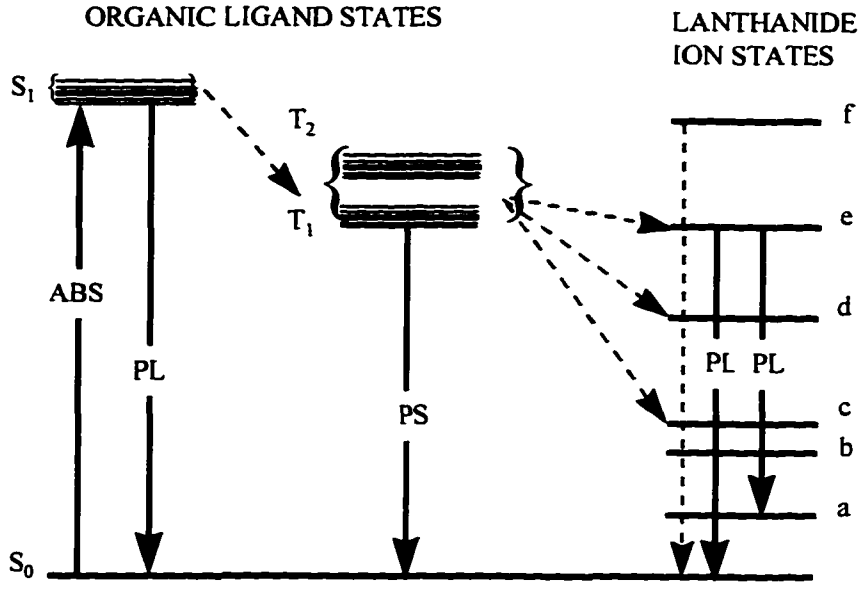

Figure 1-2. Energy Transfer in Lanthanide Chelates

The lanthanide complexes have long been known to possess narrow-line photoluminescence spectra in solution and in the solid state.[16,17] In 1992, J. Kido and K. Nagai developed the first lanthanide-organic light emitting devices based on the Tb(acetylacenato)$_3$ {Tb(ACAC)$_3$} and the Eu(thenoyltrifluoroacetonato)$_3$ {Eu(TTFA)$_3$} complexes.[18] The chemical structures of these lanthanide complexes are shown in Figure 1-3. The light emitting devices had the ITO/TPD/Tb(ACAC)$_3$/Al and ITO/PMPS:Eu(TTFA)$_3$/PBD/Mg/Ag structures, where TPD is the N,N'-diphenyl-N,N'-bis(3-methylphenyl)-1,1'-biphenyl-4,4'-diamine (a diamine derivative), PMPS is poly(methylphenylsilane) and PBD is 2-(4-biphenylyl)-5-(4-tert-butylphenyl)-1,3,4-oxadiazole. TPD and PMPS were used as hole-transporting agents and PBD was used as an electron-transporting material. The devices with the terbium complex showed narrow-line emission spectra characteristic of the Tb^{3+} ion (with the strongest

emission lines at 544 nm and 490 nm) and a maximum brightness of 7 cd/m^2. The devices containing the europium complex showed the strongest emission line at approximately 615 nm with a maximum brightness of 0.3 cd/m^2.

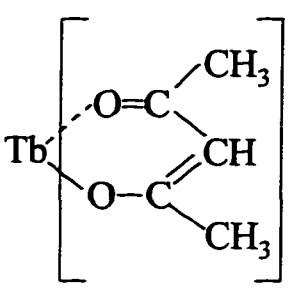

Tb(ACAC)$_3$

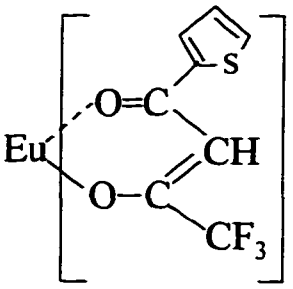

Eu(TTFA)$_3$

Figure 1-3. Chemical Structures of Electroluminescent Lanthanide Complexes

After Kido's initial efforts several monochromatic LEDs were developed from lanthanide complexes. In 1994, Kido and coworkers constructed a device based on tris(1,3-diphenyl-1,3-propanediono)(monophenanthroline)Eu(III), Eu(DBM)$_3$(Phen), a red-emitting lanthanide complex.[19] The LED cell structure was: ITO/TPD/Eu complex:butyl-PBD/ALQ$_3$/Mg:Ag, where TPD is the hole-transporting triphenyldiamine derivative, and Mg:Ag is an alloy of magnesium and silver. This device showed brightness values of up to 460 cd/m^2 with an emission line at 614 nm corresponding to the Eu^{3+} ion. Takada and coworkers also developed a similar light emitting device based on a sublimable Eu(TTA)$_3$-phenanthroline derivative {Eu(TTA)$_3$(Phen)}.[20] Takada's devices emitted a sharp line at 617 nm and had a maximum brightness of 10 cd/m^2. These devices utilized a microcavity design with a

cell structure of (SiO_2/TiO_2 bilayers)/ITO/TPD/Eu-complex/ALQ_3/Mg:Ag. The SiO_2/TiO_2 bilayers comprised a dielectric quarter-wave stack that was used as the output reflector for the microcavity. By adjusting the optical path length of the microcavity, the authors showed that there was an angular dependence of the spatial emission pattern emitted from the device. Consequently, optical display devices could be designed to optimize viewing angle by adjusting the cavity length and the reflectivity of the mirrors.

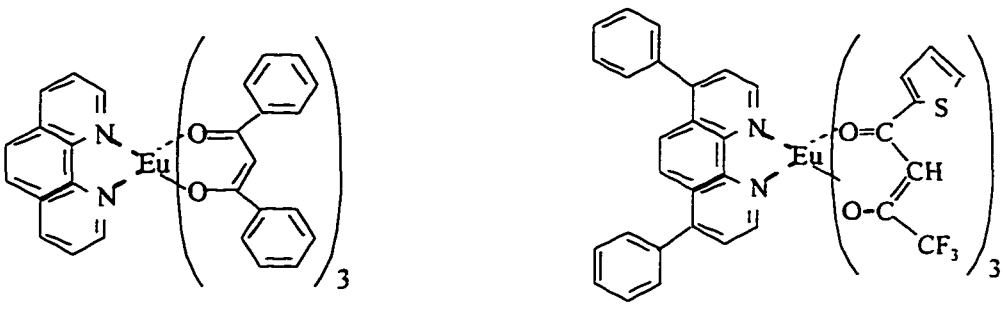

$Eu(DBM)_3(Phen)$ $Eu(TTA)_3(Phen)$

Figure 1-4. Electroluminescent Europium Complexes.

Sano et. al observed improved brightness results by modifying the side-group of the $Eu(TTA)_3(Phen)$ complex.[21] In their devices, they utilized $Eu(TTA)_3$(1,10-phenanthroline) {$Eu(TTA)_3(Phen)$ Derivative #2} using two- and three-layer cell structures (Figure 1-5). These devices showed line emission from the europium complex with maximum brightness values over 100 cd/m^2.

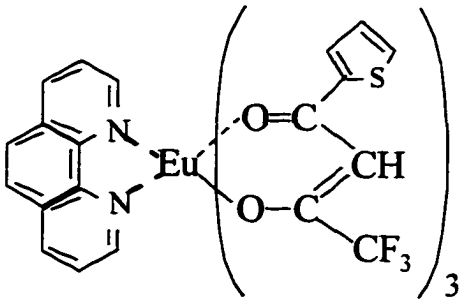

Figure 1-5. $Eu(TTA)_3(Phen)$ Derivative #2

The first white-light LED fabricated from lanthanide complexes was developed by Kido and coworkers.[22] Kido's devices were based on the mulitlayer cell: ITO/TPD/$Tb(ACAC)_3(Phen)$/$Eu(DBM)_3(Phen)$/ALQ_3/Mg:Ag. The chemical structure of $Tb(ACAC)_3(Phen)$ is shown in Figure 1-6. These devices had a maximum luminance of 90 cd/m^2. The thickness of each layer within the device was adjusted to give white emission that originated from all three metal complexes and TPD.

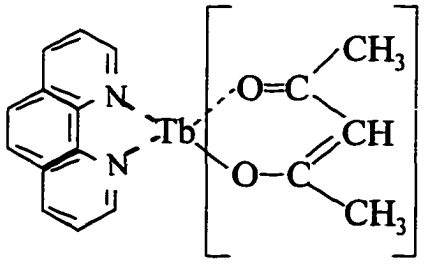

Figure 1-6. Chemical Structure of $Tb(ACAC)_3(Phen)$

In this thesis we have used new lanthanide (III) metal-organic complexes, based on terbium (III) or europium (III) ions chelated to organic ligands, as thermally-stable luminescent materials for organic LEDs. In particular, the terbium- and europium-benzoylbenzoates, emitting in the green and red regions of the visible

spectrum, respectively show good thermal stability up to 320^0 C. These lanthanide complexes have been used to fabricate single layer and multiple layer devices that emit in very narrow spectral bands with suitable efficiency.

Organic polymers have also become increasingly important for the development of electroluminescent technology. The development of conjugated polymers for the emissive layers in LEDs offers several advantages such as low cost fabrication compared to semiconductor technology. Also, organic polymers offer the advantage of relatively easy processing by spin casting from solution. For the conjugated polymer systems, the bandgap can be chemically adjusted by modifying the effective conjugation length of the polymer chain. This can be achieved by adjusting the chain length of the polymer or by adding spacer-groups to provide energy barriers for quantum confinement of the excitation energy located on the polymer backbone. Consequently, LEDs based on a variety of polymers spanning the visible spectrum have already been developed by several research groups.

The first observation of electroluminescence (EL) in organic polymers was discovered in poly(p-phenylene vinylene) (PPV) during 1990[1,23] by Burroughes et. al. Consequently, the research and commercial interest in conjugated polymers increased because of their potential use in display technology. See Figure 1-7 for the chemical structure of PPV. The light emitting devices developed by Burroughes and coworkers emitted in the green-yellow region of the spectrum.

PPV PPP

Figure 1-7. Chemical Structures of the Organic Polymers PPV and PPP

The first EL devices developed with PPV had the following structure: glass substrate/hole injecting contact/PPV/electron injecting contact. The hole injecting contact was the high work function material indium oxide. Aluminum, which has a low work function, was used for the electron injecting contact. The EL quantum efficiency of these devices was reported to be 0.05 % photons/electron. The authors also reported that the luminescence (PL and EL) is due to the radiative recombination of the polaron exciton formed by the intrachain excitation of PPV. The PL quantum yield in PPV systems is roughly 8 %. The limitation of PL quantum efficiency is attributed to the migration of excited states to defect sites that act as nonradiative recombination centers. However, with the careful design and purification of organic polymers, this quenching mechanism can be significantly reduced.

Blue electroluminescence in conjugated polymers is also important for the development of flat-panel multicolor displays. Poly(p-phenylene) (PPP) was the first conjugated polymer for which blue emitting diodes were realized.[24] Since then, blue EL has been reported from different conjugated polymers such as PPP-type ladder polymers[25,26] poly(alkylfluorene)[27], poly(pyridine)[28], non-conjugated polymers like poly(N-vinyl carbazole)[29], polymer blends[30,31] and copolymers.[32,33]

Thermally stable blue-emitting LEDs are particularly important for the development of full color displays. The high current densities generated within the thin film layers of current-driven devices may lead to high operating temperatures which necessitates the development of thermally stable emitting materials. In Chapter 7 I report the photoluminescent and electroluminescent properties of a novel polymer, poly(benzoyl-1,4-phenylene) (PBP). PBP is a PPP derivative, where the introduction of the benzoyl side group makes it soluble in common organic solvents, and thin films can be obtained by spin casting directly from solution.[34] Thus, the use of precursor routes, which is necessary for the preparation of PPP thin films, can be avoided. Additionally, PBP has high thermal stability (i.e., shows no thermal degradation below 500° C) which is desirable for good device performance.

Poly(benzoyl-1,4-phenylene) has bright photoluminescence (in solution and in solid state) in the blue region of the spectrum.[35] The PL quantum efficiency of this polymer in chloroform solution is 15 %. I have fabricated multi-layer LEDs with the PBP polymer and these devices show bright blue electroluminescence originating from PBP. The maximum brightness of these devices is 100 cd/m^2.

The results obtained from PL and EL studies of the La complexes and PBP show that these materials are promising candidates for LEDs. The experimental results will be outlined in the later sections.

1.3 Thesis Statement

Narrow-band thermally-stable light emitting diodes are important for the development of multicolor organic displays. Thermally stable blue emitting polymers are also critical for the improvement of organic display technology. This thesis is focused on studying the optical properties of lanthanide(III)-organic complexes and organic polymers that may be used in light emitting diodes. The particular compounds to be studied include terbium- and europium-tris[2-(4'-methoxybenzoyl)benzoate], terbium-tris[2-(4'-methylbenzoyl)benzoate], and poly(benzoyl-1,4-phenylene) (PBP), a soluble PPP-type polymer. To characterize each material, the optical properties are studied in dilute solution and in the solid state. Then, these novel compounds will be used to make multi-layer thin film LEDs deposited on glass substrates. The electroluminescent and device operating characteristics are studied for each set of materials used in LEDs. The optical and device-related parameters to be determined include:

1. Measurement of luminescence spectra, absorption spectra, fluorescence lifetimes, quantum efficiency of photoluminescence and energy transfer mechanisms in solution.

2. Luminescent properties of thin films.

3. Fabrication of multilayer organic LEDs

4. Characterization of LEDs including I and V vs. B curves.

5. Determination of injection, transport and recombination processes occurring within the devices.

6. Determination of energy transfer mechanisms occurring within the devices.

7. Proposals for improving existing devices and suggestions for novel device structures.

REFERENCES

1. A. J. Heeger, Oral report given at 1996 International Conference on the Science and Technology of Synthetic Metals.

2. M. Pope, H. P. Kallman and P. Magnante, *J. Chem. Phys.*, **38,** pp. 2042 - 2043, (1963).

3. M. Sano, M. Pope and H. Kallman, *J. Chem. Phys.*, **43,** pp. 2920 - 2921, (1965).

4. C. W. Tang and S. A. Van Slyke, *Appl. Phys. Lett.* **51**, No. 12, pp. 913 - 915, (1987).

5. W. E. Ohnesorge and L. B. Rogers, *Spectrochimica Acta*, pp. 27 - 31, (1959).

6. D. Z. Garbuzov, V. Bulovic, P. E. Burrows and S. R. Forrest, *Chem. Phys. Lett.* **249** pp. 433 - 437, (1996).

7. C. W. Tang, S. A. VanSlyke and C. H. Chen, *J. Appl. Phys.* **65** No. 9, pp. 3610 - 3616, (1989).

8. T. Mori, K. Miyachi, T. Kichimi and T. Mizutani, *Jpn. J. Appl. Phys.*, Part 1 No. 12, pp. 6594 - 6595, (1994).

9. Y. Hamada, T. Sano, M. Fujita, T. Fujii, Y. Nishio and K. Shibata, *Jpn. J. Appl. Phys.*, **32** L514 - L516 (1993).

REFERENCES (Continued)

10. P. E. Burrows, L. S. Sapochak, D. M. McCarty, S. R. Forrest and M. E. Thompson, *Appl. Phys. Lett.*, **64** pp. 2718 - 2720, (1994).

11. J. Kido, C. Ohtaki, K. Hongawa, K. Okuyama and K. Nagai, *Jpn., J. Appl. Phys*, **32** pp. L917 - L920, (1993).

12. G. Gustafsson, Y. Cao, G. M. Treacy, F. Klavetter, N. Colaneri and A. J. Heeger, *Nature*, **357** pp. 477 - 479, (1992).

13. Y. Yang, E. Westerweele, C. Zhang, P. Smith and A. J. Heeger, *J. Appl. Phys.*, **77** No. 2, pp. 694 - 698, (1995).

14. Y. Cao, G. M. Treacy, P. Smith and A. J. Heeger, Appl. *Phys. Lett.*, **60** No. 22, pp. 2711 - 2713, (1992).

15. J. T. Verdeyen, Laser Electronics (2nd Ed.), Prentice-Hall, pp. 137, (1989).

16. A. Heller and E. Wasserman, *J. Chem Phys.*, **42 No. 3**, pp. 949 - 953, (1964).

17. H. Samelson, A. Lempicki and C. Brecher, *J. Chem. Phys.*, **40** No. 9, pp. 2553 - 2558, (1964).

18. J. Kido and K. Nagai, *J. Alloys and Compounds*, **192** pp. 30 - 33, (1993).

19. J. Kido, H. Hayase, K. Hongawa, K. Nagai and K. Okuyama, *Appl. Phys. Lett.*, **65** pp. 2124 - 2126, (1994).

REFERENCES (Continued)

20. N. Takada, T. Tsutsui and S. Saito, *Jpn. J. Appl. Phys.*, **33** pp. L863 - L866, (1994).

21. T. Sano, M. Fujita, T. Fujii, Y. Hamada, K. Shibata and K. Kuroki, *Jpn. J. Appl. Phys.*, **34** Part1, No. 4A, pp. 1883 - 1887, (1995).

22. J. Kido, W. Ikeda, M. Kimura and K. Nagai, *Jpn. J. Appl. Phys.*, **35** Part 2, No. 3B, pp. L394 - 396, (1996).

23. J.H. Burroughes, D.D.C. Bradley, A.R. Brown, R.N. Marks, K. Mackay, R.H. Friend, P.L. Burns and A.B. Holmes, *Nature*, **347** pp. 539 - 541, (1990).

24. G. Grem, G. Leditzky, B. Ullrich and G. Leising, *Adv. Mater.*, **4** No. 1, pp. 36 - 37, (1992).

25. J. Grüner, P.J. Hamer, R.H. Friend, H.J. Huber, U. Scherf and A.B. Holmes, *Adv. Mater.*, **6** No. 1, pp. 748 - 752, (1994).

26. S. Tasch, A. Niko, G. Leising, and U. Scherf, *Appl. Phys. Lett.*, **68** pp. 1090 - 1092, (1996).

27. M. Uchida, Y. Ohmori, C. Morishima and K. Yoshino, *Synth. Met.*, **55-57** pp. 4168 - 4169 (1993).

REFERENCES (Continued)

28. D. D. Gebler, Y. .Z. Wang, J. W. Blatchford, S. W. Jessen, L. -B. Lin, T. L. Gustafson, H. L. Wang, T. M. Swager, A. G. MacDiarmid and A. J. Epstein, *J. Appl. Phys.*, **78** pp. 4264 - 4266, (1995).

29. J. Kido, K. Hongawa, K. Okuyama and K. Nagai, *Appl.Phys. Lett.*, **63** No. 19, pp. 2627 -2629, (1993).

30. C. Zhang, H. V. Seggern, K. Pakbaz, B. Kraabel, H. -W. Schmidt and A. J. Heeger, *Synth. Met.* **62** pp. 35, (1994).

31. B. Hu, Z. Yang and F. E. Karasz, *J. Appl. Phys.*, **76** No. 4, pp. 2419 - 2422, (1994).

32. W. -X. Jing, A. Kraft, S. C. Moratti, J. Grüner, F. Cacialli, P. J. Hamer, A. B. Holmes and R. H. Friend, *Synth. Met.*, **67** pp. 161 - 163, (1994).

33. I. Sokolik, Z. Yang, F. E. Karasz and D. C. Morton, *J. Appl. Phys.*, **74** pp. 3584 - 3586, (1993).

34. Y. Wang and R. P. Quirk, *Macromolecules*, **28** pp. 3495 - 3501, (1995).

35. R. W. Phillips, V. V. Sheares, E. T. Samulski and J. M. Desimone, *Macromolecules*, **27** pp. 2354 - 2356, (1994).

CHAPTER TWO

2. RESEARCH

Chapter 2 describes the synthesis techniques for developing new optical materials and the experimental methods for measuring their optical properties. This chapter also describes procedures for fabricating and characterizing electroluminescent light emitting diodes (LEDs) based on these novel materials.

2.1 Experimental

The chemical synthesis and material characterization of the lanthanide complexes and organic polymers were performed by Dr. Yoshiyuki Okamoto, Dr. Charles Claude, Dr. T. K. Kwei, Mr H. C. Yun and Mr. T. Y. Chu, all of Polytechnic University. Aluminum-(8-hydroxyquinoline) (ALQ_3) was obtained from the Eastman Kodak company. The hole transporting materials poly(n-vinylcarbazole) (PVK) and N,N'-diphenyl-N,N'-bis(3-methylphenyl)-[1,1'-biphenyl]-4,4'-diamine (TPD), and the polymer binder poly(methylmethacrylate) (PMMA) were obtained from Polytechnic university. The electron transporting material butyl-PBD was obtained from the Aldrich chemical company.

The chemical characterization was performed according to established procedures. The oxidation potential was measured on a Bioanalytical Systems CV-37 cyclic voltammograph with an Ag/AgCl reference electrode and a 10 μm platinum

electrode. Thermal analysis was performed using a DuPont 951 TGA cell with a TA2100 thermal analyzer. All chemicals were purified using standard chemical procedures prior to spectral analysis and device fabrication. Also, all compounds are dried for at least 48 hours in a vacuum oven at a temperature of 35-40^0 C to remove any traces of oxygen, water or residual solvents.

Photoluminescence (PL) spectra and lifetime (τ) measurements were collected on a Perkin-Elmer LS-50B spectrofluorometer. Absorption spectra were measured on a Perkin-Elmer Lambda 9 UV-Vis Spectrophotometer. EL spectra were measured with an Acton Research Corporation SpectraPro-150 spectrograph connected to an EG&G Princeton Applied Research Corporation (PARC) 1420 Diode Array which was controlled by an EG&G PARC 1461 Detector Interface. During the measurement of EL spectra, the LEDs were powered by an HP 214A pulse generator (square wave pulses, non-return to zero, 10 % duty cycle, 10 kHz repetition rate, 10-30 volts peak amplitude) to avoid heating effects during the measurement of the electroluminescence spectra. Figure 2-1 shows the experimental set-up for recording the EL spectra.

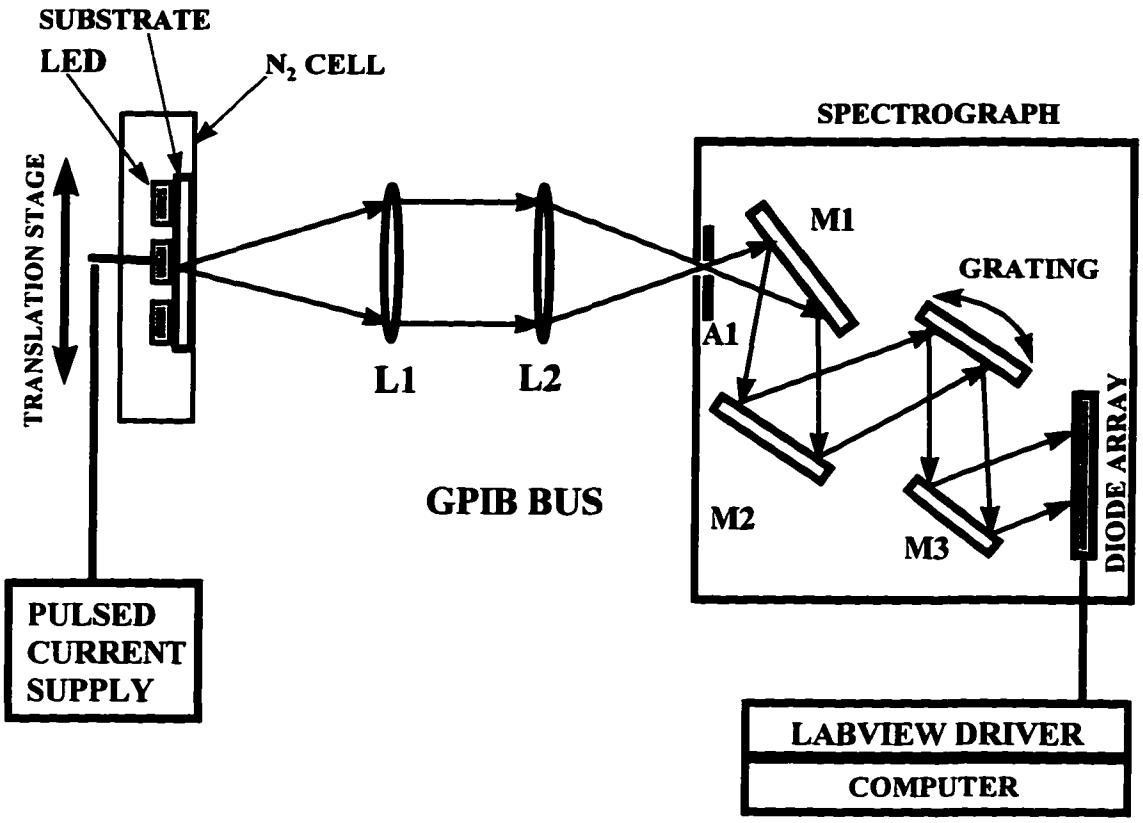

Figure 2-1. Experimental Set-up for Measuring EL Spectra

A1 - Variable Aperture/Slit; M1, M2, M3 - mirrors, L1, L2 - Biconvex Lenses

To measure the spectral properties of the LEDs, the substrate containing three LEDs was placed in a custom-made cell. This measurement cell was kept in a sealed container prior to taking measurements and was maintained under a constant flow of nitrogen during spectral measurements and when measuring current, voltage and brightness data. The cell was mounted on an XYZ translation stage. During measurements, the LED being examined was placed at the focal point of the collimating lens L1, a 15 cm focal length biconvex lens. The lens L2 (identical to L1) was used to focus the collimated LED light into the input slit of the 15 cm focal length spectrograph. The input slit was kept at a 100 to 150 μm opening during

measurements. M1, M2 and M3 are internal mirrors of the spectrograph. The LEDs were powered by the pulsed current supply during spectral measurements to avoid heating effects. The output spectra were corrected with a known standard to compensate for the optical response of the input optics and the responsivity of the detector array. The collected data were averaged over a minimum period of 60 seconds.

The LEDs' current and voltage were measured with a Keithley 6517 electrometer and the corresponding brightness data were collected with an International Light Corp. IL1700 radiometer. The electrometer and radiometer were controlled by an IBM-compatible personal computer via a GPIB interface and an RS232C interface, respectively. The computer software driver for measuring the current, voltage and brightness values was a custom-made program developed with the LABVIEW program.[1] Figure 2-2 shows the experimental arrangement for measuring the voltage-dependent behavior of the devices. During current and brightness measurements, the voltage level was increased from 0 volts to the maximum voltage in 0.1 to 2 volt increments. During each step of the voltage-increment cycle, the voltage was held constant for at least 2 seconds between voltage steps to avoid transient effects from the power supply and the LED response time. The brightness and current readings were then taken 1 second after each voltage increment.

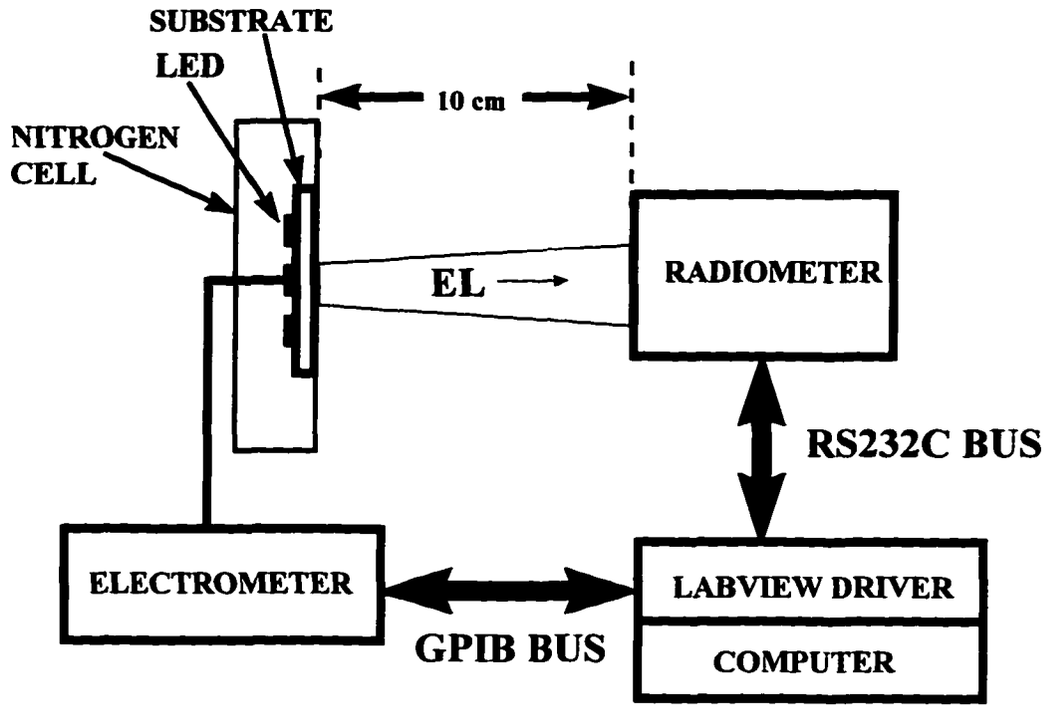

Figure 2-2. Set-up for Measuring Current, Voltage and Brightness of LEDs

LEDs (Figure 2-3) were fabricated on a glass substrate covered with indium-tin-oxide (ITO). All organic layers for the LEDs were deposited by spin casting from solution or thermal evaporation at a rate of 1-5 /s. The electrodes were deposited on top of the organic layers by thermal evaporation under a vacuum of $5x10^{-7}$ mm Hg. All stages of device fabrication and testing were done under a nitrogen atmosphere.

2.2 Device Fabrication

Light emitting diodes (Figure 2-3) are fabricated in several stages before final operation. First, each ITO-coated glass substrate is prepared before deposition of each successive thin film layer. After each organic layer is successively deposited onto the glass substrates, the metallic layer is deposited as the final step to complete the device

fabrication process. See Figure 2-4 for the structure of a single layer organic LED. Note, the single layer refers to the single organic layer present in the device. Detailed fabrication procedures are outlined in the following sections.

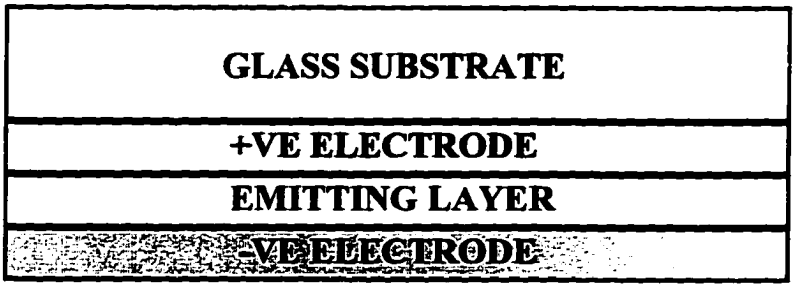

Figure 2-3. Structure of a Single Layer LED

2.2.1 *Preparation of Glass Substrates*

First, glass squares (15 mm x 15 mm), half coated with a layer of Indium Tin-Oxide (ITO), are ordered from the University of Massachusetts, Amherst or Kent State University. During the first cleaning stages these ITO-coated glass squares are prepared by cleaning with a series of polar and/or nonpolar solvents, then immediately drying under a flow of dry nitrogen between each cleaning stage. The substrates are initially cleaned in an ultrasonic bath containing an ultrasonic cleaning chemical or detergent dissolved in distilled water. The glass squares are then cleaned (in an ultrasonic bath) with acetone, dried under a flow of nitrogen, cleaned with chloroform and dried again. Next, the substrates are cleaned (in the ultrasonic vibrator) with warm methanol and then dried with nitrogen. After this cleaning stage

is completed, the substrates are dried overnight in a vacuum oven at a temperature of approximately 75 ^{0}C to remove any traces of solvents and water from the glass.

Next, five metal contacts (Figure 2-4) are attached to the ITO-covered glass substrates. These metal contacts are composed of a conducting silver-based paint that must be cured at high temperatures over a specified period of time (e.g., heating at 100 ^{0}C for twenty minutes). Two metal contacts (including one spare contact) are attached to the ITO-coated side of the substrate; one of the metal contacts will later be connected to the positive terminal of the voltage source. Second, the other three metal contacts are then deposited on the edge of the bare glass surface and will later be connected to the individual cathodes of the three diodes that will be deposited on the surface. This contact also serves as a durable connection point for the negative terminal of the power supply. The position of each electrical contact will correspond to a mask that will be placed over the substrates during evaporation of any organic layers and another mask for evaporation of the metal electrode. See Figure 2-4 for an outline of the stages involved in the preparation of each substrate.

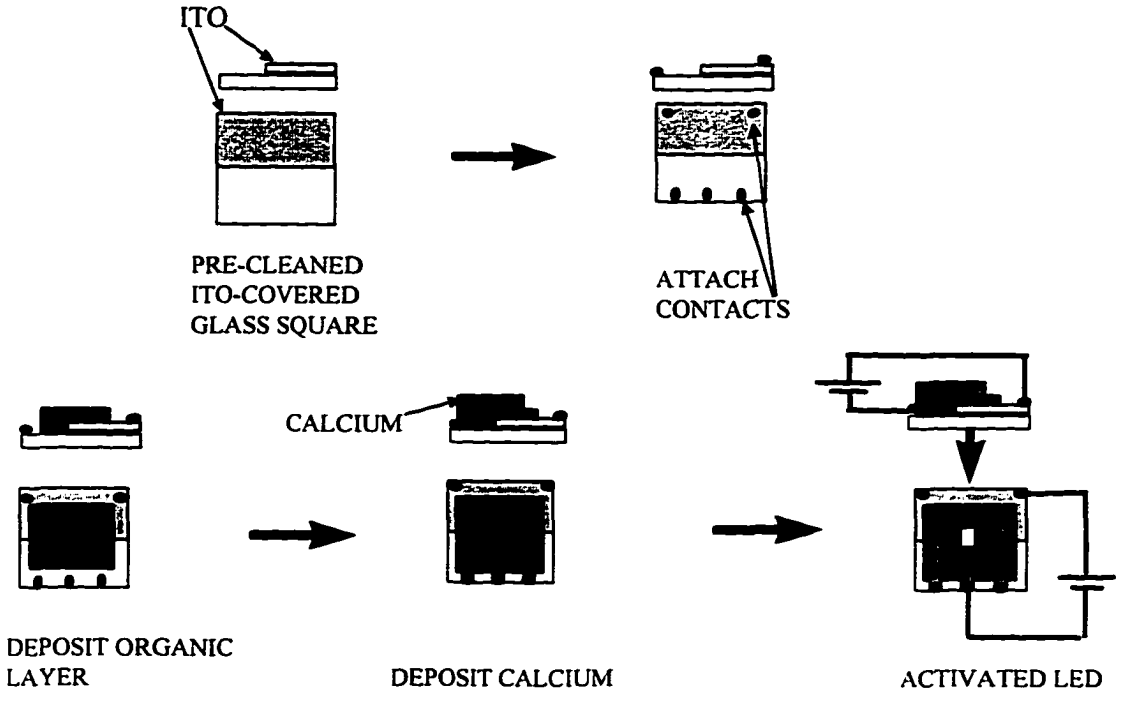

Figure 2-4. Fabrication of Organic LEDs

After attaching the metal contacts, the substrate is rinsed in distilled water, to remove any surface contaminants, and dried in a vacuum oven for at least 12 hours at a temperature of 40-50 degrees centigrade to remove any traces of water dissolved in the glass. Afterwards, the dry substrates are cleaned under an argon plasma for ten to fifteen minutes to remove any residual surface contaminants. The clean substrates are subsequently placed in a sealed container and stored in a glove box filled with dry argon (or nitrogen) until the organic films and metal cathode need to be deposited. Just prior to thin film deposition the substrates are partially cleaned again. For spin cast films, the substrates are spun rapidly (without any solvents) to remove any possible residual dust particles lying on the surface of the substrates. The spincast organic films are then kept under a high vacuum overnight to remove residual oxygen or solvents from the organic layers. For vacuum evaporated organic films, all

crucibles/containers for thermal evaporation are annealed separately at high temperature under high vacuum to remove any volatile contaminants that may affect the organic layers. The substrates covered with the organic layers (spincast or evaporated) are kept under high vacuum for at least twelve hours immediately prior to evaporation of the metal electrodes to remove any residual oxygen or solvents from the organic layers and the glass. The devices are then stored in a sealed container located in a dry argon (or nitrogen) atmosphere until they are ready for testing.

2.2.2 *Thin Film Deposition*

Thin film layers are deposited by several techniques, namely, spin casting from solution or thermal evaporation in a vacuum of $5x10^{-7}$ mmHg at a rate of 3-5 Å/s. All substrates are kept under vacuum or stored in an inert atmosphere between deposition stages.

2.2.2.1 *Spin Casting*

The spin casting is performed in a nitrogen or argon atmosphere. Every solvent used for the spin casting solutions is of high purity — either HPLC grade or spectroscopic grade. Furthermore, water is removed from the solvents by adding at least one-third volume of molecular sieves for at least 36 hours. After the solvent is dried of water the solution is prepared using a solute concentration of about 10-30 mg/ml, depending on the solute material and desired thickness of the layer. The spinner is calibrated for thickness control by varying: the concentration of the solute

in the solution, the spin-rate of the substrate and the spin-time. Thin film thicknesses are verified with a Tencor Instruments Alpha Step 1000 stylus profilometer.

To perform spincoating, a solution with a known concentration of organic material is then prepared for spin casting to achieve the desired thickness. This solution is filtered using a 2 μm millipore filter and placed in the glove box containing the water-free and oxygen-free nitrogen atmosphere. The filtered solution is then dropped onto the ITO-covered glass substrate, entirely covering the surface. Next, the stationary substrate is immediately rotated on a spinner (which is also located inside the glove box with dry nitrogen) for 45-60 seconds at an angular frequency of 1000-4000 revolutions per minute. Additional organic layers may then be deposited onto the first layer, providing that the solvents or solutes used for the upper layers do not react with or dissolve the underlying layer. Finally, the organic-covered substrate is transported in a sealed container and stored in a glovebox containing an inert atmosphere for later processing. Any additional metallic or organic layers will be deposited later by thermal evaporation.

2.2.2.2 *Thermal Evaporation*

Thermal evaporation is carried out in a custom-made glass evaporator that is assembled under argon atmosphere. Organic or metallic layers (aluminum or calcium) are deposited in a vacuum on the order of 10^{-7} mmHg. All substrates are loaded into the evaporator while in the argon atmosphere. The substrates are transported inside the sealed glass evaporator before and after evaporation with the evaporator

containing an inert atmosphere (argon or nitogen) or a high a vacuum, respectively. After evaporation of the organic and metallic layers, the diodes are put into an air-tight container and stored in the glovebox until they are tested. For testing, the diodes are placed in a custom-made cell with electrical contacts, unloaded from the glovebox and tested under a flow of nitrogen.

2.3 Material and Device Characterization

The optical characteristics of the organic compounds are measured to determine their potential applications in light emitting devices. The absorption spectra, photoluminescence spectra, excitation spectra of photoluminescence and fluorescence lifetimes are measured according to established procedures using the equipment mentioned in earlier sections. The quantum efficiency of photoluminescence (Φ_{PL}) defined as the ratio of the number of photons absorbed to the number of photons emitted is measured relative to a known standard. The PL quantum efficiency, measured relative to a known standard, is given by:[2]

$$\Phi_{PL} = \Phi_{FR} \frac{n^2 \int_0^{\infty} F(\bar{\upsilon}) d\bar{\upsilon}}{n_R^2 \int_0^{\infty} F_R(\bar{\upsilon}) d\bar{\upsilon}} \qquad \text{Equation 2-1}$$

where ν is the wavenumber in cm^{-1}; n and n_R are the indices of refraction for the sample and the reference materials in solution, respectively; Φ_{FR} is the fluorescence

quantum yield of the reference material; and Φ and Φ_R are the corrected fluorescence spectra of the sample and the reference material, respectively.

The thin film light emitting devices are characterized according to their electroluminescence spectra, current-voltage curves, brightness-voltage curves and quantum efficiency of electroluminescence (η_{EL}). η_{EL} is defined as the total number of photons emitted from the LED divided by the total number of electrons injected into the device.[3] In this case η_{EL} is given by:

$$\eta_{EL} = \frac{q_e}{IhC} \int_{\lambda_{min}}^{\lambda_{max}} P(\lambda)\lambda d\lambda \qquad \text{Equation 2-2}$$

where q_e is the charge of an electron, I is the current through the device, h is Planck's constant, C is the speed of light, λ is the wavelength, $P(\lambda)$ is the optical power emitted at wavelength λ, λ_{min} is the minimum emitted wavelength and λ_{max} is the maximum emitted wavelength.

The brightness of the LEDs is measured in units of candelas/m^2 (cd/m^2). The measurement in candelas (lumens/Ω) accounts for the emitted power corrected for the responsivity of the human eye (lumens) and the divergence of the emitted radiation as a function of the solid angle (Ω) subtended by the radiation from the source. The units of m^{-2} accounts for the intensity of light emitted by the source. The optical correction for the human eye's sensitivity was done using a spectral filter that was placed

immediately in front of the detector. The average optical power response function of the human eye is shown in Figure 2-5.

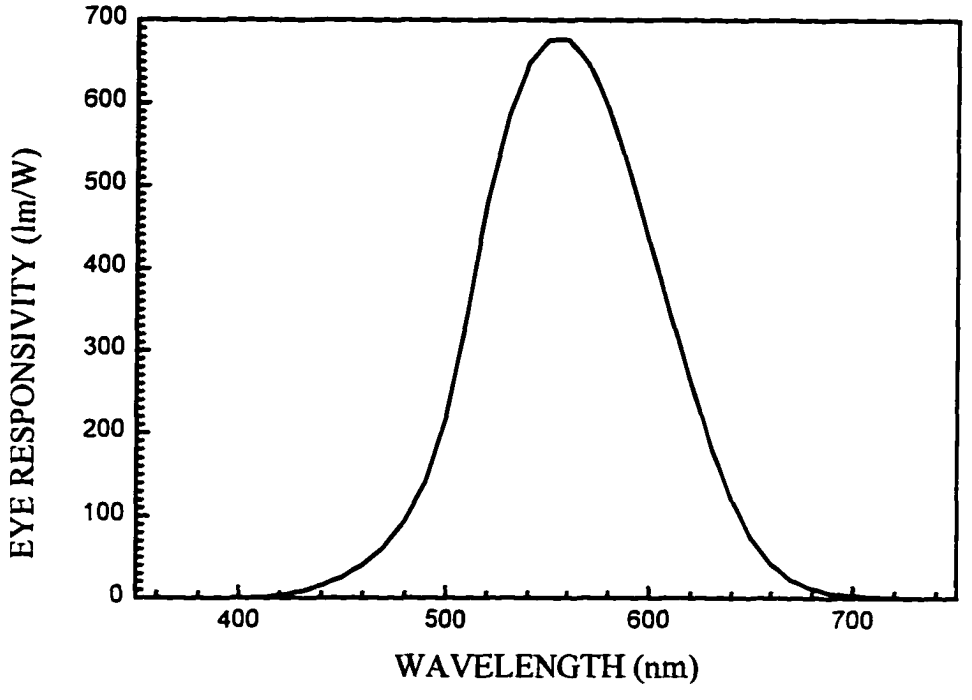

Figure 2-5. Optical Response Function of the Human Eye

To ensure that the 2 mm x 3 mm LED could be treated as a point source according to the inverse square law for optical power, the distance between the LED and the detector must be at least ten times the maximum dimension (3 mm) of the diode. In our case the LED was placed 10 cm away from the radiometer during brightness measurements. The brightness (B) in cd/m^2 was measured according to:

$$B = \frac{P_{lum}}{\Omega A}$$ Equation 2-3

where P_{lum} is the received optical power in lumens, Ω is the solid angle of the source (from source to detector) and A is the surface area of the LED.

The light emitted from an organic LED can also be characterized by several means for example, its optical spectrum. For very narrow band emission, the spectrum can be described fairly accurately by the color of the light (e.g., red, blue, yellow etc.) in terms of the central emission wavelength and spectral bandwidth. However, in many cases, the emitted spectrum may consist of a complex mixture of colors and hence may not be described accurately by central emission wavelength or perceived color alone.

Since organic LEDs may be used in display applications, it is also useful to characterize the light according to coordinates corresponding to the perception of the human eye. The perceived color is measured in terms of the chromaticity diagram which is a graphical representation of the weighted response of the three types of color receptors (cones) in the human eye.[4] The chromaticity diagram was established by the Commission Internationale de l'Eclairage (CIE) in 1931. Figure 2-6 illustrates the CIE Chromaticity diagram.

For the chromaticity diagram (Figure 2-6), two values of the CIE chromaticity coordinates (x, y) are plotted in a two dimensional graph. The third coordinate (not plotted) can be determined from the relation $x + y + z = 100$ %. The range of visible colors is enclosed by the curved and straight solid lines. Points located closer to the solid-line borders are more monochromatic in spectrum and points closer to the center

become more white in color. The value of each color can be specified quantitatively by its x, y and z (implied) coordinates. The dotted lines demarcate the major color regions that are labeled in the diagram. The triangle (dashed line) specifies the range of colors achievable with most traditional CRT displays.

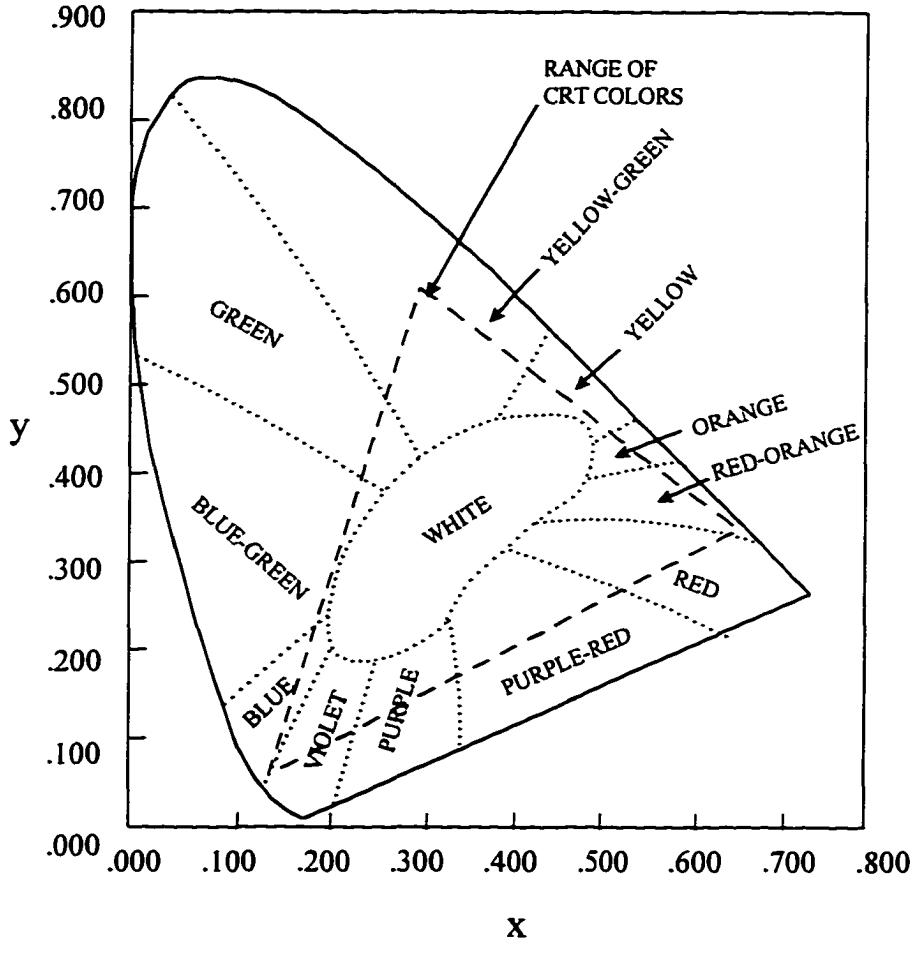

Figure 2-6. CIE Chromaticity Diagram

The coordinates of the CIE chromaticity diagram are based on the human eyes' response to three primary colors (wavelengths). These primary wavelengths, the tristimulus values (X, Y and Z) are given by:[5]

$$X = \int_{380}^{770} I(\lambda)\bar{x}(\lambda)d\lambda,$$
$$Y = \int_{380}^{770} I(\lambda)\bar{y}(\lambda)d\lambda, \qquad \text{Equation 2-4}$$
$$Z = \int_{380}^{770} I(\lambda)\bar{z}(\lambda)d\lambda,$$

where I(λ) is the intensity function of the source; 380 and 780 nm correspond to the range of visible wavelengths; and $\bar{x}(\lambda)$, $\bar{y}(\lambda)$ and $\bar{z}(\lambda)$ are the color-matching functions corresponding to the responsitivities of the human eye (over three different wavelength regions) at the wavelength λ.

The chromaticity coordinates (x, y and z) of any color can then be expressed in terms of the tristimulus values by the functions:

$$x = \frac{X}{X+Y+Z} \text{ and } y = \frac{Y}{X+Y+Z} \qquad \text{Equation 2-5}$$

where the value of z can be determined from x and y because the total percentage (x + y + z) is 100 %. The CIE chromaticity coordinates of white light are: (x = 0.333, y = 0.333). In general, the whiter or more pastel colors are located near the central portion of the CIE chromaticity diagram.

2.4 Conclusions

The procedures outlined in the previous sections describe the criteria used for evaluating the material's optical properties and the device operating characteristics. The results of these measurements will be reported in Chapters 4, 5 and 6.

REFERENCES

1. LABVIEW is a registered trademark of the National Instruments Corporation.

2. J. B. Birks, *Photophysics of Aromatic Molecules*, pp. 98, John Wiley & Sons Ltd., New York, (1969).

3. C. W. Tang, S. A. VanSlyke and C. H. Chen, *J. Appl. Phys.* **65** N0. 9, pp. 3610 - 3616, (1989).

4. G. W. Wicks, *Compound Semiconductor*, July/Aug, pp. 39 - 40, (1995).

5. R. J. Kubesh, *Am. J. Phys.*, **60**, No. 10, pp. 919 - 923, (1992).

CHAPTER THREE

3. MULTILAYER DEVICE DESIGN

Chapter 3 is concerned with the design criteria for multiple layer light emitting devices (LEDs). Organic LEDs consist of single or multiple organic layers sandwiched between metal electrodes. These light emitting devices are designed by (1) considering the energy levels in the emitting layer, (2) carefully selecting complementary materials to improve the injection of charge carriers from the electrodes, (3) using high mobility materials to transport charges away from the electrodes and into the emitting layer, (4) ensuring bipolar recombination within the emitting layers, leading to radiative decay of the excited emitters and (5) extracting the light from the emitting layer. The following sections will consider the LED materials' properties and the design techniques for optimizing the radiative output of these multilayer optoelectronic devices

3.1 Energy Levels in Solid State Materials

Electroluminescent devices may contain single layer or multiple layer cell structures. The single layer device consists of a single organic layer sandwiched between an anode and a cathode. In this case the organic layer serves as the emitting layer for the device and should therefore have a relatively high photoluminescence quantum efficiency (Φ_{PL}). This emissive layer must also have good bipolar charge

transport properties which are necessary for the transport of holes (injected from the anode) and electrons (injected from the cathode) through the organic layer. These holes and electrons, driven into the emitting layer by the applied electric field, will later recombine on the emitter molecules to form singlet and triplet excitons or polaron-excitons. The radiative decay of the singlet excitons or polaron-excitons is largely responsible for the electroluminescent radiation from most materials. Consequently, the mobility of charge carriers, the energy bands located within each layer, the probability of electrons and holes recombining to decay radiatively and the placement of each layer within the device structure are important for optimizing device performance.

The energy levels and carrier mobilities in solid state materials determine their charge injection and charge transport characteristics. In organic electroluminescent devices, the electroluminescent radiation originates from the radiative recombination of the excess charges injected from the electrodes into the organic layer. Therefore, the injection characteristics of the metal-insulator interface should be properly understood. For the purposes of this discussion the metal-insulator interface will be defined as an electrical contact.

The electrical contacts' main purpose is to enable or block carrier injection into the organic layer by providing a low- or high-energy barrier to charge carriers leaving the metal, respectively. The electrons in a metal may be free to move within the bulk of the metal, but the electrons must surmount a potential energy barrier

before they can be injected into a vacuum or any organic material adjoining the metal. This potential barrier, the work function of the metal (ϕ_m), is the difference between the highest energy level of the electrons in the metal (the Fermi level) and the lowest energy level of an electron in a vacuum (vacuum level). See Figure 3-1 for the energy levels of a metal in a vacuum. The work function corresponds to the amount of work needed to liberate the electron from the metal. Therefore, ϕ_m corresponds to the cohesive energy of the metal. In other words, metals with higher work functions will have higher cohesive energies.

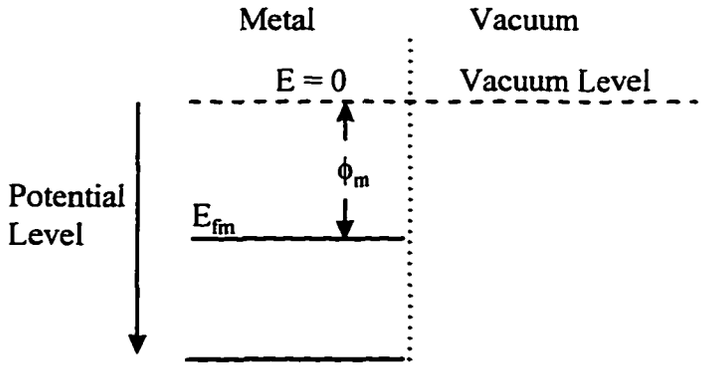

Figure 3-1. Energy Levels in Metals

In dielectrics, the electrons may move within the lowest unoccupied molecular orbital (LUMO). See Figure 3-2 for the energy levels in dielectrics. Analogously, holes may travel in the highest occupied molecular orbital (HOMO). The energy gap (E_g), defined as the energy difference between the LUMO and the HOMO levels, corresponds to the energy of radiative transitions within the materials because radiative decay usually occurs from the lowest excited singlet state to the ground states. Therefore, E_g determines the energy level of excitons in the material and hence

the wavelength of light emitted from the material. In some cases the radiative decay may originate from impurity or exciton levels located within the band gap and may introduce a relative red-shift of the electroluminescence spectrum. The electron affinity (χ) is the difference in energy between the vacuum level and the LUMO. Materials with high electron affinities will easily form negative ions because these materials will readily accept electrons due to the relatively small energy barrier seen by electrons entering the materials through their lower-lying LUMO. The ionization potential (I_p), the energy difference between the HOMO and the vacuum level, measures how readily the dielectric molecules will form positive ions (See Figure 3-2). Materials with low ionization potentials will form positive ions easily and materials with high ionization potentials do not readily form positive ions. To form holes within organic materials, a low ionization potential is a highly desirable property. When designing electroluminescent devices, the electronic properties of the adjoining layers must also be considered in detail.

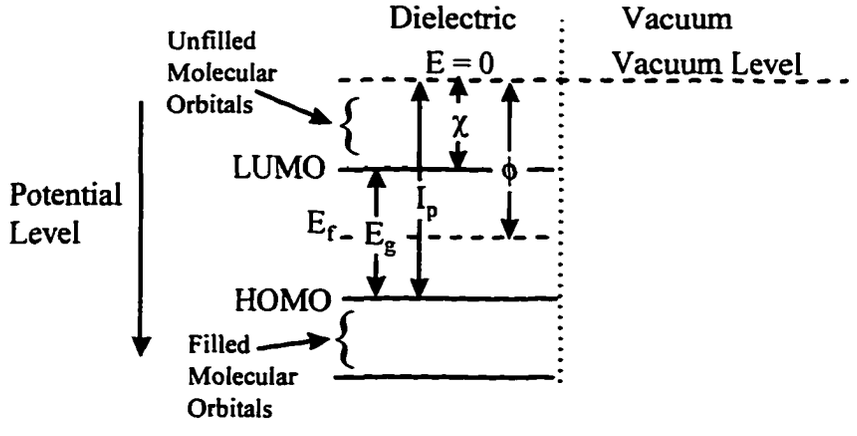

Figure 3-2. Energy Levels in Dielectrics

3.1.1 Device Layers

Thin film organic electroluminescent diodes usually consist of multiple organic and metallic layers deposited on an ITO-covered glass square. These layers may be deposited by various methods such as plasma deposition, thermal evaporation, langmuir-blodget deposition or spin casting from solution. In our case, only thermal evaporation and spin casting techniques were used to deposit the organic layers.

The physical and chemical properties of each layer are important for optimizing device performance. To provide reliable device operation, each layer must be thermally stable to withstand the intense heat caused by the high current densities produced in the device layers. Vacuum deposited layers must be homogeneous optical quality thin films. Spin coated layers must also be homogeneous and optical quality. Also, any solvents used while spin casting must not react with, dissolve or quench the luminescence from the underlying layers. All deposited materials should be free of dissolved solvent molecules, impurities, surface contaminants and pin-holes, and should also have a uniform thickness. In addition, all layers should be chemically stable, especially under ambient and device operating conditions, and be resistant to oxidation or photooxidation. The materials used in the device layers should not form excimers during photoexcitation ⊗ unless excimer emission is desirable for device operation. Furthermore, adjoining layers should not react chemically at their interfaces, neither form exciplexes (during photoexcitation) nor charge transfer complexes (during electronic excitation). In most cases, the formation of exciplexes

or charge transfer complexes within the emission layer are undesirable for good device performance.

In addition, the optical properties of each layer should be considered when designing the device structure. For higher efficiency light output, the device layers should be highly transparent to the emitted radiation. The thickness of each layer must be adjusted to ensure bipolar charge recombination within the emitting layer. Finally, the total layer thickness and the reflectivity of each interface must be adjusted to minimize (for wide-band emission) or enhance (for narrow-band emission) microcavity interference effects which become more pronounced as the device thickness approaches the wavelength of visible light.

Except for the anode and cathode, electroluminescent devices may contain single layer or multiple layer structures. The single layer device consists of a single organic layer sandwiched between the anode and cathode. In this case the organic layer serves as the emitting the layer for the device and should therefore have a relatively high photoluminescence quantum efficiency (Φ_{PL}). This emissive layer must also have good bipolar charge transport properties which is necessary for the transport of holes (injected from the anode) and electrons (injected from the cathode) through the organic layer. These holes and electrons, driven into the emitting layer by the applied electric field, will later recombine on the emitter molecules to form singlet and triplet excitons or polaron-excitons; the radiative decay of singlet excited states is largely responsible for electroluminescent radiation. Consequently, the mobility of

charge carriers within the emitting layer is important for device performance. The energy level diagram for a single layer device (i.e., a dielectric layer sandwiched between two electrodes) is shown in Figure 3-3.

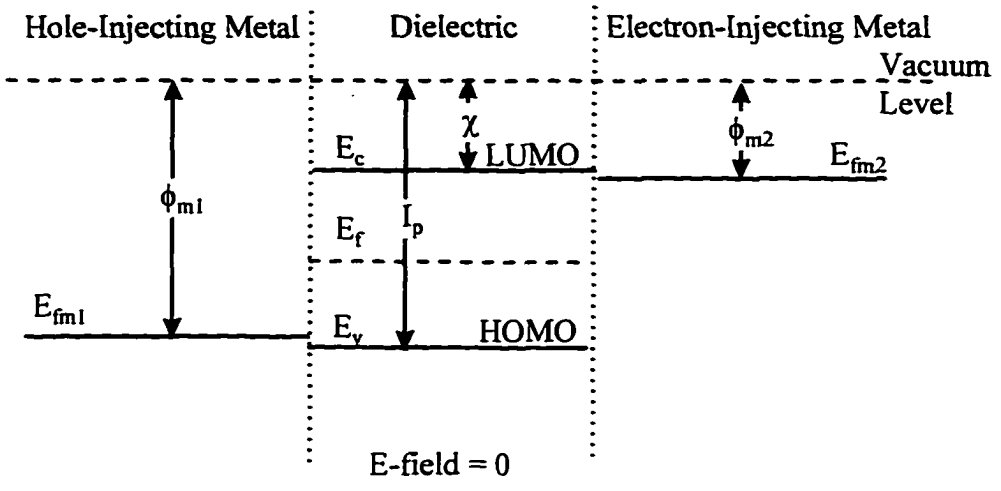

Figure 3-3. Energy Level Diagram for a Dielectric Layer Between Metal Electrodes

The organic LED functions through the bipolar injection of charge carriers into the organic layer. These carriers are injected under the influence of an applied electric field when the LED is forward biased. To forward bias the LED, the anode, usually high work function materials such as indium tin oxide (ITO) or polyanile (PANI), is connected to a positive potential. In our case low work function metals such as calcium (Ca) or aluminum (Al) were used as the negatively biased electrode (cathode). Whenever calcium was used as the electrode, an outer layer of aluminum was added to retard oxidation of the underlying calcium layer. In the forward bias condition, the carriers are driven through the device layers by the applied electric field (See Figure 3-4). Electron transport will occur through the lowest unoccupied

molecular orbital (LUMO) which is analogous to the conduction band (E_c) in semiconductors. Holes are transported through the highest occupied molecular orbital (HOMO) which corresponds to the valence band (E_v) in semiconductors. The efficiency of electron and hole transport is determined by the mobilities of both of the charge carriers in the organic layer.

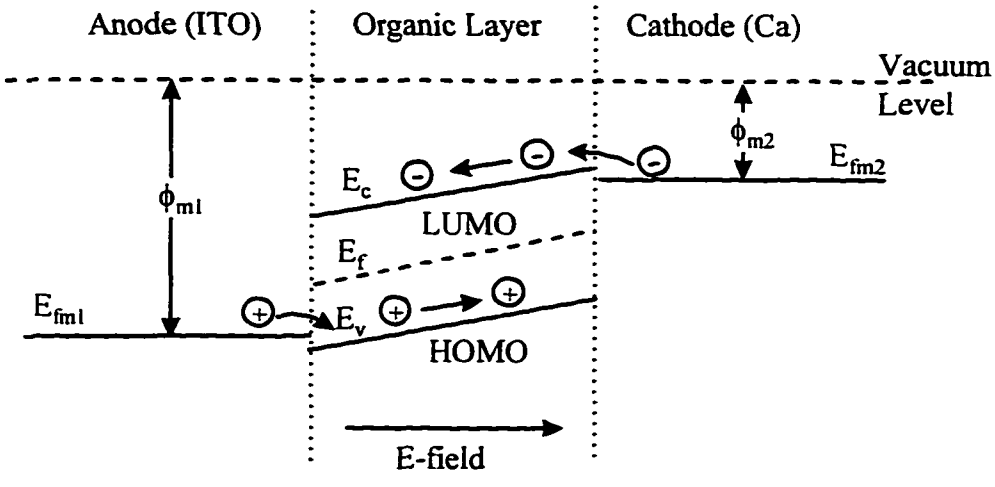

Figure 3-4. Energy Level Diagram for a Forward-Biased Single-Layer Device

Some of the most highly fluorescent materials do not have high carrier mobility and low carrier mobilities may impede device performance. Since light output from the emitting layer of the diode originates from the radiative decay of singlet excitons produced by the recombination of electrons and holes injected from the other layers, the electron and hole mobilities should be considered when designing OLEDs. In the ideal case, the emitting layer should have bipolar transport properties and a small barrier to the injection of electrons and holes.

To improve the efficiency of bipolar injection and carrier recombination within the luminescent layer, the energy levels and transport properties of each layer must be considered when designing EL devices. For good performance of the EL devices, the anode and cathode must be carefully selected to improve the injection of holes and electrons into the internal organic layer(s), respectively. Instead of using single layer structures, additional layers can be added to the organic electroluminescent (EL) device to improve charge transport and injection. In a multilayer device the layers may consist of the: anode, hole transport layer (HTL), emission layer (EML), electron transport layer (ETL) and cathode. See Figure 3-5 for the structure of a three layer light emitting device with electrodes, HTL, EML and ETL.

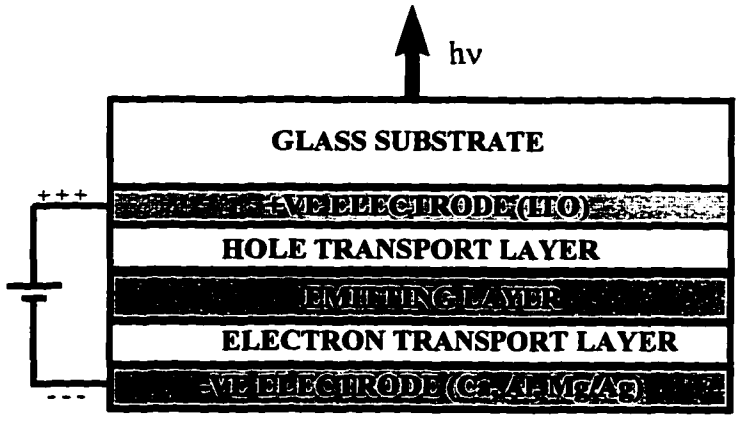

Figure 3-5. Structure of a Three Layer LED

Each of these layers in the multilayer LED helps to enhance electroluminescence. The specific role of each layer will be outlined in the immediately following sections.

3.1.2 *Anode*

The positively biased electrode (anode) serves as a source of holes for the emitting layer of the device. To enhance hole injection from the anode, the anode the material should have a high work function to lower the energy barrier for hole injection. The anode molecules should not diffuse into the adjoining organic layer. Polyaniline (PANI) and indium-tin-oxide (ITO) are common anode materials. In our case ITO was used as the anode for hole injection and as the transparent electrode that allows the emitted light to exit the electroluminescent cell.

3.1.3 *Hole Transport Layer*

The hole transport layer (HTL) mainly transports holes within the HOMO level and to a lesser degree, may transport electrons within the LUMO level. Therefore, the HTL material should have a high hole mobility. HTL materials should also have a low ionization potential for the efficient injection of holes from the anode. After bipolar charge recombination, the hole transport layer should help block the migration of excitons from the emitting layer. Therefore, the HTL should have a higher exciton energy level than the emission layer (EML) to help confine excitons within the EML. Finally, the HTL should be transparent to the radiation emitted from the EL cell to reduce the optical losses within the device.

Many organic materials have hole transport properties. Poly(n-vinylcarbazole) (PVK) and N,N'-diphenyl-N,N'-bis(3-methylphenyl)-[1,1'-biphenyl]-4,4'-diamine (TPD) are commonly used hole transport materials.[1] PVK and TPD have relatively

high hole mobilities of $\approx 10^{-6}$ $cm^2/(Vs)$ and $\approx 10^{-3}$ $cm^2/(Vs)$, respectively. Figure 3-6 shows the structures of PVK and TPD.

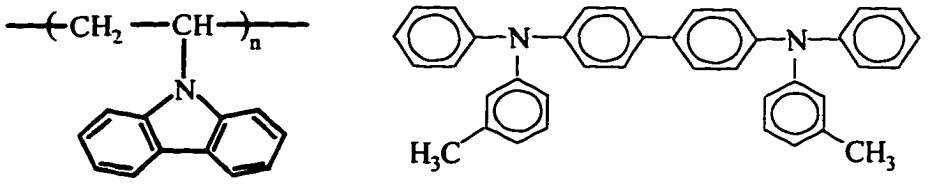

PVK TPD

Figure 3-6. Common Hole Transport Materials

3.1.4 *Emission Layer*

To produce electroluminescent radiation, electrons are injected from the electron transport layer and holes are injected from the hole transport layer into the emission layer. After bipolar charge injection and transport, holes and electrons may recombine to produce singlet excitons which may decay radiatively within the luminescent layer. Therefore, the emission layer must also function as the charge recombination layer. As such, emitting layers must also have a high quantum yield of photoluminescence and electroluminescence. To enhance the probability of recombination, the EML should have a low density of impurity quenching sites that may serve as traps for charge carriers. Trapping processes generally lead to nonradiative decay. However, the energy levels of the emitting layer should function as recombination centers that is, confine charge carriers which will recombine and form singlet excitons that will eventually decay radiatively.

After recombination but prior to deactivation, the singlet excitons formed within the EML may diffuse toward either electrode. To prevent the loss of excitons

due to diffusion to quenching sites within the transport layers or at the polymer/electrode interface, the excitons must be confined within the emissive layer to produce light. To ensure exciton confinement within the EML, the exciton energy levels of both layers (HTL and ETL) adjoining the charge recombination layer should be higher than the exciton energy level of the recombination layer. These energy barriers will prevent the quenching of EL due to the diffusion of excitons into the adjoining transport layers. If there are no HTL or ETL layers between the EML and either electrode, or the adjoining layers do not effectively confine the excitons, the thickness of the EML should be adjusted to account for the diffusion of the excitons away from the recombination zone. To reduce optical losses, the emitting layer should have a low extinction coefficient for the range of emitted wavelengths.

Nonradiative losses should also be minimized by controlling layer thickness and molecular content. For example, any dopants located within the emitting layer should not quench electroluminescence through the transfer of excitons to non-radiative sites located within the organic materials. Furthermore, no excimers should exist within the layer and no exciplexes should be formed at the interfaces between layers. In most cases, excimer or exciplex formation may lead to luminescence quenching or change the nature of the luminescence significantly. On the other hand, there are some exceptions for example, PVK, where exciplex formation and radiative deactivation is responsible, and hence desirable, for electroluminescence.[2]

In some cases the luminescent layer may also have electron or hole transport properties and consequently a separate hole transport or electron transport layer may not be necessary for good device performance. For example, if an EML layer shows good electron transport properties, then electron injection and transport can occur via the EML and only a separate HTL becomes necessary for hole injection into the EML. In this case a two layer device with Anode/HTL/EML/Cathode structure is sufficient. Conversely, an EML layer with hole transport properties might only require a separate ETL for electron injection. Consequently, the Anode/EML/ETL/Cathode cell structure can be used. Otherwise, bipolar charge transport and luminescence may occur in the same layer as in the case of a single layer cell structure: Anode/EML/cathode. The chemical structures of several materials used as the emitting layers of organic LEDs are shown in Chapter 1.

3.1.5 *Electron Transport Layer*

The electron transport layer (ETL) primarily transports electrons and may, to a lesser degree, transport holes. As such, the electron transporting material should have a high electron mobility to facilitate the transport of electrons from the cathode through the ETL to the EML. The ETL also facilitates electron injection from the cathode into the emission layer. Consequently, ETL materials should have a large electron affinity to decrease the energy barrier seen by the electrons exiting the cathode. The ETL compounds should also have an exciton energy level that is higher than the exciton energy level of the EML to prevent the diffusion of excitons from the

EML to the ETL. Finally, to reduce absorption losses, the ETL material should also be transparent to the radiation of the EML.

Several organics have been used as electron transport layers. The oxadiazoles such as 2-(4-biphenyl)-5-(4-tert-butylphenyl)-1,3,4-oxadiazole (butyl-PBD) have been used as electron transport layers because their electron mobilities are $\approx 10^{-6}$ $cm^2/(Vs)$[3]. Tris(8-hydroxyquinoline)-aluminum (ALQ_3), a widely studied luminophor, is also commonly used as an electron transporting agent. The chemical structures of ALQ_3 and butyl-PBD are shown in Figure 3-7.

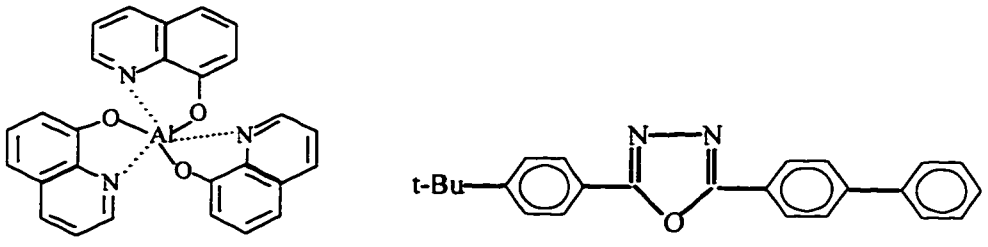

ALQ_3 butyl-PBD

Figure 3-7. Chemical Structures of Common Electron Transport Materials

3.1.6 *Cathode*

The cathode serves as the electron injecting contact. The cathode material should have a low work function to facilitate electron injection into the electron transport layer. In addition, the cathode material should not react with the underlying layer to form any exciplexes which could affect device performance. Also, the cathode molecules should not diffuse into the underlying layers. In most cases, the cathode materials are deposited last and may be directly exposed to the ambient environment.

Therefore, the cathode should be air stable (i.e., oxygen stable and water stable). In some cases, as in calcium, metals with very low work functions are highly reactive or easily oxidized and must be protected by an outer metallic layer such as aluminum. Otherwise, the entire device must be encapsulated for reliable performance in ambient conditions. In some cases, alloys such as Mg:Ag or Mg:In are also used as cathodes.

3.1.7 *Novel Electrode Structures and Device Junctions*

In some cases, graded layers instead of undoped layers have been used to improve carrier injection at the electrode/organic interface and to improve bipolar carrier injection into the emissive layer. Heeger and coworkers have employed two approaches to increase carrier injection. The first approach for improving injection at the anode/HTL uses a protonated form of polyaniline (PANI), a porous organic polymer with a correspondingly high surface area due to the roughness of its surface, and a layer of poly(2-methoxy-5-(2'-ethyl-hexyloxy)-1,4-phenylene vinylene) (MEH-PPV) which has emissive and hole transporting properties.[4] The PANI layer was protonated with camphor-sulfonic acid (CSA) which caused the PANI layer to become porous with a high degree of roughness. The MEH-PPV layer was then deposited on top of the PANI-CSA layer leading to a mixture of MEH-PPV within the porous PANI network. The interpenetration of the MEH-PPV polymer units within the PANI network increased the effective surface area of the injecting contact and produced localized regions of intense electric fields which helped to improve injection. The light emitting devices with the ITO/PANI-CSA/MEH-PPV/Ca/Al:Li

structure showed lower operating voltages than devices with the ITO anode alone or the ITO/PANI bilayer anode.

The second approach adopted by Heeger and coworkers involves the development of a pn junction due to the motion of carriers in a light-emitting electrochemical cell (LEC).[5] The LEC contains an emitting layer of MEH-PPV mixed with an electrolyte. The MEH-PPV layer was located between two electrodes. When a voltage was applied across the electrodes, localized p-type and n-type regions (near opposite electrodes) develop within the emissive layer of the LEC. The mobile carriers then meet in an electrochemically-induced p-n junction to produce light. These devices showed symmetric IV characteristics when forward or reversed biased. Also, the color of light emitted did not depend on the polarity of the voltage and could be tailored by adjusting the bandgap of the emitting polymer. These electrochemical cells also showed significantly lower operating voltages. The next section discusses the current dependent behavior of organic LEDs.

3.2 Carrier Injection and Charge Transport in Organics

Several theories have been proposed to explain the electrical transport phenomena in solids. The band model and hopping model have been suggested to explain the conduction mechanisms occurring in inorganics and organics, respectively. Recently several authors have suggested the tunnelling model and space charge limited models to explain the processes governing electric currents in organics. The following sections will discuss the band model in passing, and, the hopping,

tunnelling and space-charge limited models in more detail. Although several of these processes may occur simultaneously, the dominant current-limiting processes will determine the overall conduction characteristics in the organic layers. The following sections will discuss these current-limiting processes in organic semiconductors.

The effective electric current in organics or semiconductors may be due to drift of carriers under the influence of an electric field or may be caused by motion due to variations in the spatial distribution of charges. For low electric fields (E), the hole current (J_P) and electron current (J_N) are given by:[6]

$$J_P = J_{Pdrift} + J_{pdiffusion} = q\mu_p pE - qD_p(dp/dx) \qquad \text{Equation 3-1}$$

$$J_N = J_{Ndrift} + J_{Ndiffusion} = q\mu_n nE + qD_N(dn/dx) \qquad \text{Equation 3-2}$$

where the drift current terms vary with the electric field (for low electric fields) and the diffusion current terms vary with the spatial gradients of the charge distributions (n and p). D_p and D_N are the diffusion constants for holes and electrons, respectively; q is the electron charge; and m_p and m_n are the mobilities of holes and electrons, respectively. The total current through the device is the sum of the hole and electron currents:

$$J = J_P + J_N \qquad \text{Equation 3-3}$$

3.2.1 *Band Model Transport*

The traditional band model assumes that an electron with a given kinetic energy, under the influence of the periodic potential of the crystal lattice, can only exist in certain energy levels (bands).[7] Those electrons not involved in covalent bonding are free to move within the conduction band, thereby contributing to the electrical current in the semiconductor. Analogously, holes may move throughout the valence band of the semiconductor to generate an electrical current. The band model has been successively used to determine the carrier mobility of inorganic semiconductors such as silicon and germanium. Although band theory can explain the anisotropy of conductivity and mobility, and the temperature dependence of mobility, this model does not fully consider the electron-lattice interaction. To date, several research groups have demonstrated evidence of strong electron-phonon interactions in many organic compounds such as the polyacetylenes and poly(phenylene-vinylenes).

The electronic structure of organic materials determine their charge transport properties. In conjugated organic systems the π-electrons may be delocalized over the backbone of an individual molecule but the poor overlap of wavefunctions between molecules limits the mobility, from molecule to molecule, of excess injected carriers. The band theory inherently assumes carrier mobilities much larger than those intrinsic to organic semiconductors and hence the band model may be limited in describing carrier transport in organic systems. Modified band theories have been proposed for

organics but the limitations of these theories have led to the consideration of other mechanisms such as the hopping conduction.

3.2.2 *Hopping Conduction*

Hopping conduction may occur by several methods. A hole (M^+) may be generated on a molecule by the liberation of an outer electron from an initially neutral molecule (M). This hole may then jump to another neutral molecule, under the influence of an electric field, by accepting an electron from that other molecule (Figure 3-8). Similarly, an excess electron may become trapped on an initially nuetral molecule to produce a negatively charged molecule (M^-). This trapped electron may then jump from molecule to molecule under the influence of an electric field (Figure 3-8).

Figure 3-8. Electron and Hole Hopping

Electrons or holes may hop from one molecule to another. Before hopping is initiated, the electron must surmount an energy barrier before it can jump to an acceptor molecule. The hopping process can be initiated either thermally or through interactions with the lattice. In the latter case, there must be a strong electron-phonon coupling with the lattice. In organic systems this electron-lattice coupling is usually

appreciable enough to affect hopping charge transport processes. See Figure 3-7 for an illustration of hopping conduction over a square potential barrier.

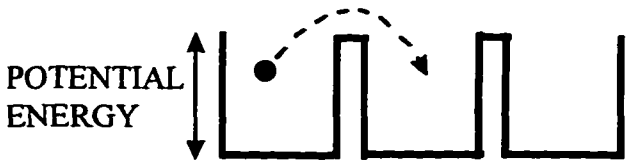

Figure 3-9. Hopping Over a Potential Barrier

The theoretical calculations and experimental observations of Bassler and coworkers have shown that in hopping conduction, the carrier-mobility obeys the electric field-dependent relationship:[8]

$$\mu(E) = \mu_0 e^{E/E_0} \qquad \text{Equation 3-4}$$

where E is the electric field and μ_0 is the mobility of charges when E=0. In this case the electrical current in the device, which varies linearly with the carrier mobility, can be derived from Maxwell's equations:[9]

$$I = q\mu_p pAE + q\mu_n nAE \qquad \text{Equation 3-5}$$

where E is the electric field, A is the cross sectional area of the diode, μ_p is the hole mobility, μ_n is the electron mobility, p is the hole density and n is the electron density.

The transport mechanisms that govern the motion of charge carriers in insulators may be limited by injection processes occurring at the contacts or the bulk properties of the organic material. If an electrical contact can serve as a reservoir for

excess carriers for the organic layer with relatively low carrier mobility, then the excess injected carriers may set up a localized space charge within the organic. The space charge phenomenon can only be observed if at least one of the electrical contacts is ohmic.

3.2.3 *Conduction Limited by Tunnelling Processes*

Tunnelling theory can reliability predict the injection and transport of charge carriers in some organic compounds when the limiting process is due to carrier injection at the electrodes. Otherwise, the bulk properties of the organic layer(s) determine their electrical characteristics. The tunnelling model assumes that an excited electron on a molecule may either return to the ground state or tunnel through a potential barrier to excite a neighboring molecule. The energy-receiving molecule must have a vacant energy level capable of accepting the electron. Figure 3-9 illustrates an electron tunnelling through a square potential barrier. In general, energy is conserved during the tunnelling process but in organics the probability of returning to the ground state is much higher than the tunnelling probability. The tunnelling probability also increases with the increasing electric field. Due to band-bending effects the effective potential energy barrier becomes triangular under the influence of the applied electric field and electrons see a lower effective energy barrier as their energy increases. In the case of the triangular barrier, tunnelling theory can, in some instances, provide a good estimate of the electric current.

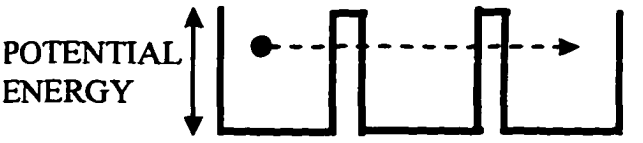

Figure 3-10. Tunneling Through a Square Potential Barrier

Fowler and Nordheim showed that under the influence of intense electric fields, the electrons may tunnel through the barriers at the electrode-organic interface. Tunnelling through the interface barrier becomes appreciable at electric fields on the order of 10^6-10^7 volts/cm. The tunnelling current of an organic layer sandwiched between metal electrodes is given by.[10]

$$I = k E^2 e^{-a/E} \qquad \text{Equation 3-6}$$

where E is the electric field; k is a constant depending on the carrier mobility and the work function of the metal; and "a" is a constant determined by the work function of the metal. Later, Heeger et. al. and Parker fabricated electroluminescent devices and based on the Fowler-Nordheim theory, they have proposed that tunnelling processes govern the charge transport in PPV derivatives.[11,12] The conditions for a good empirical fit for the tunnelling model usually apply at very high electric fields. However, the results of the tunnelling model for carrier conduction in PPV has been contested by other researchers. One alternate model, space charge limited conduction, will be discussed in the next section.

3.2.4 Space-Charge Limited Conduction

The current conduction in organic LEDs may be limited by the bulk properties of the organic layer and may not be necessarily limited by the contacts. Under thermal equilibrium conditions both positive and negative charge carriers may be thermally excited inside the organic layer but the average current across the electrode/organic interface is zero. The space charge conduction process occurs when excess charges are injected into an insulator with low carrier mobility. When these excess carriers are injected though the electrodes into the insulating organic layer the injected carriers produce a localized electric field near the electrode/organic interface. This internal field then limits the flow of additional electrons and hence determines the current-dependent properties of the organic layer. Space charge limited effects are observed when the electrode contacts are ohmic.

Space charge currents can exist when the injected free carrier density n exceeds the thermal equilibrium carrier density n_0. The space charge current is observed at a threshold voltage:[13]

$$V_t \approx n_0 q_e d^2/2\varepsilon \qquad \text{Equation 3-7}$$

where q_e is the elementary (electron or hole) charge, d is the thickness of the organic layer and ε is the permitivity of the organic material. At voltages below V_t the current follows Ohm's law:[10]

$I_\omega = q_e \mu n_0 AV/d$ Equation 3-8

where μ is the mobility of the charge carrier. For voltages above V_t, the current obeys Child's law for solids:[10]

$I_c = (9/8)\mu\varepsilon AV^2/d^3$ Equation 3-9

In the case of insulators with traps, the current-dependent behavior will depend on the energy levels and energy distributions of the trap levels within the band gap. If the traps have an exponential energy distribution then the density of traps per unit energy is:

$h(E) = (H/kT_c)\exp(-E/KT_c)$ Equation 3-10

where E is the energy measured from the top of the valence band, H is the total trap density and T_c is the characteristic temperature of the distribution greater than the measuring temperature. In this case the current-voltage relationship is:[10]

$$i_t = N_0 \mu A q_e e_0^{l-1} \left(\frac{\varepsilon l}{H(l+1)}\right)^l \left(\frac{2l+1}{l+1}\right)^{l+1} \left(\frac{V^{l+1}}{d^{2l+1}}\right)$$ Equation 3-11

where l is equal to T_c/T and N_o ($\approx 2.4 \times 10^{25}$ m^{-3}) is the effective density of states in the valence band at room temperature. The exponent (l+1) of the voltage (V) is always greater than 1. The exponent varies from 1 at low voltages to 8or 9 at high voltages. In general the current $I_t < I_c$ provided that $n < n_t$.

As the current increases the trap states become filled and the carriers begin to populate the conducting levels. When n increases above n_t, the current becomes governed by Child's law (Equation 3-7) and the conduction models the behavior of an insulator without traps. The transition from to the trap-limited conduction to trap-filled conduction occurs at a voltage:[10]

$$V_{t-c} \approx \frac{q_e d^2}{\varepsilon}\left[\frac{9}{8}\frac{H^l}{N_0}\left(\frac{l+1}{l}\right)^l\left(\frac{l+1}{2l+1}\right)^{l+1}\right]^{1/(l-1)} \qquad \text{Equation 3-12}$$

This voltage dependence has been observed in a wide range of organic materials including metal-organic complexes and organic polymers. This model has been used to describe the current dependent behavior of devices over a wide range of electric fields.

3.2.5 *Energy Transfer Processes*

In addition to bipolar conduction and recombination mechanisms, an excited molecule within the emitting layer may be produced by the energy transferred from an initially excited molecule to a previously unexcited molecule. In this case the energy of the excited molecules may be transferred to other molecules of the same species or molecules of a different species. The energy transfer process may be radiative — originating from the radiative decay of an excited donor molecule followed by the absorption of energy by a receptor molecule. In this case, the donor's

emission band must overlap with the acceptor's absorption band for efficient energy transfer to occur.

The energy transfer process may also involve nonradiative energy transfer due to dipole-dipole interactions between two spatially separated molecules with (1) energy transfer occurring between molecules with similar energy levels, or (2) energy transfer originating from a donor molecule with a given energy level to an acceptor molecule with lower energy. This process occurs during the excitation lifetime of the donor molecule before the emission of a photon. As in radiative energy transfer, the donor's emission spectrum should overlap the acceptors absorption band. For coulombic (dipole-dipole) interaction to occur, the molecules must be separated by intermolecular distances ~ 20-60 . Electron exchange interactions may also occur between molecules separated over distances of ~ 6-15 . In other cases, nonradiative energy transfer may occur by collisional processes. These collisional processes may yield excimers or exciplexes (as intermediate states) which then dissociate as a mechanism for energy transfer. The collisional interactions usually occur in fluid solutions and probably do not play a significant role in electroluminescent devices.

3.2.6 *Recombination of Charge Carriers*

The organic LEDs are designed so that the charge carriers will recombine in the emitting layer. The carriers injected from the electrodes or adjoining layers will be transported away from the electrodes into the recombination zone of the emitting layer. For small organic molecules, for example ALQ_3, the charge carriers are

primarily electrons or holes.[14] In the case of organic polymers such as poly(p-phenylenevinylene) PPV and its derivatives or poly(paraphenylene) (PPP) the charge carriers are positive or negative polarons due to the coupling of the charge carriers to the lattice.[15]

Since the electroluminescence originates from the radiative decay of excited molecules produced by recombination processes, the excited states of organic emitters should be clearly understood. For small organic molecules such as ALQ_3, the molecular excitation is confined within the vicinity of one molecule.[16] As such the excited states are usually Frenkel excitons which can diffuse away from the recombination zone. For large organic molecules such as conjugated polymers, the electrons may be delocalized along the polymer backbone. Consequently, the excited states may be polaron-excitons due to the coupling of the charge carriers to the lattice.[17] The subsequent motion of the excitation may be governed by the motion of neutral polaron-like states across the lattice. The eventual radiative decay of these singlet excited states, whether excitons or polaron-excitons, are largely responsible for electroluminescence in organic materials.

REFERENCES

1. D. M. Pai, Y. F. Yanus and M. Stolka, *J. Phys. Chem.*, **88** pp. 4714 - 4717, (1984).

2. M. Pope and C. E. Swenberg, *Electronic Processes in Organic Crystals*, Oxford University Press, New York, pp. 704 - 706, (1982).

3. H. Tokuhisa, M. Era, T. Tsutsui and S. Saito, *Appl. Phys. Lett.*, **66,** No. 25, pp. 3433 - 3435, (1995).

4. Y. Yang, E. Westerweele, C. Zhang, P. Smith and A. J. Heeger, *J. Appl. Phys.*, **77**, pp. 694 - 698, (1995).

5. Q. Pei, G. Yu, C. Zhang, Y. Yang, and A. J. Heeger, *Science*, **269** pp. 1086 - 1088, (1995).

6. G. W. Neudeck, *The PN Junction Diode*, Modular Series on Solid State Devices (2^{ND} Ed.), Addison-Wesley, New York, pp. 47, (1989).

7. E. S. Yang, *Fundamentals of Semiconductor Devices*, McGraw-Hill, New York, pp. 5 - 9, (1978).

8. H. Bassler, G. Schonherr, M. Abkowitz and D. M. Pai, *Phys. Rev. B,* **26** pp. 3105 - 3106 (1982).

REFERENCES (Continued)

9. G. W. Neudeck, G. W. Neudeck and R. F. Pierret Eds., *The PN Junction Diode*, Modular Series on Solid State Devices, Vol. II, 2nd Ed., Addison-Wesley, New York, pp. 56, (1989).

10. R. H. Fowler and L. Nordheim, *Proc. R. Soc. (London)*, Ser. A, **119** pp. 173 - 181, (1928).

11. A. J. Heeger, I. D. Parker and Y. Yang, *Synthetic Metals*, **67** pp. 23 - 29, (1994).

12. I. D. Parker, *J. Appl. Phys.*, **75** No. 3, pp. 1656 - 1666, (1994).

13. P. Mark and W. Helfrich, *J. of Appl. Phys.*, **33** No. 1, pp. 205 - 215, (1962).

14. C. W. Tang and S. A. Van Slyke, *Appl. Phys. Lett.*, **51** No.12, pp. 913 - 915, (1987).

15. M. Onoda, S. Morita, H. Nakayama and K. Yoshino, *Jpn. J. Appl. Phys.*, **32**, Part 2, No. 1A/B, pp. L82 - L85, (1993).

16. Z. Shen, P. E. Burrows, V. Bulovic, D. M. McCarty, M. E. Thompson and S. R. Forrest, *Jpn. J. Appl. Phys.*, **35**, Part 2, No. 3B, pp. L401 - L404, (1996).

17. D. Braun and A. J. Heeger, *Thin Solid Films*, **216** pp. 96 - 98, (1992).

CHAPTER FOUR

4. CHARACTERIZATION OF ALQ_3 DEVICES

This chapter considers the physical, optical and electroluminescent properties of tris(8-hydroxyquinoline)-aluminum (ALQ_3), a green emitting metal-organic complex. We will be studying ALQ_3 because this material is chemically stable, shows good electroluminescent properties and is a widely used emitting material in organic light emitting diodes. As such, ALQ_3 can serve as a reference standard for comparison with the novel emitting materials to be studied and reported in Chapters 5 and 6.

4.1 Electroluminescence in Metal-Hydroxyquinoline Chelates

Several hydroxyquinoline-derivative metal complexes have already been used to fabricate organic light emitting diodes (LEDs).[1,2] The Be, Mg, Zn, Al, Ga, In and Sc metals have all been chelated to various hydroxyquinoline-type ligands. In particular, both two- and three-ligand complexes have been synthesized from 8-hydroxyquinoline, 2-methyl-8-hydroxyquinoline and 7-n-propyl-8-hydroxyquinoline derivatives. See Figure 4-1 for the chemical structures of these 8-hydroxyquinoline ligands. The luminescence in these metal complexes occur in the green or yellow region of the visible spectrum and these emission spectra are broad, which is characteristic of most organic systems. For all cases involving the class of previously

mentioned metal-hydroxyquinoline chelates, the photoluminescence peaks lie between 500 and 580 nm and are correlated with the emission spectra of the corresponding ligands.

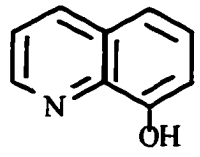

8-Hydroxyquinoline

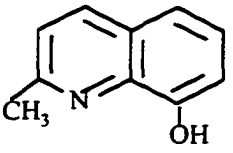

2-Methyl-8-Hydroxyquinoline

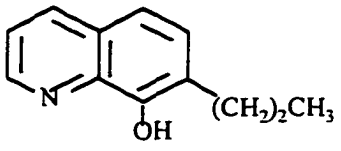

7-n-Propyl-8-Hydroxyquinoline

Figure 4-1. 8-Hydroxyquinoline Derivatives

Tris-(8-hydroxyquinoline)-aluminum (ALQ_3), the most widely used emitting material for organic LEDs, is an aluminum chelate whose luminescent properties have been studied since the 1950's.[3,4] The chemical structure of ALQ_3 is shown in Figure 4-2. The chemical and physical properties of ALQ_3 have also been studied in later years.[5-7] This metal complex is chemically stable and shows good fluorescent properties in solution and in the solid state. Several researchers have developed light emitting devices based on ALQ_3 and achieved brightness output values well in excess of 1000 cd/m^2.[8,9] The following paragraphs will discuss the chemical, physical and luminescent properties of ALQ_3 and the electroluminescent measurements obtained for ALQ_3-based light emitting devices.

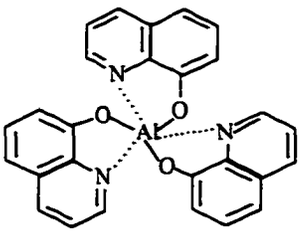

Figure 4-2. Chemical Structure of ALQ_3

4.2 Chemical and Physical Properties of ALQ_3

Since Tang and Van Slyke first fabricated ALQ_3 electroluminescent (EL) devices, several research groups have developed thin film organic EL devices based on ALQ_3 because it has desirable chemical and physical properties. ALQ_3 shows good film-forming properties, and evaporated thin film layers tend to form uniform layers with a microcrystalline structure. This material has a hole mobility of $\approx 10^{-7}$ cm^2/Vs but preferentially transports electrons with a mobility of $\approx 10^{-5}$ cm^2/Vs.[10] Though holes have a limited diffusion length of a few hundred angstroms, the electrons are the majority carriers in ALQ_3 LEDs.[11]

The energy transfer processes determine the nature of the emission spectra of the aluminum chelate compounds. In the aluminum-quinolate systems, the optical excitation energy is initially absorbed by the ligand because the Al ion has very weak absorption bands in the UV. The majority of photoluminescence (PL) lines from the Al atom occur in the UV region of the spectrum.[12] These PL lines originate from excited state levels (e.g., a_1 and a_2 in Figure 4-3) located at or above 3.3 eV.[13] Therefore, energy transfer from the ligand's excited states to the Al energy levels

above 3.3 eV is energetically prohibited. Additionally, energy transfer from the ligands to the remaining Al ion resonance levels (located below 3.3 eV) is spin-forbidden. As a result, the hydroxyquinoline ligands determine the energy transfer processes occurring in ALQ_3. Since the Al atom does not contribute directly to the luminescent properties of ALQ_3, it serves to bond the ligands together in a chemically stable configuration.

The photoluminescence in ALQ_3 originates from the radiative decay of the ligand's excited states (See figure 4-3). Therefore, the electronic levels of the 8-hydroxyquinoline ligands determine the optical properties of ALQ_3.[14] The highest occupied molecular orbital (HOMO) level and the lowest unoccupied molecular orbital (LUMO) level are located at 6.65 eV and approximately 3.8 eV, respectively. ALQ_3 has a corresponding bandgap of about 2.7-2.9 eV but the luminescence originates from the deactivation of shallow trap levels, located within the bandgap, 2.3 eV above the HOMO level.[15] Consequently, there is a red-shift between the wavelength corresponding to the optical badgap (428-460 nm) and the emitted optical spectrum (peak wavelength at 517-519 nm).

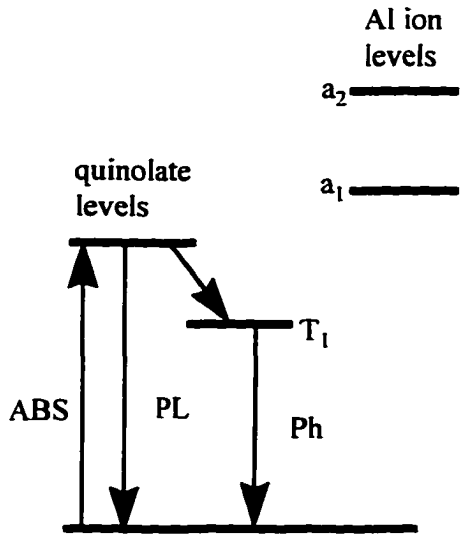

Figure 4-3. Energy Transfer in Al-Quinolate Systems

This aluminum chelate also shows excellent long term chemical stability under ambient conditions. However, the chemical stability of the aluminum chelate films during device operation is also important for LED performance. Recently, ALQ_3 thin films have been shown to photooxidize in the presence of oxygen and water.[16] In fact, under intense UV photoexcitation, the chemical by-products of photooxidation are responsible for the quenching of (1) the singlet excited states in ALQ_3 and (2) the photoconductive response of ALQ_3.[17] During device operation the organic compounds used for LEDs may suffer premature degradation due to residual oxygen within the layer. Therefore, the chemicals used in light emitting devices need to be purified of oxygen, water and other quenching agents to improve long term device stability. Also, LEDs should be encapsulated to prevent degradation from atmospheric quenchers such as oxygen. Studies have shown that the device operating lifetimes can be increased by over two orders of magnitude by using encapsulation procedures.[18]

The organic thin films in devices should also show good thermal stability because localized heating may occur at high operating current densities. ALQ_3 films show a temperature-dependent behavior of the luminescence. In fact, the photoluminescence of thin films and the electroluminescence of thin film devices show a decline of luminescence intensity with increasing temperature.[19] Although the operating lifetimes of the best ALQ_3-based devices have exceeded 100,000 hours, the device heating must be reduced to improve long term LED performance. Heating effects may be minimized by driving the LEDs with low duty cycle pulsed currents instead of DC currents.

The organic layers used in LEDs should also show good physical stability. ALQ_3 films deposited on glass substrates remain exceptionally stable (even after a few years) in ambient conditions. ALQ_3 films also show good stability at elevated temperatures of up to 80^0 C.[18] However, the interface between the Al chelate and adjoining layers are not always stable over long periods. N,N'-diphenyl-N,N'-bis(3-methylphenyl)-[1,1'-biphenyl]-4,4'-diamine. (TPD), a common used hole transporting agent crystallizes under ambient conditions. Burrows and coworkers observe that when ALQ_3 and TPD are deposited as an ALQ_3/TPD bilayer, there –is a profound change in the surface topology due to crystallization of ALQ_3 layer ---- the TPD begins to protrude through the ALQ_3 layer. This morphological change occurs faster with time and increasing temperature. There is also deterioration of the interfacial region between the hole-conducting diamine and the aluminum chelate. This deterioration was caused by interdiffusion of ALQ_3 and TPD. This interfacial

region had a yellowish-green luminescence that appeared through the surface of the bilayer films. Neither crystallized TPD nor ALQ_3 films showed the appearance of this new emission band, thereby confirming that there is a chemical change at the interface.

Morphological changes in the organic/electrode interfacial layer have also been shown to affect the outer electrodes, for example, by forming domes in the aluminum cathodes of ITO/TPD/ALQ_3/Al devices. These domes are created by the evolution of gases formed from chemical reactions at the metal interface. These dome-like formations led to the appearance of dark spots on the surface of the operating LEDs. As time progressed, these dark spots increased in size and caused the premature failure of LEDs. In the case of organic polymer/Al interfaces, the electron-induced diffusion of aluminum into the polymer layer has led to the formation of dark non-emissive spots which then led to premature device failure. ITO electrodes have also been shown to form regions of volcanic-like craters by the degradation of the indium tin-oxide. This degradation is strongly dependent on the electric field strength and independent of joule heating, conjugation structure of the polymer deposited on the ITO, and the light emission process.

4.3 Photoluminescence of ALQ_3 in Solution

The photoluminescence in organic materials such as ALQ_3 usually originates from the radiative decay of the lowest excited singlet state. When excited at 330 nm, this aluminum chelate emits in the green region of the spectrum with a peak

wavelength of about 501 nm in dilute chloroform solution ($5x10^{-6}$ M concentration). Based on studies of metal-(8-hydroxyquinoline) systems, the photoluminescence of ALQ_3 originates from the electronic transitions which are localized on the quinolate ligands. The absorption and luminescence spectra of ALQ_3 in dilute chloroform is shown in Figure 4-4. The corresponding photoluminescence quantum efficiency is fairly constant when exciting above 280 nm and has been estimated to be 32 % in solution.[1] The absorption band of ALQ_3 is located below 450 nm with the strongest absorption peak at 389 nm along with smaller peaks located at 318 nm and 334 nm. There is also a very strong absorption band located below 380 nm however, the PL emission from the 500 nm emission band solution was less efficient when photoexciting ALQ_3 at these shorter wavelengths (below 300 nm). The lineshape of the PLE spectrum (for emission at 520 nm) spectrum closely resembles the absorption lineshape between 270 nm and 450 nm, indicating that the same absorbing states are responsible for luminescence. There is a small (6 nm) red-shift of the PLE spectrum compared to the absorption spectrum.

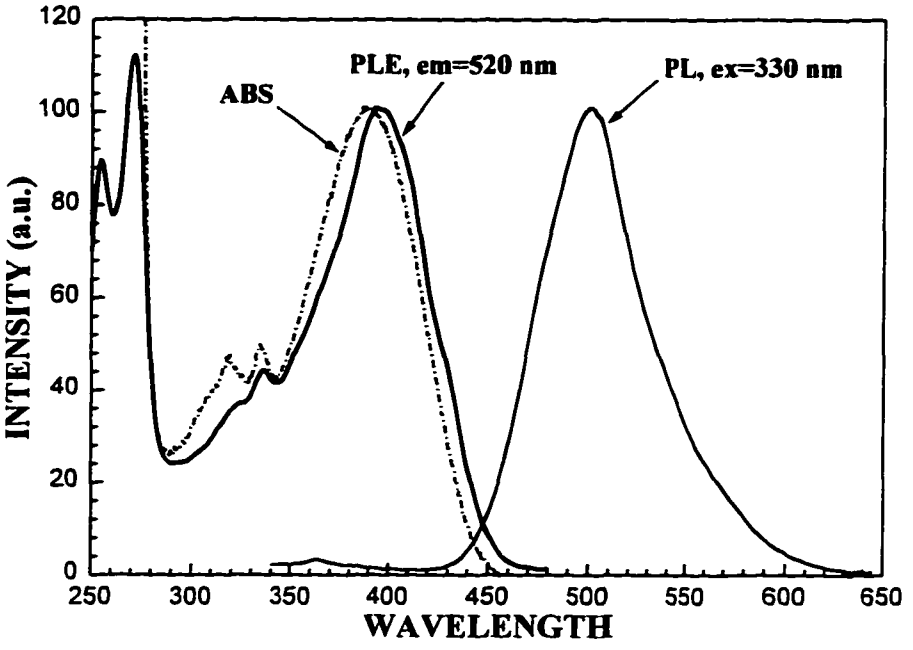

Figure 4-4. Absorption and Luminescence of ALQ_3 in Chloroform ($5x10^{-6}$ M)

4.4 Photoluminescence of ALQ_3 in the Solid State

In the solid state, ALQ_3 shows bright green photoluminescence, with a maximum at 502 nm when excited at 355 nm that corresponds to the PL spectrum in chloroform solution (See Figures 4-4 and 4-5). Other researchers have observed emission peaks at different wavelengths (519 nm) and attributed the emission to deactivation of trap states located within the band gap. I have found a correspondence between the PL (solution and solid state) and EL spectra, suggesting that in my samples the trap levels are shallower than those observed by Burrows et. al. Also, since the PL spectrum in solution matches the solid state PL spectrum and the EL spectrum I cannot attribute this effect to structural disorder of the thin films as does

Burrows and coworkers. The PL quantum efficiency has been reported to be 8 % in the solid state.[6] For ALQ_3, the absorption and PLE spectra extend from 450 nm through the UV region (See Figure 4-4). The absorption band at 389 nm was slightly red-shifted compared to the solution spectra, and the PLE maximum (for emission at 500 nm) was located at 394 nm.

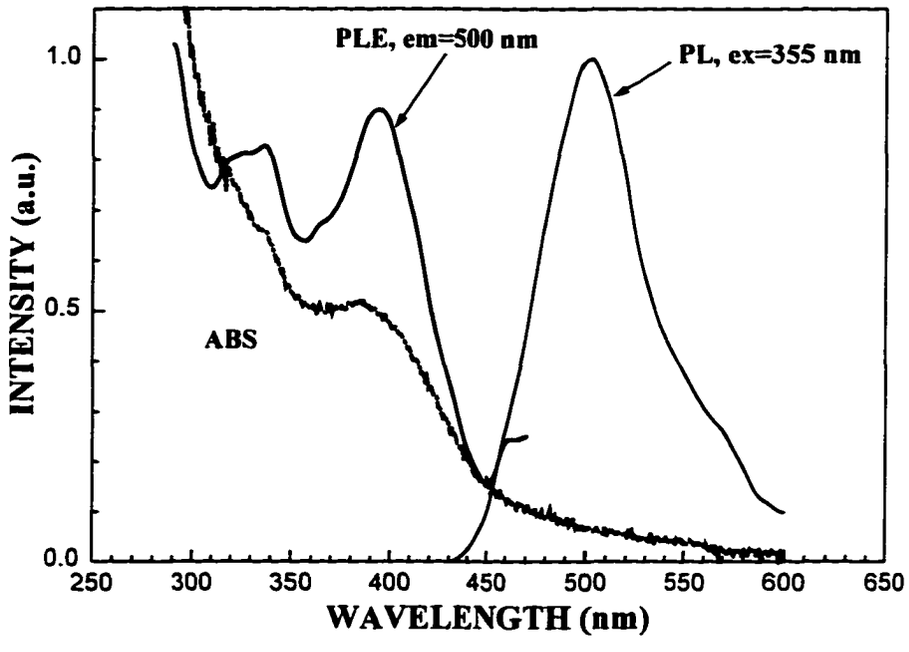

Figure 4-5. Absorption and Luminescence Spectra of ALQ_3 Thin Film

4.5 Electroluminescence of ALQ_3

To test the cleanliness of the substrates, operation of the vacuum system, spin coating procedures, structures of the diode layers, film thickness, and the overall device fabrication and optical measurement procedures, two-layer electroluminescent

devices were fabricated using the aluminum-oxinate, ALQ_3, as the emitting layer. The initial test samples were fabricated with the following structure: ITO/TPD(400 Å)/ALQ_3 (600 Å)/Ca/Al. TPD is the hole transporting diamine derivative, commonly used in LEDs. The TPD and ALQ_3 layers were both deposited by vacuum evaporation at a rate of 3-5 Å/s under a vacuum of $5x10^{-7}$ mmHg. The thickness of the TPD and ALQ_3 layers were 500 Å and 600 Å, respectively. The metallic layers were deposited by thermal evaporation under a vacuum of $5x10^{-6}$ mmHg. The combined thickness of the Ca and Al layers was over 4000 Å.

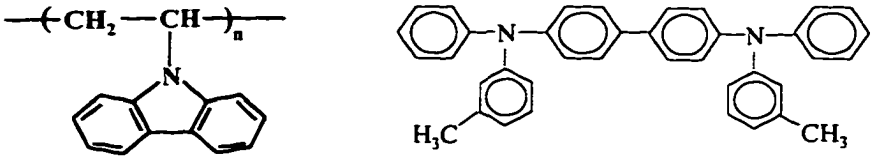

PVK TPD

Figure 4-6. Chemical Structures of PVK and TPD

Green electroluminescence was observed from ALQ_3 when the LEDs were forward biased. To forward bias these LEDs, the ITO and Ca electrodes were connected to the positive and negative terminals of the current supply, respectively. The green electroluminescence corresponded to emission from the ALQ_3 layer, indicating that holes are transported through the TPD layer and bipolar charge recombination occurs in the ALQ_3 layer. These devices tended to fail prematurely at high voltages due to crystallization of the TPD layer. Consequently, subsequent devices were fabricated with poly(n,vinylcarbazole) (PVK) as the hole transporting

material to improve the operating lifetime and overall reliability of the devices (See Figure 4-6).

The layers for the ALQ_3 devices were selected to optimize the injection and transport of carriers. The energy level diagram of an ITO/PVK/ALQ_3/Ca device is shown in Figure 4-7. For electron injection, the barrier at the Ca/ALQ_3 interface was low (approximately 0.1 eV). Therefore, it should be relatively easy to inject electrons from Ca into ALQ_3. However, the barrier for hole injection was much higher (approximately 0.9 eV). To compensate for this relatively large energy barrier, the PVK layer was kept very thin to ensure transport of the holes that were injected into the PVK layer. The thickness of the PVK layer was approximately 250 - 300 . Once inside the PVK layer the holes will see a barrier of only 0.1 eV at the PVK/ALQ_3 interface. Therefore, it should be relatively easy to inject holes from PVK into ALQ_3. On the other hand, the electrons traveling through the ALQ_3 layer will see a 0.7 eV barrier for injection from ALQ_3 into the PVK layer. Since the holes experience a small barrier for injection from PVK into ALQ_3 and electrons will more likely be confined to ALQ_3, the recombination occurs in the ALQ_3 layer. Also, since holes have a limited difffusion length inside ALQ_3, recombination should occur very near to the PVK/ALQ_3 interface. Using this energy level design, two layer LEDs were fabricated.

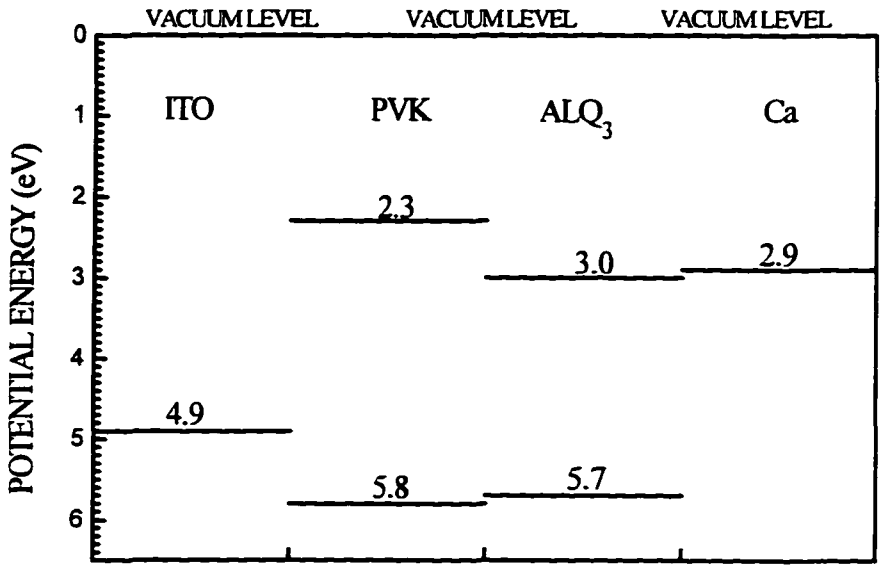

Figure 4-7. Energy Level Diagram of an ITO/PVK/ALQ_3/Ca Device

The organic layers for the new devices were deposited according to established procedures. The PVK layer was spin coated from a chloroform solution onto the ITO-coated glass surface and the aluminum oxinate layer was deposited by thermal evaporation (under a vacuum of 4 x 10^{-7} mmHg at a rate of 3-5 Å /s.) The thickness of the PVK layer was approximately 250-300 Å and the thickness of the ALQ_3 layer was 300-700 Å. When the diodes were forward biased, green electroluminescence was observed from the ALQ_3 layer — indicating that electron-hole recombination occurs in the ALQ_3 layer. The EL spectra of the devices corresponded to the PL of the thin films and the maximum EL emission was located

at 503 nm. The electroluminescence spectrum and the cell structure of the ALQ_3-based diodes is shown in Figure 4-8.

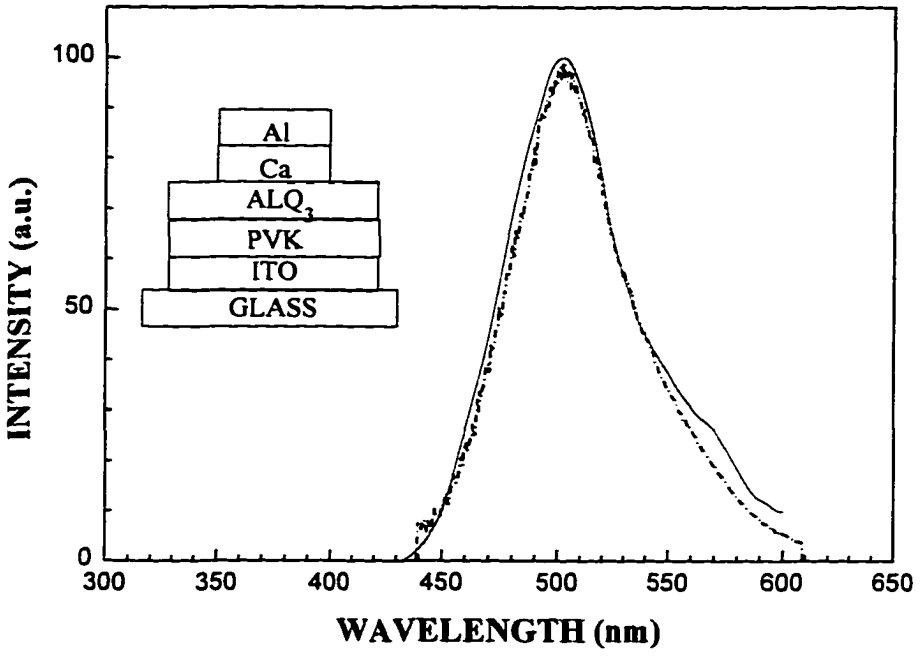

Figure 4-8. PL of ALQ_3 Films (solid line) and EL (dashed line) of ALQ_3 Devices

The devices containing PVK for HTL operated longer than the devices with TPD as HTL because of the better thermal stability of PVK. The voltage-dependent curves and brightness curves are shown in Figure 4-9. The turn-on voltage for these devices was approximately 11 volts and the maximum brightness was on the order of 80-120 cd/m^2 when the ALQ_3 layer thickness was 600-700 Å (See Figure 4-9). These

devices showed good operational stability and could be operated for several days at low driving voltages.

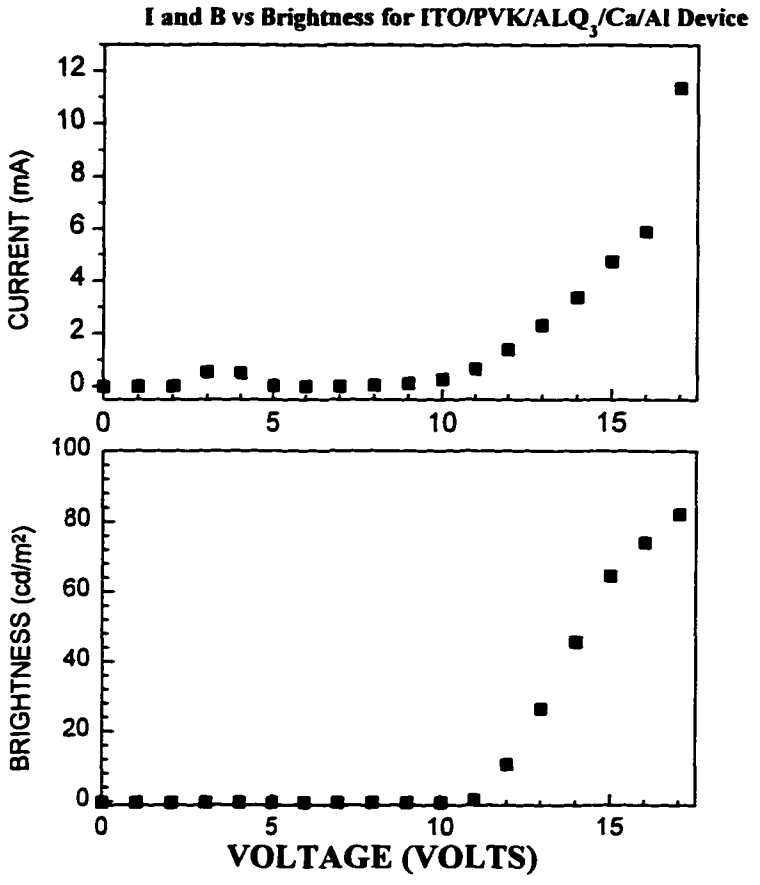

Figure 4-9. I and B vs. V Curves for an ITO/PVK/ALQ_3/Ca/Al LED

The devices' brightness depended on the thickness of the emitting layer. After decreasing the ALQ_3 layer thickness to 350 Å, the brightness of these layers increased to 1030 cd/m^2 (See Figure 4-10). No microcavity effects were observed from the EL spectra of the ALQ_3 devices, probably due to the low reflectivity of the ITO electrode.

These devices showed stable operation but tended to fail at voltages above 20 V DC. The mechanism of failure is probably due to crystallization caused by heating of the organic layers or the electrode-organic interface. To reduce the heating effects I checked device operation while using a pulsed current source. The maximum brightness increased to 4200 cd/m^2 when using a pulsed current source (10 % duty cycle) to drive the LEDs. This suggests that a maximum brightness of 42,000 cd/m^2 or more should be achievable with a DC driving voltage however localized heating effects may play a major role in limiting the brightness and operational stability of the devices.

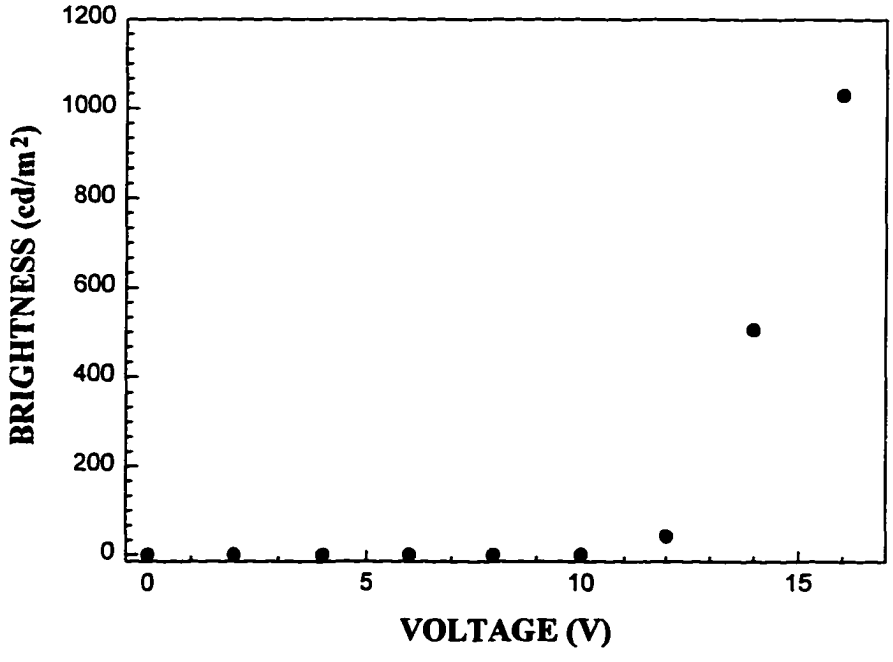

Figure 4-10. Brightness Curves for a Two-Layer ALQ_3 LED

The device operation was checked by measuring the quantum efficiency of electroluminescence (η_{EL}). Figure 4-11 displays the results of η_{EL} measurements for an ALQ_3 LED. Although the maximum brightness was obtained at about 16 volts, the maximum value of $\eta_{EL} \approx 0.2$ % was obtained at a driving voltage of 15 volts. Therefore, the conditions for maximum brightness also corresponds to the conditions for maximum radiative recombination.

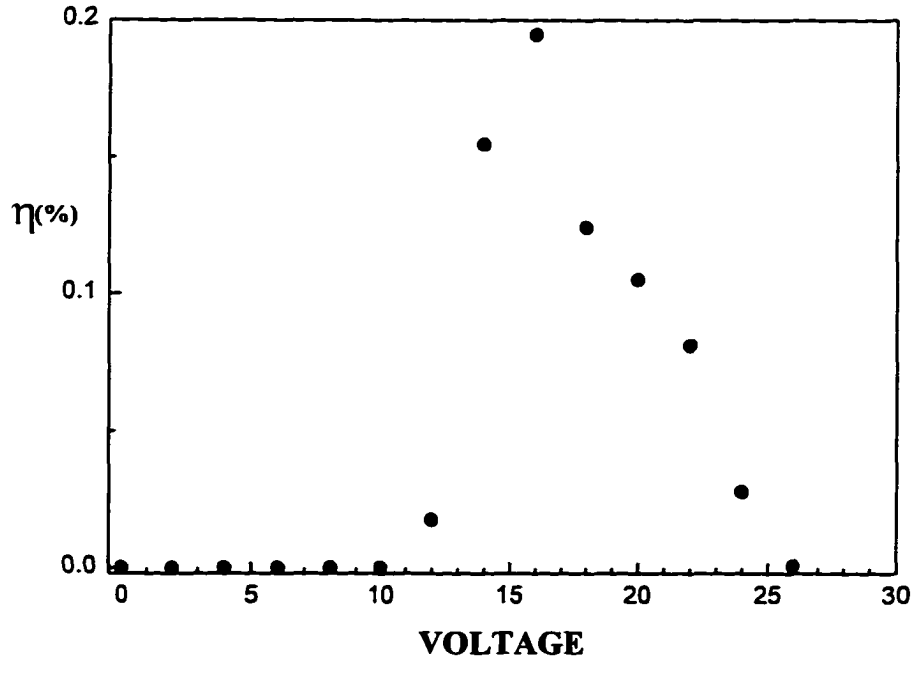

Figure 4-11. EL Quantum Efficiency of an ALQ_3 LED

The transport properties of ALQ_3 are determined by the charge carriers' mobilities and the influence of impurity levels within the films. Based on the studies of Burrows et. al., the current in this aluminum complex is controlled by the trap-limited transport of electrons (the majority carriers) through the layer.[10.13] In addition,

the electroluminescence is determined by the efficiency of holes (the minority carrier) injected from the hole transport layer into the ALQ_3 layer.

4.6 Conclusions

Light emitting diodes have been fabricated from ALQ_3. These devices show high brightness values of approximately 1000 cd/m^2 under DC currents and up to 4,400 cd/m^2 under pulsed driving currents. Without heating effects, these brightness values may be as high as 44,000 cd/m^2 or more. These devices show EL intensity that is limited by the injection of minority carriers (holes). However, device brightness may be significantly improved by the selection of higher work function anodes compared to ITO. Consequently, the corresponding efficiency values may also be improved with the selection of alternate anodes. The EL emission corresponds to the PL emission in solution and the solid state. The luminescence in ALQ_3 originates from the radiative deactivation of trap states located within the bandgap.

REFERENCES

1. Y. Hamada, T. Sano, M. Fujita, T. Fujii, Y. Nishio and K. Shibata, *Jpn. J. Appl. Phys.*, **32** pp. L514 - L515, (1993).

2. P. E. Burrows, L. S. Sapochak, D. M. McCarty, S. R. Forrest and M. E. Thompson, *Appl. Phys. Lett.*, **64** No. 20, pp. 2718 - 2720, (1994).

3. W. E. Ohnsorge and L. B. Rogers, *Spectrochimica Acta*, pp. 27 - 40, (1959).

4. W. E. Ohnsorge and L. B. Rogers, *Spectrochimica Acta*, pp. 41 - 48, (1959).

5. B. C. Baker and D. T. Sawyer, *Analytical Chem.*, **40** No. 13, pp. 1945 - 1951, (1968).

6. H. F. Steger and A. Corsini, *J. Inorg. Nucl. Chem.*, **35** pp. 1621- 1636, (1973).

7. H. F. Steger and A. Corsini, *J. Inorg. Nucl. Chem.*, **35** pp. 1637 - 1643, (1973).

8. C. W. Tang, S. A. VanSlyke and C. H. Chen, *J. Appl. Phys.*, **65** No. 9, pp. 3610 - 3616, (1989).

9. N. Takada, T. Tsutsui and S. Saito, *Jpn. J. Appl. Phys.* **33**, pp. 863 (1994).

10. P. E. Burrows, Z. Shen, V. Bulovic, D. M. McCarty and S. R. Forrest, *J. Appl. Phys.*, **79** No. 10, pp. 7991 - 7995 (1996).

REFERENCES (Continued)

11. C. W. Tang and S. A. Van Slyke, *Appl. Phys. Lett.*, **51** No. 12, pp. 913 - 915, (1987).

12. G. Herzberg, *Atomic Spectra and Atomic Structure*, Prentice-Hall, New York, pp. 198 (1937).

13. W. F. Meggers, C. H. Corliss and B. F. Scribner, *Tables of Spectral-Line Intensities Part I*, National Bureau of Standards Monograph 32-Part I, pp. 3, (1961).

14. K. Sugiyama, D. Yoshimura, E. Ito, T. Miyazaki, Y. Ouchi and K. Seki, *Mol. Cryst. Liq. Cryst.*, To be published.

15. P. E. Burrows and S. F. Forrest, *Appl. Phys. Lett.*, **64** No. 17, pp. 2285 -2287, (1994).

16. I. Sokolik, A. D. Walser, R. Priestley, R. Dorsinville and C. W. Tang, *Materials Research Society Symposium Proceedings*, **413** pp. 65, (1996).

17. R. Priestley, I. Sokolik, A. D. Walser, C. W. Tang and R. Dorsinville, *Synthetic Metals*, **84** Nos. 1-3, pp. 915 - 916, (1997).

18. P. E. Burrows, V. Bulovic, S. R. Forrest, L. S. Sapochak, D. M. McCarty and M. E. Thompson, *Appl. Phys. Lett.*, **65** No. 23, pp. 2922 - 2924, (1994).

REFERENCES (Continued)

19. Y. Abe, K Onisawa, S. Aratani and M. Hanazono, *J. Electrochem. Soc.*, **139**, No. 3, pp. 641 - 642 (1992).

CHAPTER FIVE

5. CHARACTERIZATION OF NARROW LINEWIDTH DEVICES

Chapter 5 discusses the synthesis and optical characterization of new thermally stable lanthanide-(benzoylbenzoate) complexes that emit visible light with narrow spectral lines. This chapter also covers the characterization of single and multiple layer light emitting diodes fabricated from these novel metal-organic complexes.

5.1 Introduction

Recently, there has been a significant interest in organic-lanthanide ion complexes for the development of electroluminescent devices.[1-6] These lanthanide (La) complexes have luminescence spectra that are characterized by the absorption (ABS) of energy by the ligand and emission that originates from the La ion, exhibiting sharp, well defined spectral lines.[7,8] In some cases, such as europium tris(thenoyltrifluoroacetonate), $Eu(TTFA)_3$, the photoluminescence (PL) quantum efficiency in solution may be as high as 56 %.[9] When the 2-benzoylbenzoate derivatives are used as ligands, these complexes possess better thermal and oxidative stability compared to other La complexes such as the dibenzoylmethines and thenoyltrifluoroacetonates.[10] In this chapter the synthesis and optical characterization of new terbium- and europium-(benzoyl)benzoate complexes are reported. In

addition, single- and multi-layer light emitting diodes (LEDs) based on these complexes are fabricated and their electroluminescence (EL) is characterized.

5.2 Energy Transfer in Lanthanide Chelates

The lanthanide elements of the periodic table consist of the first fourteen transition elements following lanthanum {i.e., from cerium (Z=58) through lutetium (Z=71)}. These elements are all metals and can be classified as having their last electron in the f orbital. The lanthanides europium (Z=63) and terbium (Z=65) have the electronic configurations of $[Xe]6S^2 4f^7$ and $[Xe]6S^2 4f^9$, respectively where [Xe] is the electronic core of xenon (Xe).[11] The lanthanides normally form the +3 oxidation state with the Eu^{3+} and Tb^{3+} ions having the $[Xe]4f^6$ and $[Xe]4f^8$ outer electronic configurations, respectively. Since the 4f orbitals are shielded by the filled 5S and 5P orbitals, the f-f transitions are usually protected from environmental factors. As a result, the PL spectra of a wide range of lanthanide chelates are fairly independent of the ligands.

The absorption and luminescence spectra of the lanthanide ions depend on the electronic transitions between the La ion's energy levels. For absorption, these transitions occur between the ground state and the ion's upper resonance levels. The absorption bands corresponding to the f-f transitions of the Eu^{3+} ions are located at 376 and 394.1 nm and the corresponding peaks for Tb^{3+} are located at 284, 350, 368 and 487 nm.[10] The Tb and Eu atoms are difficult to photoexcite because of their extremely weak and narrow absorption bands. These absorption bands are normally

very weak because the f-f transitions are spin-forbidden. The corresponding extinction coefficients (ε) are on the order of 10 $cm^{-1}|M^{-1}$ or less. For better absorption properties and subsequent energy transfer to the metal atoms, these lanthanides are usually used in chelated systems.

For the lanthanide complexes, energy transfer to the La ions occurs via the ligand. The ligands in the lanthanide chelates have strong absorption bands which allow for the initial excitation to the S_1 excited state of the ligand. This excitation process is usually followed by intersystem crossing (under the influence of the heavy metal atoms) to the triplet states (T_2 or T_1) of the ligand. Energy transfer from the triplet state of the ligand to the upper resonance levels of the metal ion may then occur by dipole-dipole interactions. The efficiency of energy transfer will of course be determined by the degree of matching between the ligand's triplet level and the lanthanide ion's emitting level – generally $^5D_0$ or $^5D_1$ for Eu and $^5D_4$ for Tb. The $^5D_0$, $^5D_1$ and $^5D_4$ energy levels will be described in the next paragraph. In some cases, higher energy levels may be excited by the ligand but nonradiative relaxations occur from these higher energy levels until the energy has decayed to the emitting levels where visible radiation originates. To improve energy transfer to the lanthanide ions, the triplet states of the ligand must be closely matched to or slightly above the metal ion's emitting resonance levels. Figure 5-1 shows the excitation and energy transfer mechanisms for the lanthanide chelates.

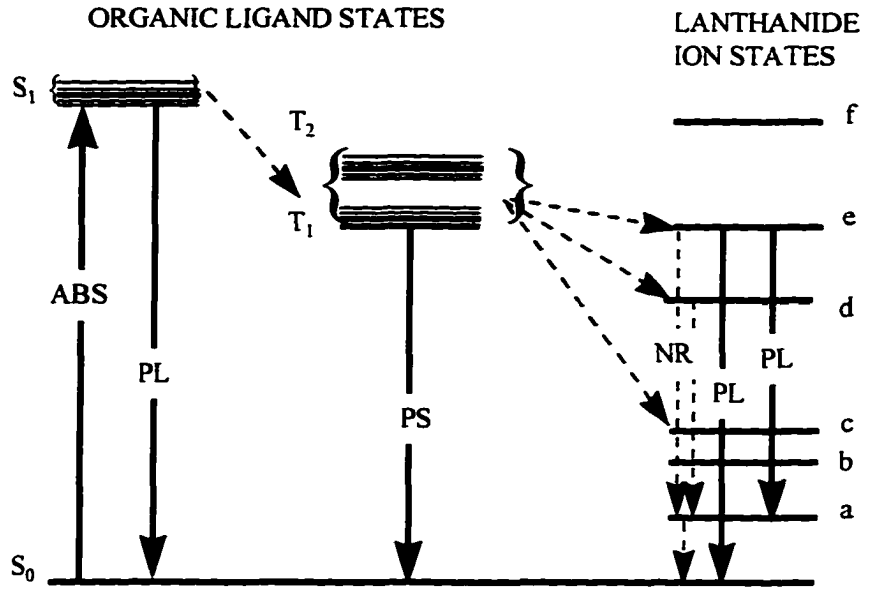

Figure 5-1. Energy Transfer in Lanthanide Complexes

ABS: Absorption; PS: Phosphorescence; PL Photoluminescence;

NR: Nonradiative decay; a, b, c, d, e and f: lanthanide ion energy levels

The energy levels in lanthanide atoms are normally described using the term symbol notation. The term symbol $^{2S+1}L_j$ describes the electronic orbital of the atom, where L is the total orbital angular momentum, j is the total angular quantum number, S is the total spin angular quantum number, and the exponent 2S+1 describes the multiplicity of the term.[12] In general the value of L may be 0, 1, 2, 3, 4, ··· , and corresponds to the letters S, P, D, F, G, ··· , respectively. In $EuCl_3$ the energy levels that participate in the visible-emitting radiative transitions are the $^5D_0$ (~ 17,270 cm^{-1}), $^5D_1$ (~ 19,270 cm^{-1}), $^7F_1$ (~ 400 cm^{-1}) and $^7F_2$ (~ 30-1000 cm^{-1}).[13] For $TbCl_3$ the energy levels that participate in the radiative transitions for visible light emission are: $^5D_4$ (~

20,500 cm^{-1}), $^7F_6$ (~ 100 cm^{-1}), $^7F_5$ (~ 2,100 cm^{-1}), $^7F_4$ (~ 3,400 cm^{-1}) and $^7F_3$ (~ 4,400 cm^{-1}).

The Tb and Eu complexes emit visible radiation that originates from the radiative transitions between the lanthanide ions' ^5D and ^7F levels. The emission spectrum from the Tb^{3+} ions is due to electronic energy transitions between the $^5D_4 \rightarrow {}^7F_6$, $^5D_4 \rightarrow {}^7F_5$, $^5D_4 \rightarrow {}^7F_4$ and $^5D_4 \rightarrow {}^7F_3$ states of the Tb^{3+} ion, respectively. The radiation emitted from the Eu^{3+} ions originates from the $^5D_0 \rightarrow {}^7F_1$, $^5D_0 \rightarrow {}^7F_2$ and $^5D_1 \rightarrow {}^7F_4$ energy transitions. The lanthanide-(benzoylbenzoate) complexes such as terbium tris(4-methyl benzoylbenzoate) {$Tb(MeBB)_3$} also show these radiative transitions; the chemical structure of $Tb(MeBB)_3$ is shown in Figure 5-2. The absorption and luminescence spectra of $Tb(MeBB)_3$ in dilute chloroform solution is shown in Figure 5-3. This chelate was also used to fabricate light emitting diodes and the results of the electroluminescence studies will be discussed in later sections.

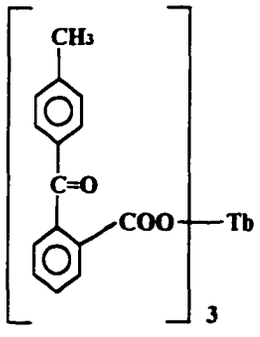

$Tb(MeBB)_3$

Figure 5-2. Chemical Structure of $Tb(MeBB)_3$

The absorption and PL excitation spectra of $Tb(MeBB)_3$ resemble the absorption and PL excitation spectra (See Figure 5-3) of the ligand, 4-methyl benzoylbenzoic acid (MeBB). This similarity in lineshapes indicates that the initial excitation of the complex occurs via the ligand. The PL spectrum of the terbium complex shows emission lines from the terbium(III) ion and an absence of the PL emission band from the ligand (peak emission $\approx$ 300 nm) because of intersystem crossing within the ligand. After energy transfer to the terbium ion's emitting level, we observe emission from the Tb^{3+} ion. The other optical properties of the terbium chelate are discussed in later sections and the results of these optical measurements are summarized in Table 5-1. The next section discusses the synthesis of the lanthanide-benzoylbenzoate complexes.

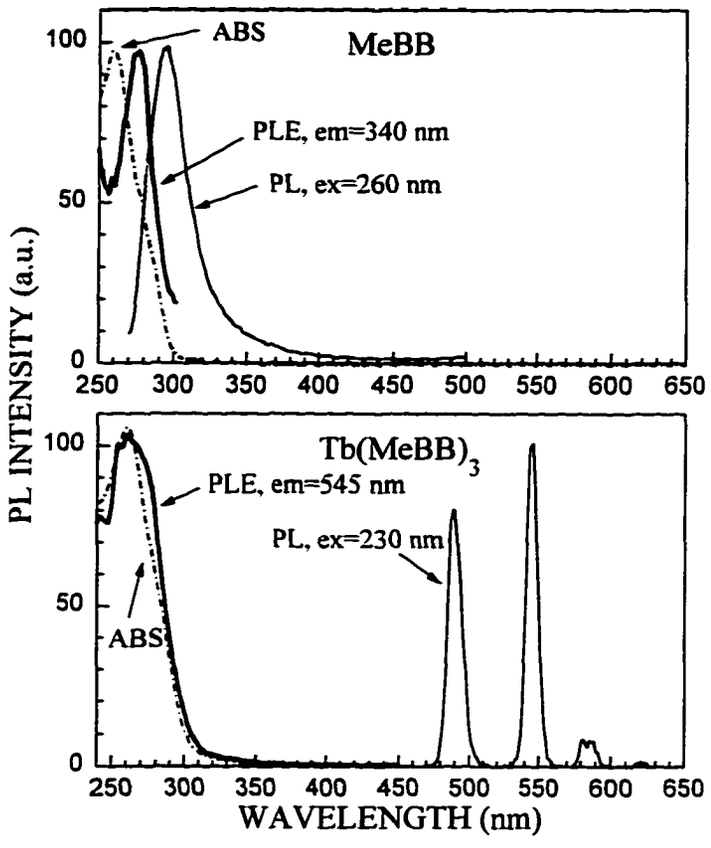

Figure 5-3. Absorption and Luminescence Spectra of $Tb(MeBB)_3$ in Solution

Concentration of MeBB : $3x10^{-6}$ M in Methylene Chloride; Concentration of $Tb(MeBB)_3$: $5x10^{-6}$ M in Methylene Chloride

5.3 Synthesis of Lanthanide(benzoylbenzoate) Complexes

The lanthanide complexes were synthesized according to established procedures by the research team led by Dr. Y. Okamoto from Polytechnic University.[12] One of the ligands, 4-methoxy benzoylbenzoic acid (MeOBB), was prepared by the Friedel-Crafts reaction of phthalic acid and methoxybenzene using

anhydrous aluminum chloride (See Figure 5-4). The crude product was recrystalized from ethanol, m.p. 144^0 C. The resulting compound was characterized by measuring FT-IR and H NMR spectra. The other ligand, 4-methyl benzoylbenzoic acid (MeBB), was prepared using procedures similar to those methods used to synthesize MeOBB.

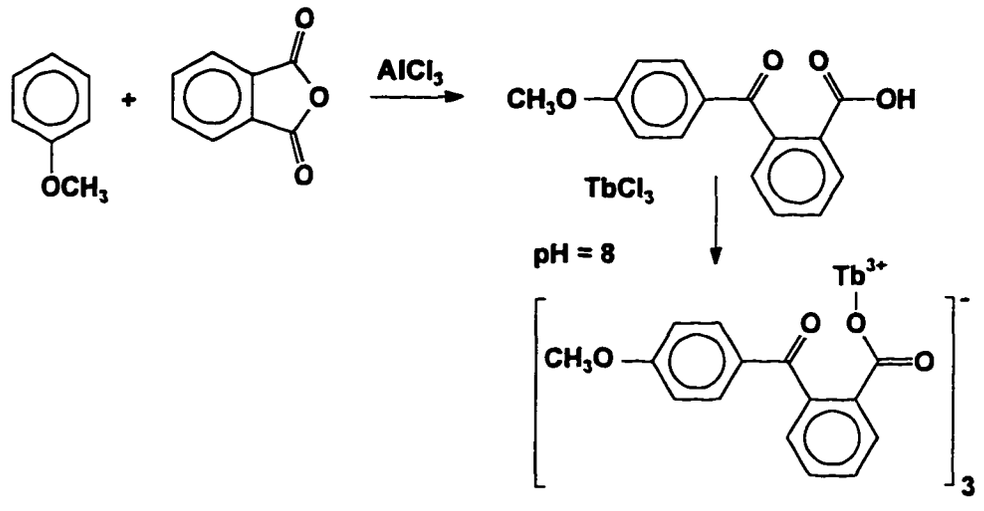

Figure 5-4. Preparation of 2(4'-methoxy-benzoyl)benzoic acid and Tb tris[2(4'-methoxybenzoyl)benzoate

Terbium tris(4-methoxy benzoylbenzoate), $Tb(MeOBB)_3$, was prepared by the addition of $TbCl_3$ aqueous solution into sodium 4-methoxy benzoyl benzoate (1:3 molar ratio) – See Figure 5-4. The precipitate product was washed with water and methanol. The solid product was dried under reduced pressure at 50^0 C for 4 days. The Tb content in the complex was determined by converting the terbium benzoate to Tb_2O_3 using a thermal gravimetric analyzer (TGA) while the sample was heated from room temperature to 1000^0 C at a rate of 10^0 C/min under an air atmosphere (Calc.: 19.2 %; Found: 17.5 %). A typical TGA profile of $Tb(MeOBB)_3$ is shown in Figure 5-5. $Tb(MeOBB)_3$ is thermally stable up to about 340^0 C and has a decomposition

temperature of 450^0 C in air. This metal complex has an oxidation potential of 1.71 volts in methylene chloride solution. The other lanthanide-(benzoyl)benzoates complexes, Tb(MeBB)$_3$ and Eu(MeOBB)$_3$, also possessed good thermal stablility up to the range of 320 - 340^0 C.

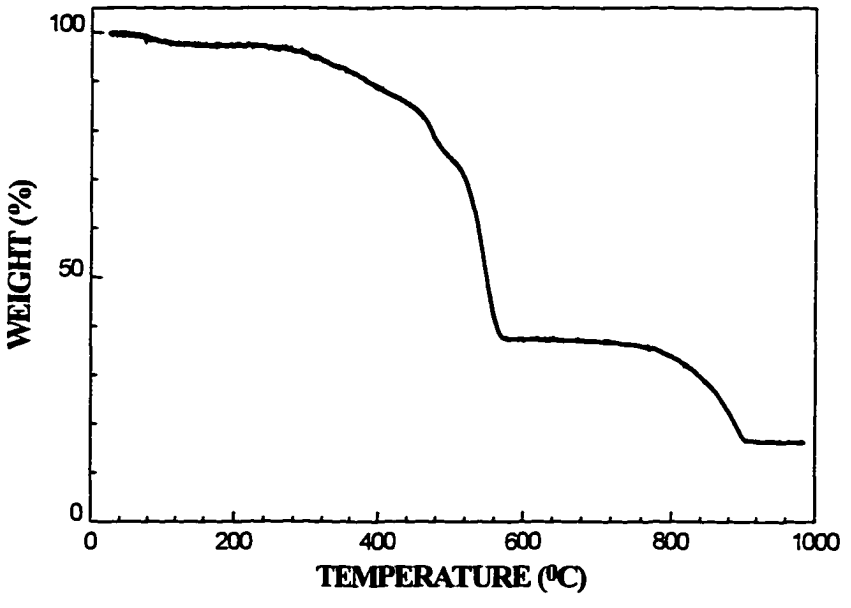

Figure 5-5. TGA Analysis of Tb(MeOBB)$_3$

Heating rate = 10^0 C/min, heating range: room temperature to 1000^0 C in air.

Eu(MeOBB)$_3$ (decomposition temperature = 450^0 C, oxidation potential = 1.60 volts in methylene chloride solution) was synthesized using procedures similar to the synthesis of the Tb complex. Eu(TTFA)$_3$ was synthesized as described by Whan and Crosby.[6,14] Terbium tris(acetylacetonate), Tb(ACAC)$_3$ was synthesized as described by Hayes and Drickamer.[15] The Tb(MeBB)$_3$ complex was prepared according to procedures similar to those used for synthesizing Tb(MeOBB)$_3$.

5.4 Device Structures

Single and double layer devices were fabricated to study electrominescence in the lanthanide complexes. The single-layer devices were fabricated on ITO-covered glass substrates. Since the lanthanide complexes are not volatile and do not form optical quality pin-hole free films, spin casting techniques were used to fabricate devices. The device configurations were: ITO/La(benzoyl)benzoate complex:PBD:PVK/Ca/Al for the single layer cell structures. The poly(N-vinylcarbazole) (PVK) layer was used as a polymer matrix for the other dopant materials and as a hole transporting agent.[16] The PVK layer (| 850) also helped to provide uniform optical quality films for the active layer. Thirty weight percent of 2-(4-biphenyl)-5-(4-tert-butylphenyl)-1,3,4-oxadiazole (butyl-PBD), an electron transporting agent, was added to the PVK layer to increase bipolar charge transport.[17] The lanthanide complexes were added to the PVK layer at doping concentrations of 1 - 40 mole %.

The device layers were deposited according to conventional procedures. The organic layers for the LEDs were deposited by spin casting from chloroform solutions with concentrations of 25-35 mg/ml. The metal electrodes (Ca covered by Al) were deposited, on top of the organic layers, by thermal evaporation under a vacuum of $5x10^{-7}$ mm Hg. The Al layer was deposited over the Ca to retard oxidation. The thickness of the calcium layer was 250 - 300 nm and the aluminum layer had a 150 - 200 nm thickness. All stages of device fabrication and testing were done under a nitrogen atmosphere.

The double-layer LEDs were also fabricated on ITO-covered glass substrates. The device structures were: ITO/La(MeOBB)$_3$:PVK/PBD:PMMA/Ca/Al, where the poly(methyl methacrylate) (PMMA) was used as a polymeric binder to obtain uniform films and to retard the crystallization of the butyl-PBD. The doped PVK ($\sim$ 650) and combined PBD:PMMA ($\sim$ 300) layers for the LEDs were deposited by spin casting from chloroform and acetonitrile solutions, respectively. The concentrations of the PVK and PBD solutions were approximately 14-18 mg/ml and 14 mg/ml, respectively. The metal electrodes were deposited according to procedures described in the preceeding sections.

5.5 Photoluminescence in Lanthanide-(benzoyl)benzoates

The luminescent properties of the three new thermally stable lanthanide-organic complexes namely, terbium tris(4-methyl benzoylbenzoate) {Tb(MeBB)$_3$}, terbium tris(4-methoxy benzoylbenzoate) {Tb(MeOBB)$_3$} and europium tris(4-methoxy benzoylbenzoate) {Eu(MeOBB)$_3$} were studied. The UV absorption bands in these compounds are attributed to the ligand while the emission originates from the respective lanthanide ions' electronic transitions. The photoluminescence spectra, absorption spectra, quantum efficiency of photoluminescence and fluorescence lifetimes were measured in solution. These results will be reported in this section. In later sections narrow-band electroluminescence from these complexes are studied by fabricating and characterizing single- and multi-layer organic light emitting diodes (OLEDs).

The absorption and luminescence spectra of the MeOBB ligand in $1x10^{-6}$ M methylene chloride solutions are shown in Fig. 5-6. The PL spectrum of the ligand contains a broad featureless UV-blue emission band extending from 350 to 500 nm with an emission peak at approximately 390 nm. The photoluminescence excitation (PLE) spectrum of MeOBB is similar to the absorption spectrum indicating that the initially excited states are responsible for emission.

The absorption spectra of the $Tb(MeOBB)_3$ and $Eu(MeOBB)_3$ complexes exhibit features that are representative of the MeOBB ligand (Fig. 5-6). The corresponding excitation spectra for emission from the respective La ions are similar to the absorption spectrum of the ligand, indicating that the Tb^{3+} and Eu^{3+} ions are excited via energy transfer from the initially excited MeOBB ligand through the triplet states of the ligand.[7,11,12] The lack of PL from the ligand indicates that the heavy lanthanide ions probably enhance the rate of intersystem crossing from the singlet states of the ligand to the ligand's triplet states.[18,19]

Consequently, emission from the Tb^{3+} and Eu^{3+} complexes is mostly due to the respective La^{3+} ions. The PL spectrum from the Tb(III) complex shows emission peaks at approximately 490 nm, 545 nm, 585 nm and 620 nm which are assigned to the electronic energy transitions between the $^5D_4 \rightarrow {}^7F_6$, $^5D_4 \rightarrow {}^7F_5$, $^5D_4 \rightarrow {}^7F_4$ and $^5D_4 \rightarrow {}^7F_3$ states of the Tb^{3+} ion, respectively. The Eu(III) complex has emission peaks at about 585 nm and 617 nm corresponding to the electronic energy transitions between the $^5D_0 \rightarrow {}^7F_1$ and $^5D_0 \rightarrow {}^7F_2$ states of the Eu^{3+} ion, respectively. The $^5D_1 \rightarrow {}^7F_4$ energy transition of the Eu^{3+} ion, which is red-shifted approximately 2 nm from 617 nm, may

have been present but could not be resolved from the $^5D_0 \rightarrow {}^7F_2$ energy level transition. The excitation energy is usually transferred from the triplet state of the ligand to the nearest lower resonance level of the lanthanide ion.[7,11,12] Therefore the singlet and triplet energy levels of the MeOBB ligand should be higher than the energy corresponding to the $^5D_4 \rightarrow {}^7F_6$ transition of the Tb^{3+} ion at 490 nm (i.e., approximately $20.5x10^3\ cm^{-1}$ or 2.54 eV).

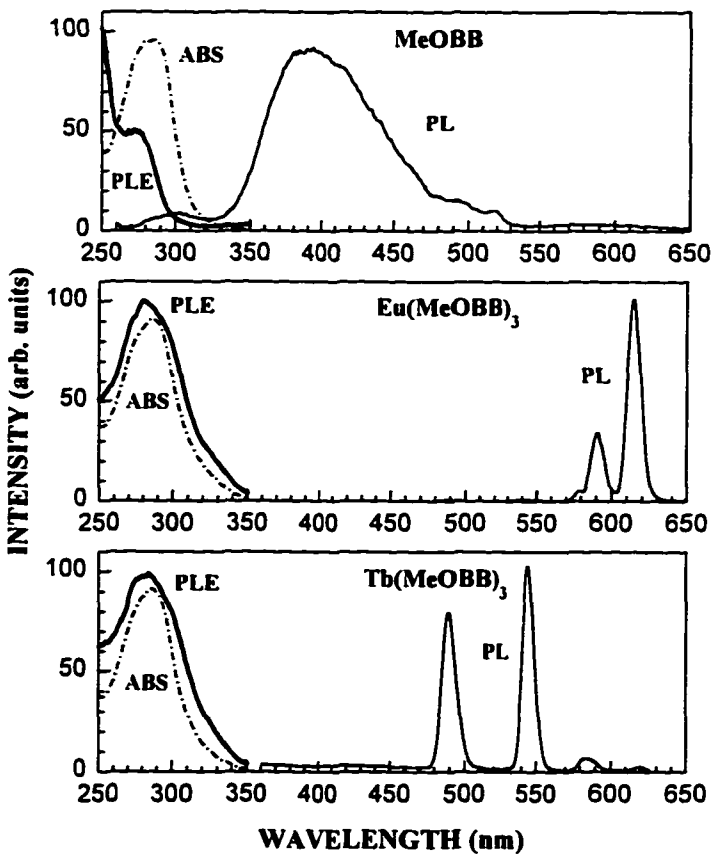

Figure 5-6. ABS, PL & PLE of MeOBB, $Eu(MeOBB)_3$ & $Tb(MeOBB)_3$ in Solution Concentration: $1x10^{-6}$ M in methylene chloride; PL for excitation at 280 nm; PLE for emission at 400 nm (MeOBB), 615 nm {$Eu(MeOBB)_3$}, and 545 nm {$Tb(MeOBB)_3$}.

The PL quantum efficiencies, Φ, and fluorescence lifetimes, τ, for $Eu(MeOBB)_3$ $Tb(MeOBB)_3$, and $Tb(MeBB)_3$ were measured in chloroform and methylene chloride solutions ($5x10^{-4}$ M) at room temperature. PL quantum efficiencies were measured relative to the published values for $Eu(TTFA)_3$ ($\Phi = 0.53$) and $Tb(ACAC)_3$ ($\Phi = 0.19$) (See Table 5-1).[12,20] The lower quantum efficiencies and fluorescence lifetimes, measured for both complexes in chloroform solutions, are probably due to the higher degree of their dissociation in the more polar solvent. The lower quantum efficiency values obtained for $Eu(MeOBB)_3$ compared to $Tb(MeOBB)_3$ might be due to a slight mismatch of the triplet energy level of the MeOBB ligand and the europium ion's $^5D_0$ resonance level – assuming a high rate of intersystem crossing in the ligand along with the presence of the heavy La ions. The fluorescence lifetimes of these lanthanide complexes was measured and found to be in the microsecond to millisecond range. These characteristically long lifetimes were probably due to the spin-forbidden electronic transitions of the lanthanide ions.

MATERIAL	SOLVENT	Φ	τ (μsec)
$Eu(MeOBB)_3$	Methylene chloride	0.16	541
	Chloroform	0.08	440
$Tb(MeOBB)_3$	Methylene chloride	0.27	743
	Chloroform	0.22	641
$Tb(MeBB)_3$	Methylene chloride	0.04	1085
	Chloroform	0.01	1009

Table 5-1. Optical Parameters of the Lanthanide-(benzoyl)benzoates in Solution

Concentration: 10^{-6} M in methylene chloride or chloroform; PL lifetimes measured at 615 nm (Eu complex) and 545 nm (Tb complexes).

To determine the suitable candidate materials for device emitting layers, the solid state optical properties of the lanthanide complexes were also studied. Solid state spectra measured for thin films of lanthanide-(benzoylbenzoates) were qualitatively similar to the spectra of the solutions. These lanthanide complexes in the solid state show absorption and PLE spectra that are characteristic of the ligands. The corresponding PL spectra of the complexes show line emission spectra that originate from the lanthanide ions (terbium or europium). The absorption, PL and PLE spectra of the MeOBB ligand and the lanthanide-(methoxybenzoyl)benzoate complex films are shown in Figure 5-7.

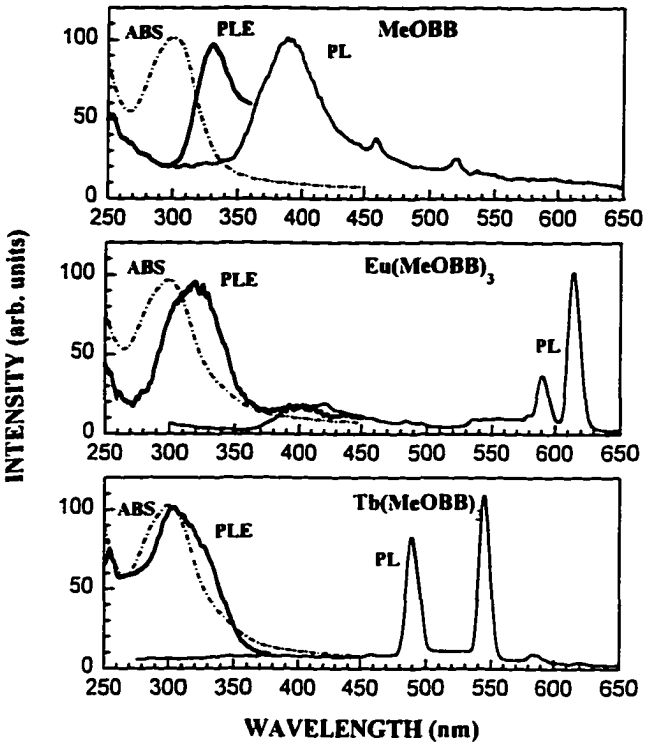

Figure 5-7. ABS and PL Spectra of MEOBB, $Eu(MeOBB)_3$ & $Tb(MeOBB)_3$ Films

Since the solid state spectra showed bright line emission from the La complexes and no evidence of strong quenching effects, these materials were used to fabricate single- and multi-layer LEDs. The fabrication and characterization of these LEDs is discussed in the upcoming sections.

5.6 Electroluminescence in Single Layer Devices

LEDs were fabricated to study the EL of the lanthanide complexes. The lanthanide-(benzoylbenzoate) complexes are not volatile and suitable optical-quality thin films could not be produced by thermal evaporation; instead, spin casting techniques were used to fabricate LEDs. Poly(N-vinylcarbazole) (PVK) was selected

as a host matrix for the LEDs because of its good hole transport and film-forming properties.[17] The chemical structure of PVK is shown in Figure 5-8. The absorption spectrum and luminescence spectra of PVK are shown in Figure 5-9.

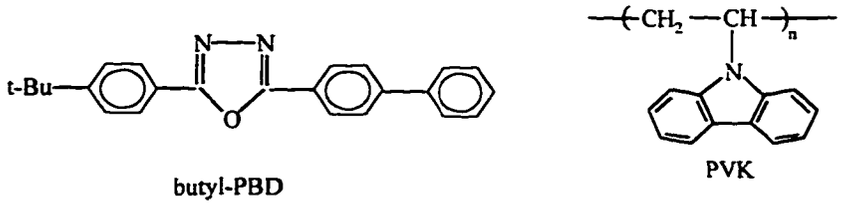

Figure 5-8. Chemical Structures of butyl-PBD and PVK

The PVK thin film layers were initially doped with the lanthanide complexes contained in single layer devices with the ITO/La Complex:PVK/Ca/Al cell structure, but these devices showed negligible light output, probably because of the poor electron transport properties of the doped PVK layer. To improve the electron transport property, 2-(4-biphenyl)-5-(4-tert-butylphenyl)-1,3,4-oxadiazole (butyl-PBD) was added to the single layer cells.[21] This composite layer (which should have bipolar charge transport properties) may be more suitable for LED fabrication.

Based on the results of PL studies for composite thin films, the butyl-PBD and PVK compounds were selected because they do not quench the luminescence of the lanthanide complexes. In other words, the absorption bands of PBD and PVK do not overlap with the emission spectra of the La complexes. Therefore, there should not be any radiative or Forster-type energy transfer from the lanthanide chelates to the PVK or butyl-PBD compounds. In addition, the PL spectra of PVK and PBD are blue-shifted relative to the lanthanide complexes. Therefore, the excited states of the

complexes will not be quenched by energy transfer to the other organic components in the layer. The chemical structure of butyl-PBD is shown in Figure 5-8. The absorption and PL spectra of butyl-PBD are shown in Figure 5-9.

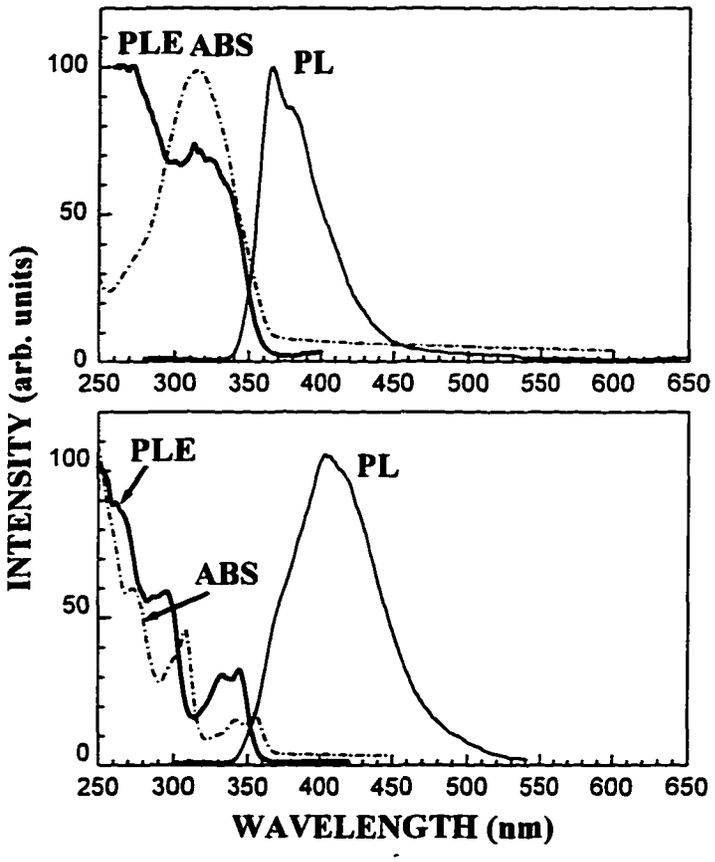

Figure 5-9. ABS, PL and PLE spectra of PBD and PVK Thin Films
Top: butyl PBD; Bottom: PVK; PL for excitation at 280 nm (PVK) and 260 nm (PBD); PLE for emission at 440 nm (PVK) and 420 nm (PBD).

The next set of single layer light emitting diodes were fabricated from terbium tris[2-(4'-methylbenzoyl)benzoate], $Tb(MeBB)_3$.[22] These light emitting diodes had the following cell structure: ITO/$Tb(MeBB)_3$:PBD:PVK/Ca/Al. The concentration of

dopants in the second set of devices was: 30 weight % of butyl-PBD compared to PVK and 1-10 mole % of $Tb(MeBB)_3$ relative to PVK. The single layer LEDs containing $Tb(MeBB)_3$ showed green electroluminescence, corresponding to the emission lines of the Tb^{3+} ion, when the devices were forward biased with the ITO electrode at positive polarity (See Figure 5-10). No emission from the ligand, butyl-PBD or PVK was observed. Assuming no energy transfer from PVK or PBD to the lanthanide complex, this suggests that there was recombination on the Tb complex but very little or no recombination on PVK or butyl-PBD. The maximum brightness of these devices was approximately 0.7 cd/m^2 for a 2 mole % doping concentration of the terbium complex. Below 1 mole % doping, there is significant EL from PVK. The maximum brightness of the LEDs decreased with increasing concentrations above 2 mole %. For doping concentrations above 10 mole %, there was no light output from the devices. Because of the very low brightness values, it was not possible to make an accurate quantitative assessment of the concentration-dependent behavior of the brightness for $Tb(MeBB)_3$ LEDs.

The brightness of the light emitting devices can be modified by the selection of stronger electron-donating or electron-accepting side-groups within the ligand. The terbium tris[2-(4'-methoxylbenzoyl)benzoate], $\{Tb(MeOBB)_3\}$ contains a methoxy sidegroup (OCH_3) instead of the methyl side-group (CH_3) found in $Tb(MeBB)_3$. This methoxy sidegroup is a stronger electron donating group and consequently shows brighter EL due to the more efficient transfer of energy from the excited ligand to the

Tb^{3+} ion. Photoluminescence studies show that the $Tb(MeOBB)_3$ complex shows a higher PL quantum efficiency (Table 5-1) than $Tb(MeBB)_3$.

Indeed, LEDs were fabricated based on a single layer device consisting of PVK doped with butyl-PBD (30 weight %) and $Tb(MeOBB)_3$ (1-40 mole %) compared to PVK. The device structures were as follows: ITO/$Tb(MeOBB)_3$:PBD:PVK/Ca/Al. The doped PVK layer had a thickness of about 80-100 nm. The thickness measurements of the calcium and aluminum layers were similar to the dimensions for the $Tb(MeBB)_3$-based devices. When the diodes were forward biased with the ITO electrode at positive polarity, green EL was also observed from the second set of Tb-complex LEDs. This EL spectrum (Figure 5-10) shows distinct emission lines corresponding to the Tb^{3+} ion. No electroluminescence was observed from the MeOBB ligand, PVK, or butyl-PBD.

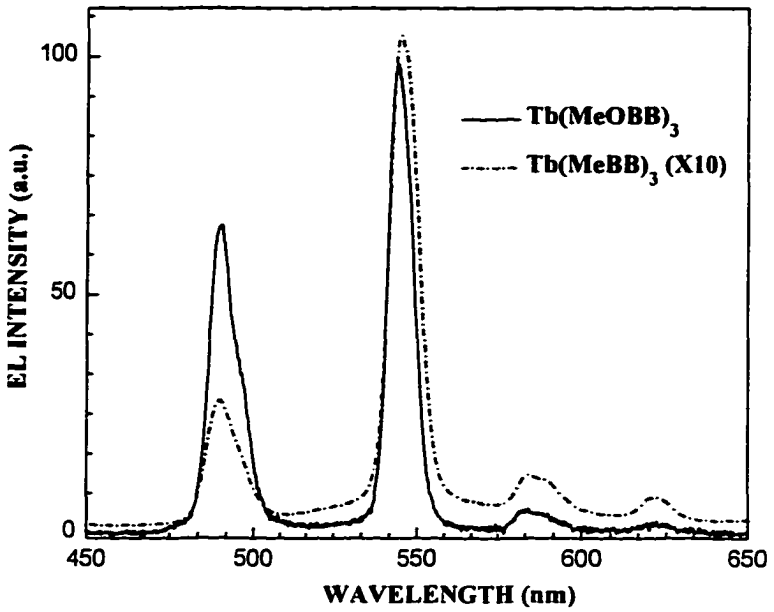

Figure 5-10. EL Spectra of Tb complex LEDs

The I-V characteristics varied with the doping concentration of $Tb(MeOBB)_3$. The current vs. voltage curves for LEDs with various concentrations of $Tb(MeOBB)_3$ are shown in Figure 5-11. The turn-on voltage for both sets of devices was relatively high (25 volts) and increased as the doping concentration of the La complexes increased. The high turn on voltage was most likely due to the single layer cell structure (note: charge injection is not optimized near the Ca and ITO contacts) and the quality of the ITO used in these devices. The increase in turn-on voltage may also have been due to the increase in the effective barriers at the electrode-organic layer interfaces To determine the nature of the barrier due to the lanthanide complexes, a more detailed study of the energy levels in $La(MeOBB)_3$ molecules is necessary. For highly doped {> 2 mole % $Tb(MeOBB)_3$ in PVK} layers, we also observed reduced

current densities compared to devices with doping concentrations of 1-2 mole %. This reduced current density may originate from a decrease in the effective carrier mobilities within the doped layer.

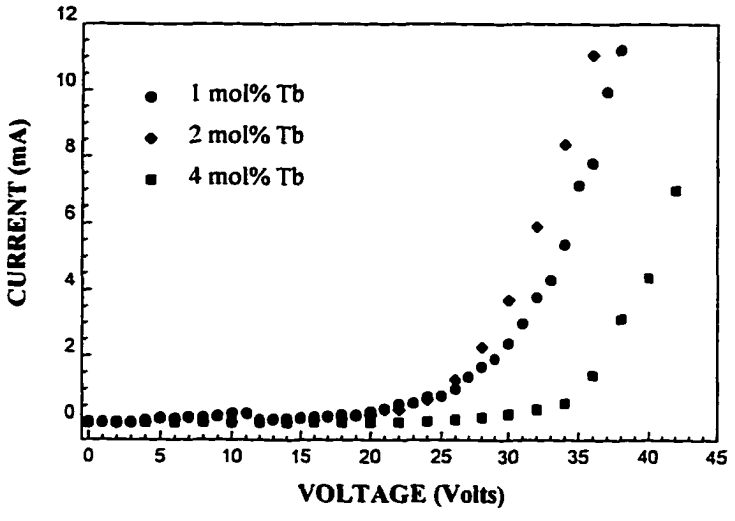

Figure 5-11. I-V Curves for $Tb(MeOBB)_3$ LEDs

We also studied the concentration dependence of electroluminescence in $Tb(MeOBB)_3$, the brighter terbium emitter, and found that the EL intensity of the light emitting devices depended strongly on the doping concentration of the terbium complex within the PVK layer. In general, the brightness of the $Tb(MeOBB)_3$-based devices was an order of magnitude brighter than the $Tb(MeBB)_3$-based devices. At doping concentrations below 1 mole % there is EL from PVK and the Tb complex. At a 1-1.5 mole % concentration of $Tb(MeOBB)_3$ in PVK, PVK EL becomes negligible and the brightest emission (9 cd/m^2) was observed from the Tb complex. For devices with 2 and 4 mole% doping, the maximum brightness was on the order of 7 and 5 cd/m^2, respectively. For concentrations above 4 mole %, the EL intensity continued to decrease as the doping concentration increased. Based on PL studies for 1-40 mole %

doping of $Tb(MeOBB)_3$:PVK and $Tb(MeOBB)_3$:PBD:PVK films, we did not observe any concentration quenching of the La luminescence. We attribute the declining brightness of the single layer devices to a progressively decreasing mobility of charge carriers within the doped PVK layer and possibly an increasing imbalance of charge carriers due to the changing barriers at the interfaces or varying carrier mobilities within the PVK layer.

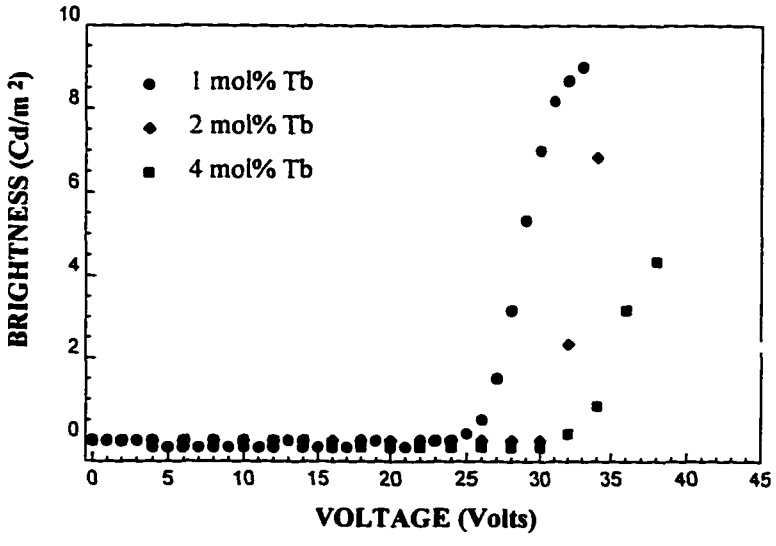

Figure 5-12. B-V Curves for $Tb(MeOBB)_3$ LEDs

By substituting the europium ion instead of the terbium ion in the benzoyl(benzoate) complex, the spectrum of EL emission can also be tailored to give line emission in the red region of the spectrum. Consequently, single layer LEDs were also fabricated using europium tris[2-(4'-methoxylbenzoyl)benzoate] {$Eu(MeOBB)_3$} as the emitting material. Again, single layer LEDs were fabricated but in this case with the ITO/$Eu(MeOBB)_3$:PBD:PVK/Ca/Al device configuration. These LEDs showed red EL with emission lines that were attributed to the Eu^{3+} ion (See Figure 5-

13); the devices showed saturated red emission with one emission peak at approximately 616 nm. The thickness of the organic layer was approximately 850 - 900 Å. For doping concentrations greater than or equal to 1 mole %, we did not observe any voltage-dependent variation in the EL spectra.

The maximum brightness of these devices was very low ⊗ less than 1 cd/m^2 at a 2 mole % concentration of $Eu(MeOBB)_3$. Since the PL quantum efficiency of $Eu(MeOBB)_3$ in solution is about one half of the value for $Tb(MeOBB)_3$, we expect the EL radiation emitted from the europium-based devices to be lower than similar terbium-based devices. Also, the lower responsivity of the human eye in the red region of the visible spectrum would lead to lower brightness readings for red devices compared to green devices. To improve the brightness output, mutlilayer devices were fabricated. The corresponding results will be discussed in the next section.

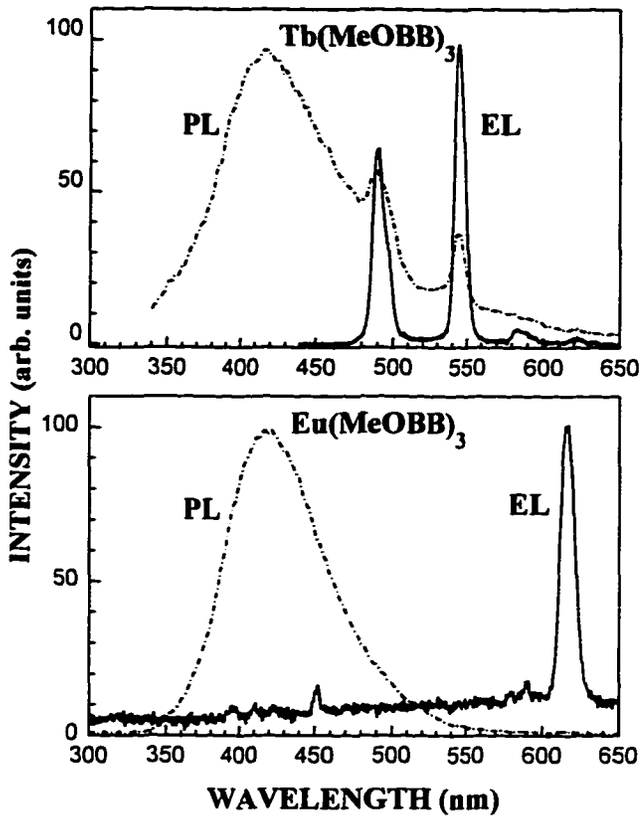

Figure 5-13. PL Spectra of $La(MeOBB)_3$:butyl-PBD:PVK (1:1:1) Films and EL Spectra of Single-Layer LEDs

LED Structure: ITO/$La(MeOBB)_3$(2 mole %):PBD(30 wt %):PVK(100 %)/Ca/Al structure; Thickness of Polymer Layer: 85 nm.

5.7 Electroluminescence in Multilayer Devices

To improve the performance of the devices, we used a two layer cell structure: ITO/$Tb(MeOBB)_3$:PVK/PBD/Ca/Al.[23] Devices containing the Tb complex showed green EL but these devices failed rather quickly because of the rapid crystallization of the butyl-PBD layer. To improve device reliability, the butyl-PBD layer was doped

with PMMA which retards premature crystallization of the butyl-PBD layer. The two layer devices had the ITO/La(MeOBB)$_3$:PVK/PBD:PMMA/Ca/Al configuration; the ratio of PBD to PMMA was 3:1 by weight. The relative proportions of the organic components in the active layer of the brightest devices were Tb(MeOBB)$_3$:PVK (1:15 weight ratio), Eu(MeOBB)$_3$:PVK (1:1 weight ratio). These devices showed better performance due to improved electron and hole injection from the cathode and anode, respectively. For the Tb-complex devices, green EL was observed with the maximum brightness of 45 cd/m^2 at a driving voltage of 24 volts (See Figure 5-14). The turn-on voltage for these two layer devices was 13 volts, approximately half of the corresponding values for single layer devices. The EL spectrum of these two layer devices shows that most of the EL emission originates from the Tb^{3+} ion but there is some EL from PVK in the short wavelength tail of the spectrum (See Figure 5-15). For low driving voltages, there was no significant variation in the EL spectrum with changing concentration. The concentrations of the active layers were 1:15, 1:10 and 1:5 by weight of Tb(MeOBB)$_3$ compared to PVK.

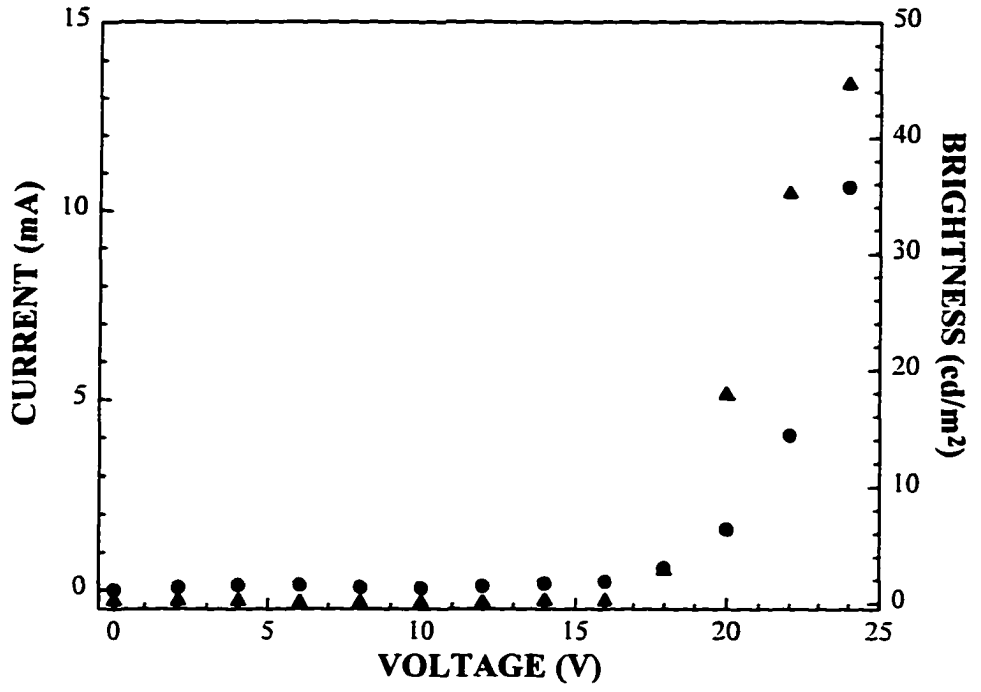

Figure 5-14. Current- and Brightness- vs. Voltage Curves for Two-Layer LEDs

LED Structure: ITO/Tb(MeOBB)$_3$:PVK/PBD:PMMA/Ca/Al cell structure. Thickness of the Tb(MeOBB)$_3$:PVK (1:15 weight ratio) layer: 65 nm. Thickness of the PBD:PMMA (3:1 weight ratio) layer: 20 nm. Current-voltage Curves: (λ); Brightness-voltage Curves: (σ)

The EL spectra of the Eu-complex devices varied considerably with the concentration of Eu(MeOBB)$_3$ within the PVK layer because of the relatively weaker EL of the Eu complex compared to PVK. For two layer devices containing Eu(MeOBB)$_3$:PVK concentrations of 1:15, 1:10, 1:5 and 1:2 by weight, the devices show lavender electroluminescence due to EL from the Eu complex and PVK. The devices with higher doping concentrations (1:1 and 2:1) showed red EL — largely

due to emission (at 616 nm) from the Eu^{3+} ion along with a relatively small PVK emission band centered at approximately 420 nm (See Figure 6). The devices with 1:1 ratio of $Eu(MeOBB_3$ to PVK showed brightness values of only 1.2 cd/m^2 due to the poor carrier mobility of the highly doped PVK layer. The EL spectra in Figure 5-15 suggest that the most of the carrier recombination occurs on the La complexes with few carriers recombining on PVK ⊗ assuming little or no energy transfer from PVK to the La complexes.

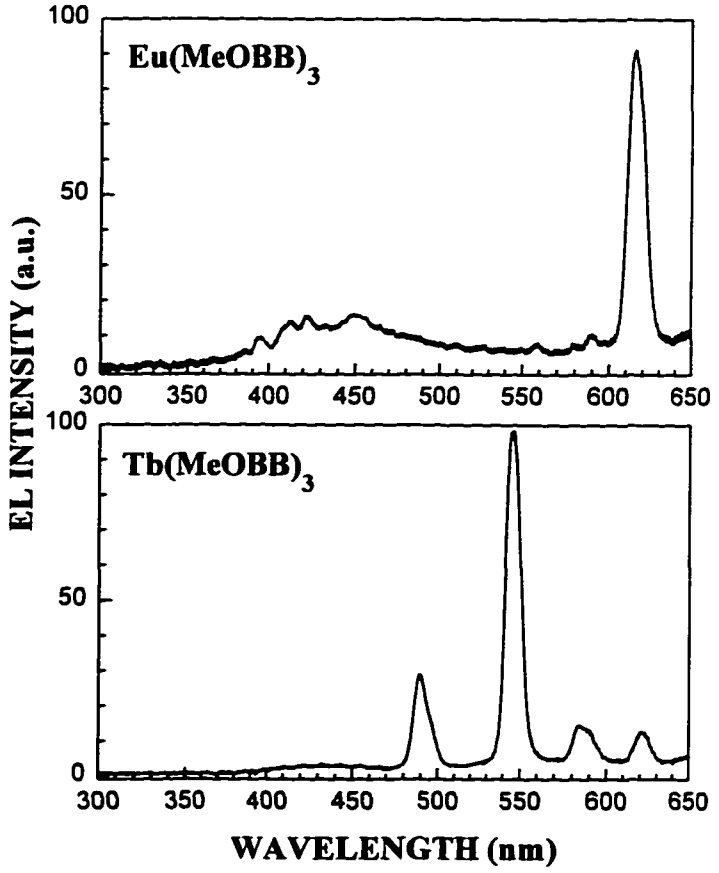

Figure 5-15. EL spectra of two-layer LEDs

LED Structure: ITO/La(MeOBB)$_3$:PVK/PBD:PMMA/Ca/Al cell structure; Thickness of La(MeOBB)$_3$:PVK layer: 65 nm; Thickness of the PBD:PMMA layer: 20 nm.

5.8 Energy Transfer in La(MeOBB)$_3$ Light Emitting Diodes

The energy transfer processes in the diodes made from the lanthanide complexes were studied by comparing the EL spectra of the devices with the PL spectra of composite thin films (See Figure 5-16). The composite thin films consist of various combinations of Tb(MeOBB)$_3$, PBD, PVK, or MeOBB. The results of electroluminescence studies have shown that the EL originates from the lanthanide ions, and, the lanthanide complexes act as charge traps and recombination centers for electroluminescence.

To further determine the mechanism for intermolecular energy transfer and bipolar charge recombination within the two layer devices we compared the EL spectra of the Tb-based devices (Fig. 5-15) to the PL spectra of thin films containing the Tb complex and PVK (1:1 weight ratio) ⊗See Fig. 5-16. The absorption spectra of Tb(MeOBB)$_3$:PVK films resemble the absorption and PLE spectra of PVK films (Fig. 5-16). From 270-310 nm, the corresponding PLE spectrum (for emission at 545 nm) of the composite film shows features similar to the Tb(MeOBB)$_3$ absorption and PLE spectra. The PLE peak at 285-290 nm is blue-shifted compared to the 295 nm PLE peak of PVK. This suggests that emission at 545 nm is mostly due to the photoexcitation of the Tb complex which in turn implies that energy transfer from the PVK matrix is probably not significant.

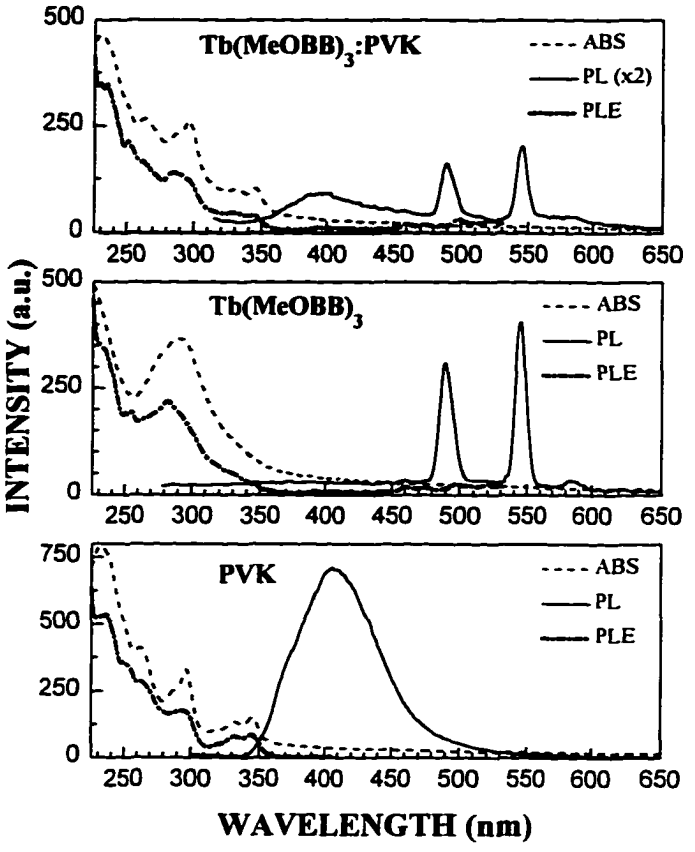

Figure 5-16. PL and PLE of $Tb(MeOBB)_3$, PVK and $Tb(MeOBB)_3$:PVK (1:1) Films

PL for excitation at 260 nm {$Tb(MeOBB)_3$, PVK and $Tb(MeOBB)_3$:PVK}; PLE for emission at 545 nm {$Tb(MeOBB)_3$ and $Tb(MeOBB)_3$:PVK}, 420 nm (PVK); All PL spectra are normalized for absorbance at 260 nm; Thin films were spin cast from chloroform solutions

The EL spectra of the Tb-based two layer devices show large emission peaks from the Tb complex but relatively little emission from PVK (See Figure 5-15). Since energy transfer from PVK to the Tb complex is not significant, the EL in the two layer devices originates (mostly) from bipolar charge recombination occurring on the

Tb complex molecules located within the PVK layer. The relative brightness of the EL will be determined by the percentage of electron-hole pairs recombining on the La complex molecules and the efficiency of energy transfer from the MeOBB ligand to the lanthanide ion's resonance level.

To verify the contribution to Tb^{3+} electroluminescence that is caused by energy transferred from PVK, we have studied the PL of $Tb(MeOBB)_3$:PVK (1:1) thin films and simulated the separate contributions to PL from $Tb(MeOBB)_3$ and PVK while accounting for the exciting energy absorbed by each material (See figure 5-17). These studies show there is little or no energy transferred from PVK to the Tb complex as evidenced by the intensities of the Tb emission peaks at 490 and 545 nm. Also, there is a significant decrease in the PL contribution from PVK (See Figure 5-17). Based on earlier studies of MeOBB:PVK (1:1) films, we have determined that the ligand (MeOBB) quenches the photoluminescence of PVK, hence the significant decrease of PVK emission in the $Tb(MeOBB)_3$:PVK films. Since PVK does not enhance the Tb PL, we can conclude that there is little or no contribution to La^{3+} EL that is generated by energy transferred from charge carriers recombining on PVK molecules.

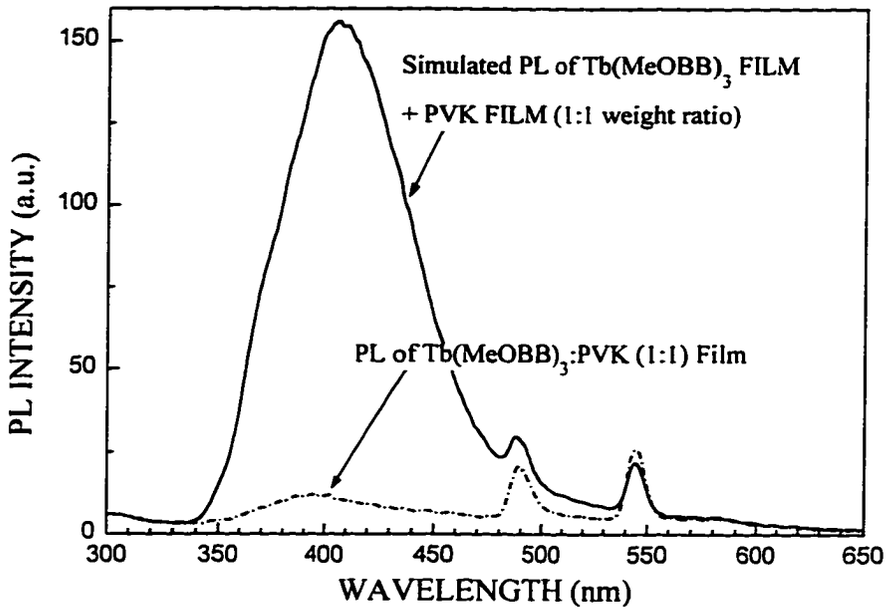

Figure 5-17. Energy transfer in $Tb(MeOBB)_3$:PVK Films

On the other hand, PVK serves as a polymer matrix {for $Tb(MeOBB)_3$ molecules} and also aids charge transport within the device. Since PVK does not show strong evidence of transfer energy to the La complexes, it may also increase the competing nonradiative processes occurring in the device. Consequently, this possible lack of energy transfer may limit the overall luminous efficiency of the LED.

The influence of trapping mechanisms in the active layer of the two layer cells was studied by observing the EL spectra of the $Tb(MeOBB)_3$ devices. The multi-layer layer devices showed voltage-dependent variations in the EL spectra. To reduce the heating effects at high injection currents and prevent premature degradation of the LEDs pulsed currents with 10 % duty cycle were used to drive the LEDs.

LEDs were fabricated with active layers containing doping concentrations of 1:1, 1:2, 1:5, 1:10 and 1:15 (by weight) of $Tb(MeOBB)_3$ compared to PVK. For all concentrations, there was a strong component of EL from the Tb^{3+} ion at all voltages above the onset voltage for electroluminescence (See Figure 5-18). At voltages below 50 volts, there was no detectable emission from PVK. However, at 50 volts we observed EL from PVK as well as Tb^{3+}. As the voltage was increased, the relative emission of PVK {compared to $Tb(MeOBB)_3$} increased. We believe the PVK emission originates from the filling of the Tb complex trap levels located within the PVK layer. As the voltage increases above the trap-filled limit, then recombination also occurs on PVK which leads to electroluminescence originating from PVK. Figure 5-18 illustrates the relative increase in PVK emission with increasing voltage.

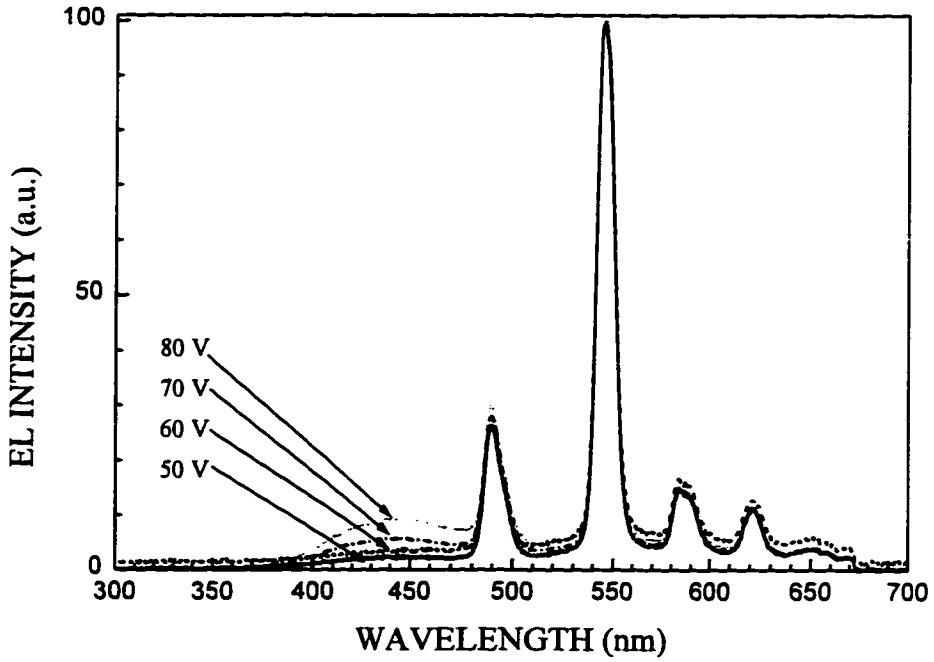

Figure 5-18. Voltage Dependence of EL Spectra for $Tb(MeOBB)_3$

LED structure: ITO/Tb(MeOBB)$_3$:PVK/PBD:PMMA/Ca/Al; Doping Concentration of Active Layer: 1:15 by weight of Tb complex compared to PVK; All EL spectra were normalized to the 545 nm emission peak of Tb.

The two layer devices fabricated from Eu(MeOBB)$_3$ also showed concentration-dependent and voltage-dependent changes in the EL spectra. The device structures were ITO/Eu(MeOBB)$_3$:PVK/PBD:PMMA/Ca/Al. For doping concentrations of 1:2, 1:5, 1:10 and 1:15 of Eu(MeOBB)$_3$ compared (by weight) to PVK, there was relatively stronger emission from PVK compared to the red-emitting Eu^{3+} ion. However, at a 1:1 concentration, there was very little emission from PVK and relatively brighter Eu ion emission (See Figure 5-19). The emission peak at approximately 616 nm was largely due to the Eu^{3+} ion (See Figure 5-19). Due to the lower brightness of the europium complex molecules, there was a relatively stronger emission from PVK as the voltage was increased. This suggests that at higher voltages, there is increased injection which leads to recombination on the PVK molecules. This voltage-dependent behavior suggests electroluminescence modified by trapping centres.

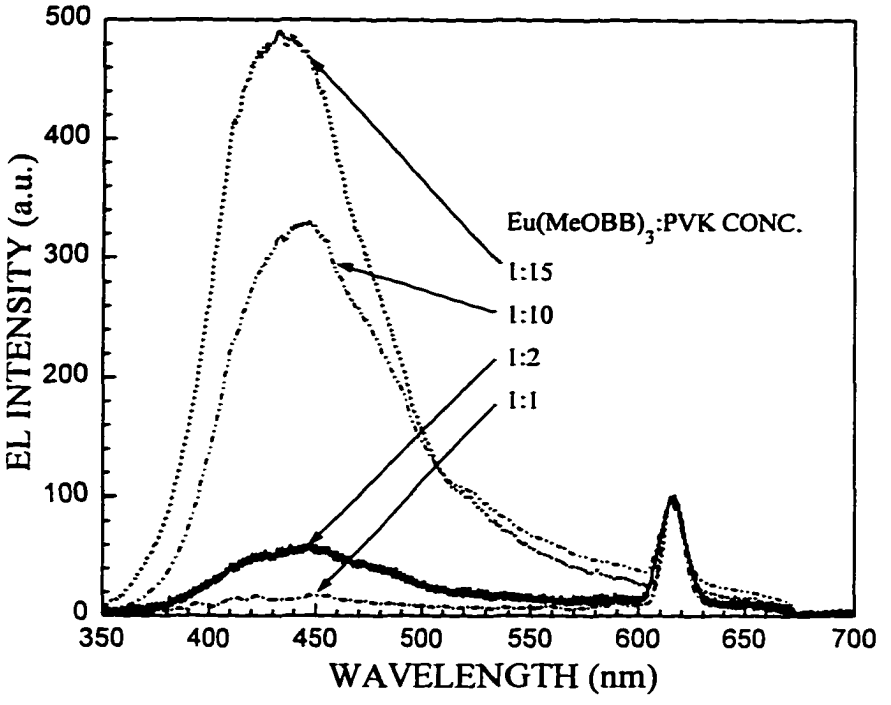

Figure 5-19. Concentration Dependence of $Eu(MeOBB)_3$ EL Spectra

The voltage-dependent behavior of the two-layer LEDs is modified by the filling of traps within the PVK layer. At low doping concentrations, there is a relatively low concentration of lanthanide-complex trapping centres compared to PVK molecules. As a result, electroluminescence originates from the trap sites and PVK molecules. For low current levels and high doping concentrations, the lanthanide-complex trap sites are the source of electroluminescence. At high current operation, the trap sites become filled and EL also originates from PVK. Figure 5-20 shows one possible scenario for the role of the lanthanide complexes as trapping centres within the PVK layer. The lanthanide-(benzoylbenzoate) molecules may serve as electron and/or hole traps within the PVK layer. However, a more detailed analysis

of the energy levels of the lanthanide complexes must be known in order to determine the current transport and carrier recombination mechanisms.

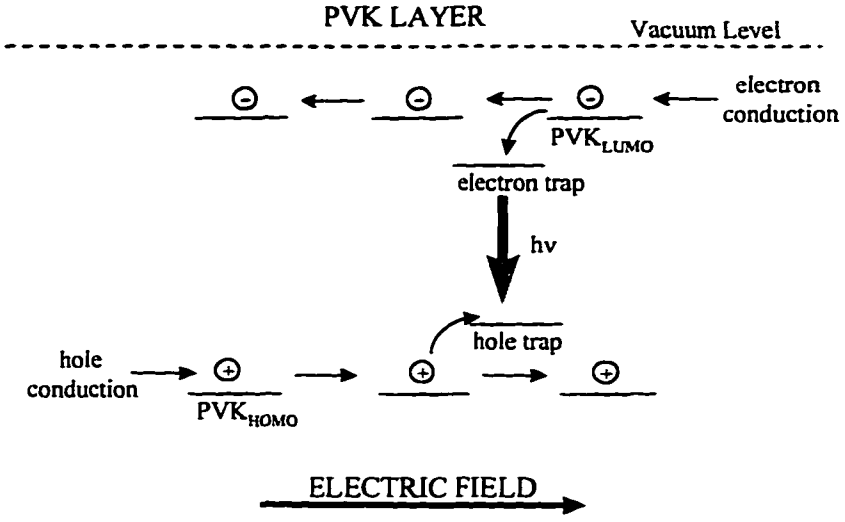

Figure 5-20. Trapping Processes in PVK

The quantum efficiency of electroluminescence in the lanthanide complexes was also studied. For the two layer devices, the maximum EL quantum efficiency was 0.08 % photons/electron at a driving voltage of 20 Volts DC. The plot of EL quantum efficiency vs. Voltage is shown in Figure 5-21.

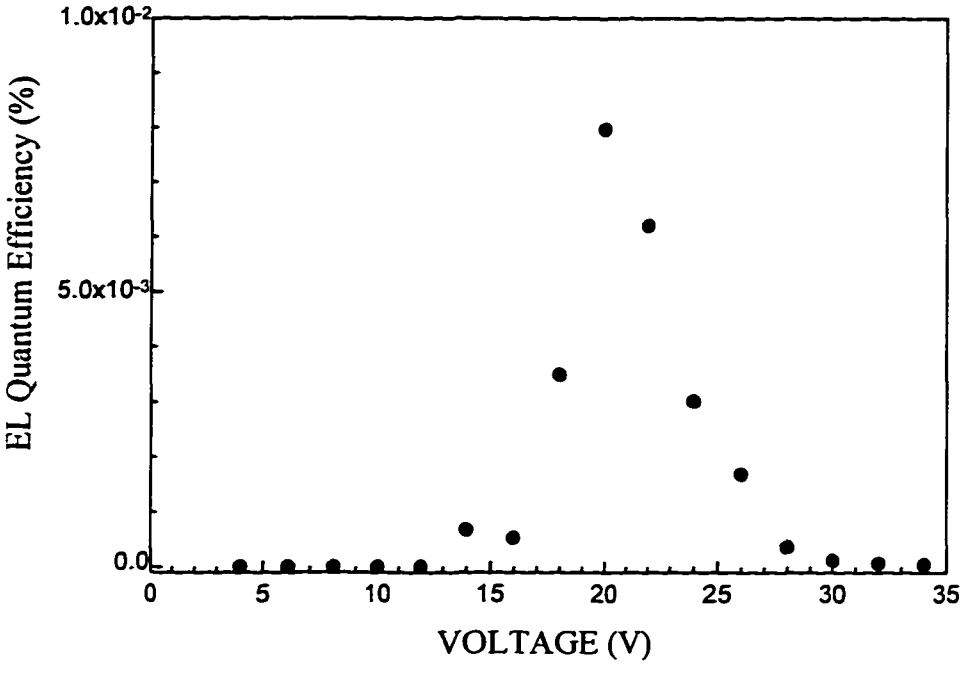

Figure 5-21. EL Quantum Efficiency vs. Voltage for Two-Layer Tb-complex LEDs Device Structure: ITO/$Tb(MeOBB)_3$:PVK (1:15)/PBD:PMMA/Ca/Al

5.9 Conclusions

New thermally stable luminescent lanthanide-(benzoyl)benzoate complexes, $Tb(MeBB)_3$, $Tb(MeOBB)_3$ and $Eu(MeOBB)_3$, were synthesized and their absorptive and luminescent properties were studied. Single layer LEDs were fabricated from the Tb or Eu complex combined with PVK and butyl-PBD, and these devices showed EL spectra that are attributed to emission from the Tb^{3+} or Eu^{3+} ions. Two layer LEDs fabricated from the Tb complex showed improved brightness, compared to single layer devices, with a maximum brightness of 45 cd/m^2 at an operating voltage of 24 volts. The two layer $Eu(MeOBB)_3$ LEDs also showed better light output compared to

the single-layer devices based on the Eu complex. The higher brightness values of $Tb(MeOBB)_3$ devices compared to $Eu(MeOBB)_3$ LEDs is due to the higher PL quantum efficiency of the Tb complex and the higher luminous efficiency of the eye in the green region of the spectrum. PL studies show that the $La(MeOBB)_3$ molecules act as recombination centers for charge carriers within the PVK layer. However, while PVK aids in charge transport, the possible lack of energy transfer from the PVK molecules to the La complexes may limit the overall brightness of the LEDs.

REFERENCES

1. J. Kido, H. Hayase, K. Hongawa, K. Nagai and K. Okuyama, *Appl. Phys. Lett..*, **65** No. 17, pp. 2124 - 2126, (1994).

2. J. Kido, K. Nagai, Y. Okamoto and T. Skotheim, *Chem. Lett.*, pp. 1267 - 1268 (1991).

3. N. Takada, T. Tsutsui and S. Saito, *Jpn. J. Appl. Phys.* **33** Part 2, No. 6B, pp. L863 - L866, (1994).

4. T. Sano, M. Fujita, T. Fujii, Y. Hamada, K. Shibata and K. Kuroki, *Jpn. J. Appl. Phys.* **34** Part 1, No. 4A, pp. 1883 - 1887, (1995).

5. J. Kido, K. Nagai and Y. Okamoto, *J. Alloys and Compounds*, **192** pp. 30 - 33, (1993).

6. J. Kido, W. Ikeda, M. Kimura and K. Nagai, *Jpn. J. Appl. Phys.* **35**, Pt. 2, No. 3B, pp. L394 - L396, (1996).

7. W. Dawson, J. Kropp and M. Windsor, *J. Chem. Phys.* **45** No. 7, pp. 2410 - 2418, (1966).

8. A. Heller and E. Wasserman, *J. Chem. Phys.*, **42** pp. 949 - 955, (1965).

REFERENCES (Continued)

9. R. Gudmundsen, O. Marsh, and E. Matovich, *J. Chem. Phys.* **39**, No. 2, pp. 272 - 274, (1963).

10. C. Claude, Ph.D. Dissertation, Polytechnic University, (1996).

11. S. R. Radel and M. H. Navidi, Chemistry (2nd Ed.), West Publishing Co., pp. 311, (1994).

12. P. Atkins, *Physical Chemistry (Fifth Ed.)*, W. H. Freeman and Co., New York, pp. 451 - 456, (1994).

13. G. H. Dieke, *Spectra and Energy Levels of Rare Earth Ions in Crystals*, Interscience Publishers, New York, pp. 243 - 261, (1968).

14. R. E. Whan and G. A. Crosby, *J. Mol. Spectr.* **8** pp. 315 - 327, (1962).

15. A. V. Hayes and H. G. Drickamer, *J. Chem. Phys.* **76** pp. 114 - 115, (1982).

16. D. M. Pai, J. F. Yanus and M. Stolka, *J. Phys. Chem.*, **88** pp. 4714 - 4717, (1984).

17. H. Tokuhisa, M. Era, T. Tsutsui and S. Saito, *Appl. Phys. Lett.*, **66**, No. 25, pp. 3433 - 3435 (1995).

18. G. E. Buono-Core, H. Li and B. Marciniak, *Coord. Chem. Rev.* **99**, pp. 55 - 87, (1990).

REFERENCES (Continued)

19. M. L. Bhaumik and M. A. El-Sayed, *J. Chem. Phys.* **42**, pp. 787 - 788, (1965).

20. M. L. Bhaumik and C. L. Telk, *Opt. Soc. Am.* **54,** No. 10, pp. 1211 - 1215, (1964).

21. H. Tokuhisa, M. Era, T. Tsutsui and S. Saito, *Appl. Phys. Lett.* **66** pp. 3433 - 3435, (1995).

22. A. Edwards, T. Y. Chu, C. Claude, I. Sokolik, Y. Okamoto, and R. Dorsinville, *Synthetic Metals*, **84**, Nos. 1-3, pp. 433 - 434 (1997).

23. A. Edwards, I. Sokolik, R. Dorsinville, C. Claude, T. Y. Chu and Y. Okamoto, *J. Appl. Phys.*, Accepted for Publication (1997).

CHAPTER SIX

6. CHARACTERIZATION OF BLUE EMITTING DEVICES

This chapter discusses photoluminescence and electroluminescence in poly(benzoyl-1,4-phenylene) (PBP). PBP is a soluble blue-emitting poly(para-phenylene)-type polymer that has good film-forming properties and shows exceptional thermal stability. The implementation of blue-emitting electroluminescent materials combined with the green and red lanthanide emitters enables the development of white light emitting diodes (LEDs) spanning the entire visible spectrum. For multicolor displays, optical filters may be employed to select the desired emission color. Multicolor displays can also be developed by combining various colored LEDs in a multipixel diode array.

6.1 Introduction

Many conjugated polymers have been used in the emitting and transport layers of organic light emitting diodes (LEDs). The application of conjugated polymers as active layers and transport materials in LEDs offers several advantages such as relatively low cost synthesis and easy processing by spin casting from solution. Also, the charge transport properties of these polymers can be improved by chemical doping or by incorporating functional groups along the chain of the polymer. Another advantage is that the bandgap, and therefore the emitting wavelength, can be

chemically tailored by using polymer engineering techniques. Consequently, LEDs based on a wide variety of polymers covering the entire visible spectral range have already been prepared by several research groups.

Electroluminescence (EL) was discovered in the conjugated polymer poly(p-phenylene vinylene) (PPV) in 1990 by Burroughes et. al.[1] The chemical structure of PPV is shown in Figure 6-1. The PPV-based devices developed by Burroughes and coworkers emitted in the green-yellow region of the spectrum with relatively moderate electroluminescence quantum efficiencies of about 0.05 % photons/electron. PPV thin films show green-yellow photoluminescence (PL) with the PL band centered near 2.2 eV. The PPV polymer can be deposited in optical quality thin films but requires a precursor route for processing. For lower cost processing, soluble organic polymers are a highly desirable alternative for producing optical quality thin films. Since Burroughes' initial work, interest in the conducting and luminescent properties of conjugated polymers systems increased because of their potential uses in optoelectronic technology.[2-5]

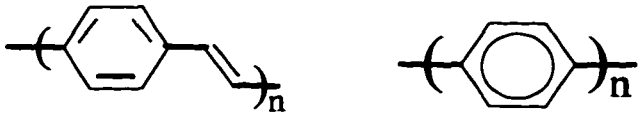

PPV PPP

Figure 6-1. Chemical Structures of PPV and PPP

The development of thermally stable blue-emitting materials is an important step for the possible application of conjugated polymers in multicolor flat-panel displays. Poly(p-phenylene) (PPP) was the first conjugated polymer system for which blue light emitting diodes were realized[6]. Poly(p-phenylene) has good thermal and luminescent properties but PPP, like PPV, requires a chemical precursor route for processing. Since the first observation of EL in PPP, blue EL has been reported from different conjugated polymer systems such as PPP-type ladder polymers[7,8], poly(alkylfluorene)[9], poly(pyridine)[10], non-conjugated polymers like poly(N-vinyl carbazole)[11], polymer blends[12,13] and copolymers[14,15]. The chemical structure of PPP is shown in Figure 6-1.

The availability of soluble organic polymers will help to provide low cost solutions for LED fabrication. Because of the poor solubility of PPP, PPP-type derivatives have been developed by attaching lateral substituents to the phenyl rings along the PPP backbone. Similar to PPV or PPP, the resulting PPP derivatives should also have good thermal, optical and conductive properties for these materials to be useful in display applications. To date, several PPP derivatives have been synthesized by attaching benzoyl substituents to poly(paraphenylene). For example, poly(4,4'-benzophenone) and poly(2,5-benzophenone) (PBP) were synthesized by Philips et. al.[16] Both of these compounds are thermally stable up to 400^0 C. Poly(4,4'-benzophenone) is completely insoluble and highly crystalline while poly(2,5-benzophenone) is soluble and amorhphous. The chemical structures of poly(4,4'-benzophenone) and poly(2,5-benzophenone) are shown in Figure 6-2.

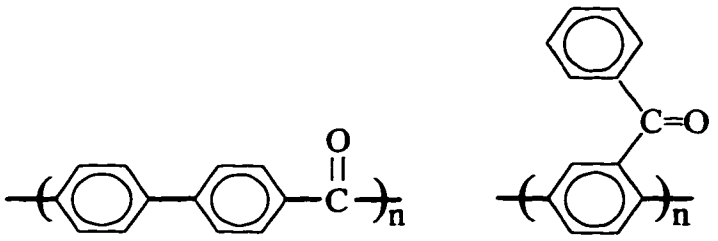

Poly(4,4'-benzophenone) Poly(2,5-benzophenone)

Figure 6-2. Chemical Structures of Benzophenone Polymers

Wang and coworker also synthesized poly(2,5-benzophenone) (PBP) derivatives and found that, based on their chemical analysis, there were several isomers of PBP.[17] From their studies, they proposed that the different isomers were due to variations in the placement of the lateral benzoyl groups along the polymer chain. The two isomers synthesized by Wang and colleague were poly(benzoyl-1,4-phenylene) types A and B (PBP-A and PBP-B, respectively). See Figure 6-3 for the chemical structures of PBP isomers.

In the upcoming sections I will report the photoluminescent and electroluminescent properties of poly(benzoyl-1,4-phenylene) (PBP). PBP is a PPP derivative, where the introduction of the benzoyl side group makes it soluble, and thin films can be readily obtained by spin casting directly from solution. Thus, the use of precursor routes, which is necessary for the preparation of PPP thin films, can be avoided. Additionally, PBP has high thermal stability (i.e., shows no thermal degradation below 500° C[12]) which is a highly desirable material property for stable device performance.

PBP shows bright blue photoluminescence and multilayer light emitting diodes (LEDs) fabricated with this polymer as the active material emit blue electroluminescence corresponding to the photoluminescence spectrum of PBP. The electroluminescence spectra of the multilayer devices will be reported in later sections.

6.2 Chemical Properties of PBP

Poly(benzoyl-1,4-phenylene) (PBP) was synthesized by the coupling of 2,5-dichlorobenzphenone using a nickel catalyst.[17] Depending on the synthesis conditions, two isomers of PBP can be realized using this procedure: head-to-head (PBP-A) or head-to-tail (PBP-B). Both PBP isomers are soluble in polar organic solvents such as chloroform and methylene chloride. Thin optical quality films can be readily produced by spincasting techniques. The chemical structures of the two PBP isomers are shown in Figure 6-3.

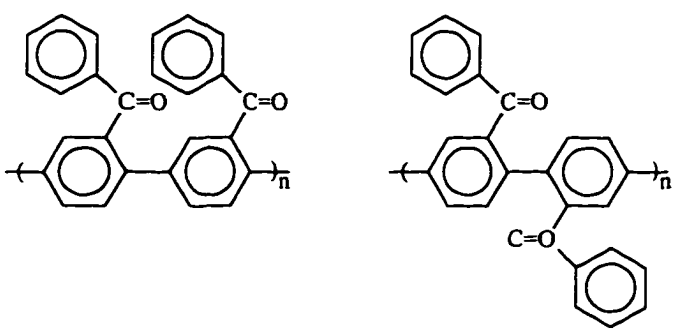

head-to-tail head-to-head

Figure 6-3. Chemical Structures of PBP Isomers

Light emitting diodes may have high current densities within the organic layers during device operation. As such, the organic layer should have a high thermal stability to improve device performance and to extend device operating lifetimes. Based on thermal gravimetric analysis (TGA) measurements, the two PBP isomers show high thermal stability up to 500^0 C which makes this class of polymers highly desirable for optoelectronic applications. The thermal gravimetric analysis curves for PBP isomers A and B in air are shown in Figure 6-4. The TGA curves were obtained while heating the samples from room temperature to 1000^0 C at a heating rate of 10^0 C/min.

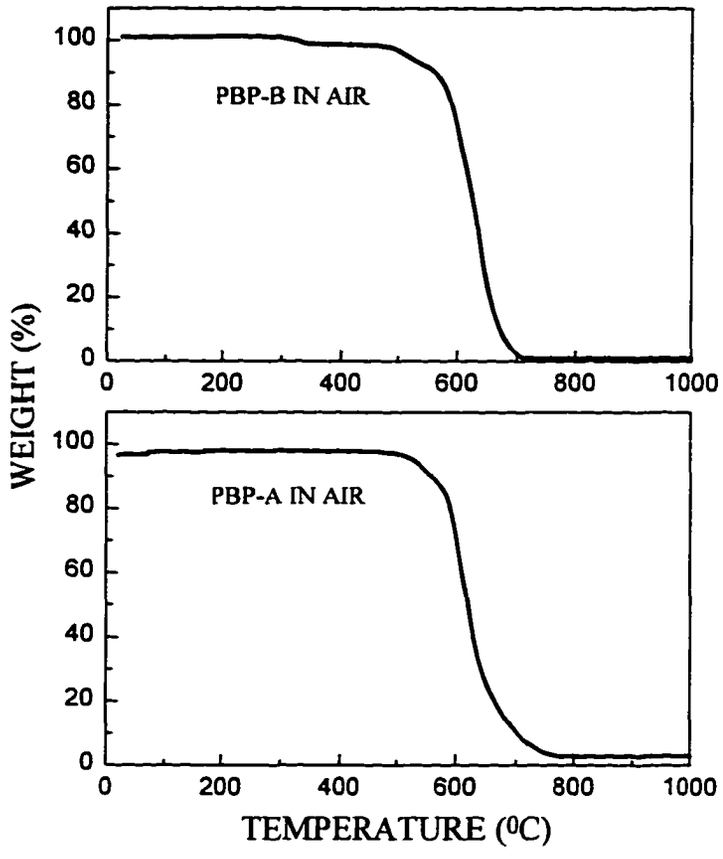

Figure 6-4. TGA Curves for PBP Isomers in Air.

6.3 Photoluminescence in PBP

The absorption and PL spectra of the PBP-A isomer were measured in dilute chloroform solution. The absorption spectrum extends in the UV region below 380 nm (See Figure 6-5). No vibronic structure was observed in the absorption spectrum. The low energy absorption maximum is located at 328 nm. From the long wavelength tail of the absorption spectrum, the energy gap is estimated to be approximately 3.3 eV. The PBP-A isomer shows a broad featureless emission band in the blue-green

region of the spectrum. For excitation at 380 nm, the PL emission peak is located at approximately 441 nm. The quantum efficiency of photoluminescence in 10^{-6} Molar chloroform solution is only 0.23 % when exciting at 366 nm.

The PLE (for emission at 440 nm) maximum is located at 387 nm and is significantly red-shifted from the absorption spectrum (See Figure 6-5). This difference cannot be explained by the familiar Stokes-shift due to energy losses occurring when the excitation energy decays from higher excited states to the lowest excited state. This is energy shift is not likely caused by impurities within the sample but is more likely due to the presence of more than one isomer within the polymer sample. This variation in isomer content leads to: (1) the presence of strongly absorbing non-emitting polymer segments (with shorter chain lengths) that give rise to the dominant absorption band below 380 nm and (2) fluorescent polymer segments with longer chain lengths corresponding to the PLE band between 380 and 440 nm.

In the solid state there is significant quenching of the PL from the PBP-A thin film samples. The corresponding PL quantum efficiency in the solid state is estimated to be much less than 0.5 %. Based on our measurements, we have estimated the fluorescence lifetime of PBP-A in solution and in the solid state to be less than 500 ps which is the best resolution of our experimental set-up. Due to the very low PL quantum efficiency in solution and in the solid state, no LEDs were fabricated from the PBP-A isomer.

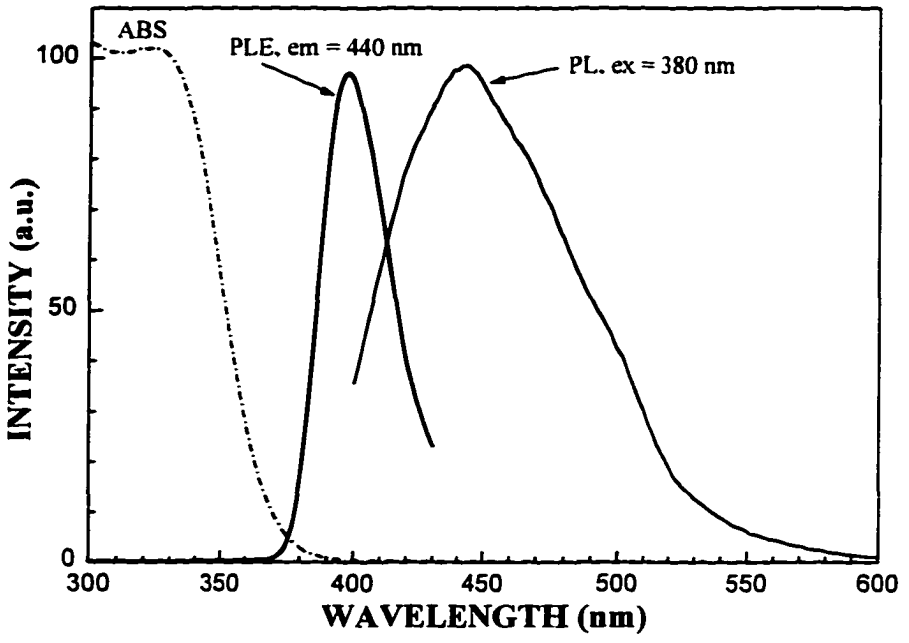

Figure 6-5. PL Spectra of PBP-A in 10^{-6} M Chloroform Solution

The optical properties of PBP-B were also studied in dilute chloroform solution and in the solid state; PBP-B shows bright blue PL in solution. In solution, the PL quantum efficiency (Φ) of the more regular structured isomer (head-to-tail) of PBP depends on the solvent. In dilute chloroform (an effective solvent for PBP which we have used for spin-coating) solution (10^{-6} M), we measured $\Phi_{PBP} \approx 15\%$ when exciting at the peak of the PLE spectrum. PBP films also show bright blue photoluminescence with a maximum at 433 nm. Due to the large UV-blue absorbance of PBP, concentration dependent effects have been observed in concentrated PBP solutions and in thick films; there is a gradual red-shift of the PL spectra with increasing solution concentration or increasing film thickness.

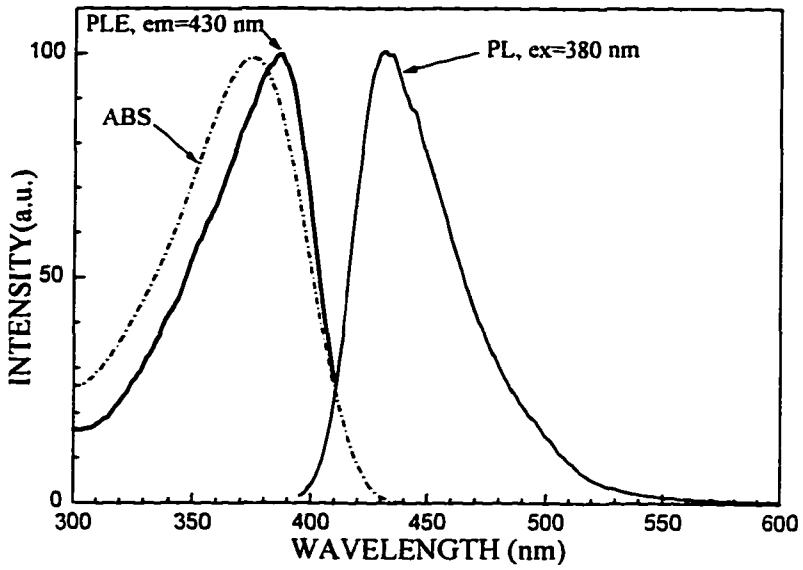

Figure 6-6. ABS, PL and PLE of PBP-B in Chloroform

PBP-B has a broad featureless absorption spectrum with a maximum at 381 nm. Figure 6-7 shows the absorption, PLE and PL spectra of a thin (*ca.* 15 nm) PBP film. By extrapolating the absorption spectrum, the optical bandgap was estimated to be 2.8 eV, which is wider than that of PPP.[18] This is probably due to the introduction of the benzoyl side groups which leads to an out-of-plane rotation of the phenyl rings and therefore to a decrease of the conjugation length relative to PPP.[19] The PL spectrum shows a partially resolved vibronic structure due to the coupling of excitonic transitions to the bond-stretching vibrations of the carbon backbone.[20,21] The emission lies in the blue with vibronic peaks at 433 nm and 454 nm. The ratio of the peak intensities depends on the film thickness because of the large penetration depth of the exciting light and reabsorption of the emitted radiation.

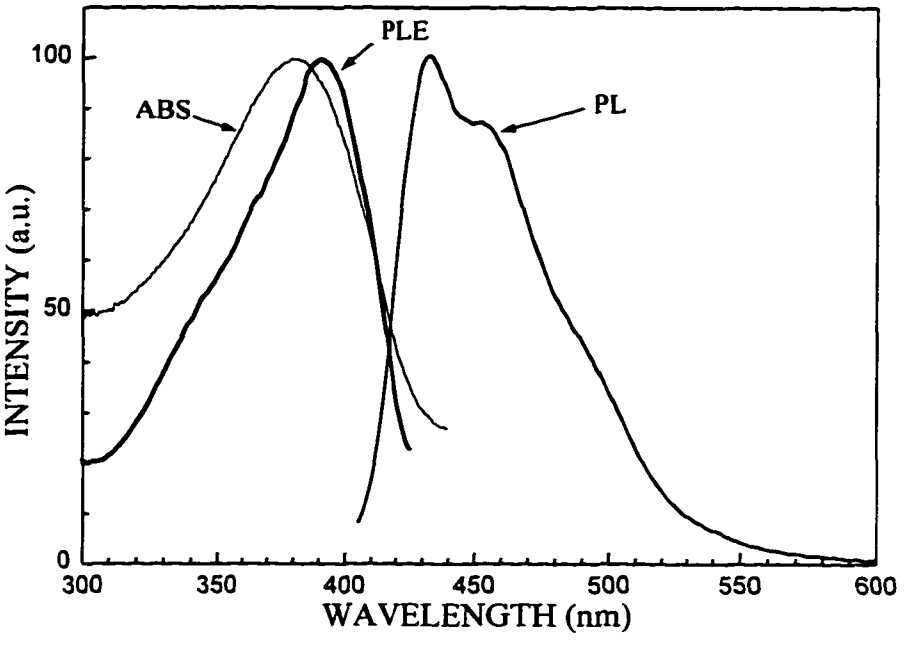

Figure 6-7. ABS, PL and PLE of PBP-B Thin Film

Absorption (dotted line), PLE (dashed line) and PL (solid line) spectra of a PBP film. The excitation wavelength for the PL spectrum is λ_{ex} = 390 nm and the emission wavelength for the PLE spectrum is λ_{em} = 430 nm. Film thickness ~ 15 nm. These measurements were performed at 300 K.

Figure 6-7 shows that the mirror image relation between absorption and emission spectra is not retained. The polymer sample consists of a mixture of chains with different conjugation lengths and thus, different π-π^* transition energies. Superposition of the absorption of species with different transition energies should lead to a broad structureless absorption spectrum. Emission always occurs from states with the lowest energy, since energy is transferred from states with higher π-π^* transition energy (polymer segments with shorter conjugation length) to states with

lower energy (polymer segments with longer conjugation length) before radiative deactivation takes place.[22] Considering that each excited state has two choices for deactivation, either to give away its energy nonradiatively to the lattice or to transfer the energy to an excited state of lower energy, it becomes clear that nonradiative losses increase when the polymer is excited into higher lying states. This is consistent with our experimental observation that the PL quantum yield decreases with increasing excitation energy and explains why the PLE spectrum is narrower and red-shifted in comparison to the absorption spectrum.

The PL quantum yield Φ of PBP films was estimated relative to a thin (*ca.* 20 nm) *tris*(8-hydroxyquinoline) aluminium (Alq_3) film. It was reported that Φ_{ALQ3} in solid state lies between 8 %[23] and 32 %[24]. We obtained, for a thin (*ca.* 15 nm) PBP film, $\Phi_{PBP} \approx 0.86\ \Phi_{ALQ3}$, when exciting the film at the peak of its PLE spectrum.

6.4 Electroluminescence in PBP-B

Electroluminescence was first observed in the benzophenone monomer (BP) by Hoshino and Suzuki.[25] These researchers employed an ITO/PMPS/BP:PMMA/PBD/Al three-layer cell structure, where PMPS is poly(methylphenylsilane), PMMA is poly(methylmethacrylate) and PBD is 2-(4-biphenyl)-5-(4-tert-butylphenyl)-1,3,4-oxadiazole (butyl-PBD). The chemical structures of BP, PMPS and PMMA are shown in Figure 6-8 and the chemical structure of butyl-PBD is shown in Figure 6-9. The PMPS and butyl-PBD layers were used for hole transport and electron transport, respectively. The active layer of the

three layer LED was composed of BP (10 wt. %) dispersed in PMMA, an inert transparent polymer binder. Unlike the vast majority of organic polymers, the electroluminescence in BP originates from the radiative decay of the triplet excited states. The electroluminescence spectrum is blue-green and shows vibronic peaks at 420, 450 and 480 nm corresponding to the phosphorescence spectrum of BP. Based on their experiments, Hoshino and Suzuki determined that carrier recombination occurs on BP monomer molecules located within the active layer. In the upcoming sections, we will study EL in the benzophenone-type polymer PBP-B.

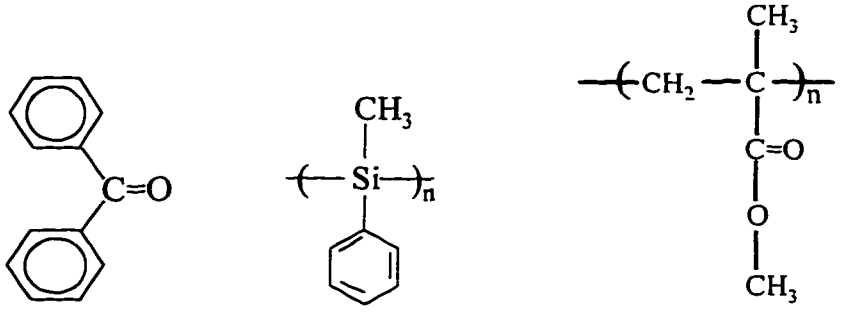

Figure 6-8. Chemical Structures of BP, PMPS and PMMA

To study electroluminescence in PBP-B, light emitting diodes were fabricated in single and multilayer cell configurations. Initially, single layer LEDs were fabricated with the ITO/PBP/Ca/Al cell structure. These devices showed very weak UV-blue EL that was barely visible in a dimly lit room. The weak EL intensity probably occurred because charge injection from the electrodes into the PBP layer was poor (due to high interfacial energy barriers) and/or unbalanced (due to uneven energy barriers). Also, charge transport may not have been efficient within the PBP-B

layer. In some cases, the brightness may be improved by varying the thickness of the organic layer. In our case, the brightness was still very low for thicknesses from 40 to 100 nm. For very thin PBP-B layers, a significant number of charge carriers may travel from the injecting electrode to the opposite electrode without recombining with carriers of the opposite sign. For very thick and possibly low-mobility PBP-B layers, a significant portion of the carriers may not reach the recombination zone to recombine with carriers of the opposite sign. Concentration quenching may have also played a significant role in limiting the EL efficiency of the single layer devices.

To improve the performance of the single layer LEDs, thin films of PBP-B were also doped with butyl PBD (to improve electron transport) and/or PVK (to enhance hole transport). See Figure 6-9 for the chemical structures of PVK and butyl-PBD. Light emitting diodes with the ITO/PBP:PBD/Ca/Al and ITO/PBP:PVK/Ca/Al structures showed blue EL spectra that were due to PBP. The initial devices' active layers contained PBP:PBD and PBP:PVK in 1:1 weight ratios. When operating at low voltages, devices doped with PBD were slightly brighter than the devices doped with PVK. However, at higher voltages, the devices containing butyl-PBD tended to fail faster than PVK-doped doped devices. Butyl-PBD has a lower melting point than PBP or PVK, and tends to: (1) crystallize slowly at room temperature and (2) crystallize rapidly when heated. The devices doped with butyl-PBD had a maximum brightness of 1-2 cd/m^2. However, the devices with PVK lasted longer and performed better at higher operating currents because of the superior thermal stability of PVK compared to butyl-PBD. The single layer devices prepared with PVK showed a

maximum brightness of approximately 21 cd/m^2 for a PBP:PVK concentration of 1:3 by weight. For doping concentrations of 1:2 and 1:4 by weight, the EL originated from PBP-B but the brightness values were significantly less than 21 cd/m^2. See Figure 6-11 for the current- and brightness vs. voltage curves for these single layer devices.

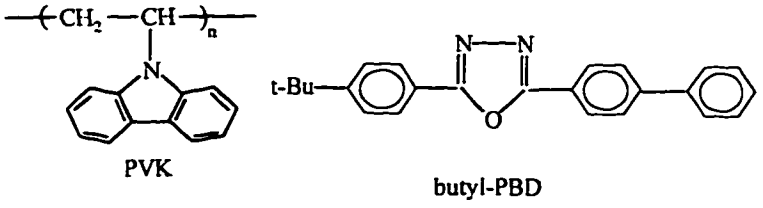

Figure 6-9. Chemical Structures of PVK and Butyl-PBD

We have used PVK as a polymer matrix for PBP-B because it has good film-forming properties and this polymer is largely a hole transport material with very low electron mobility. Also the PL spectrum of PVK overlaps with the PLE spectrum of PBP, thereby enabling efficient energy transfer from the transport material PVK to the emitter PBP. This energy transfer may play a role in improving the EL of PBP. As an electron transport material we have utilized butyl-PBD to be combined with PBP-B. PBD will also allow for efficient energy transfer to PBP-B because its emission spectrum overlaps with the absorption spectrum of PBP-B. Since PBD films tend to crystallize over time, this compound was dissolved in the PBP layer to improve electron transport in the single layer devices.

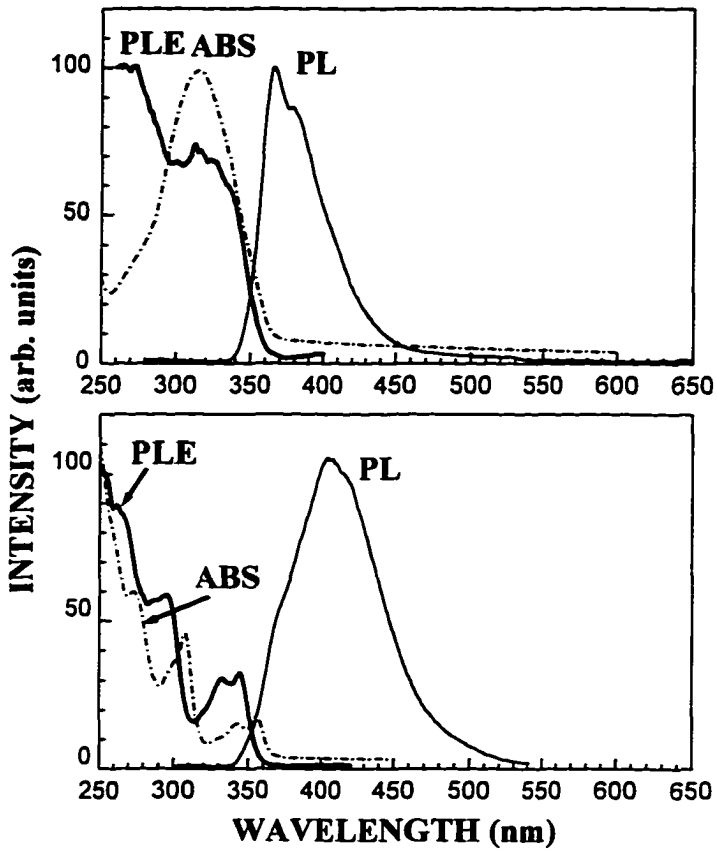

Figure 6-10. Absorption and Luminescence Spectra of PVK and Butyl-PBD

Top: butyl PBD; Bottom: PVK; PL for excitation at 280 nm (PVK) and 260 nm (PBD); PLE for emission at 440 nm (PVK) and 420 nm (PBD).

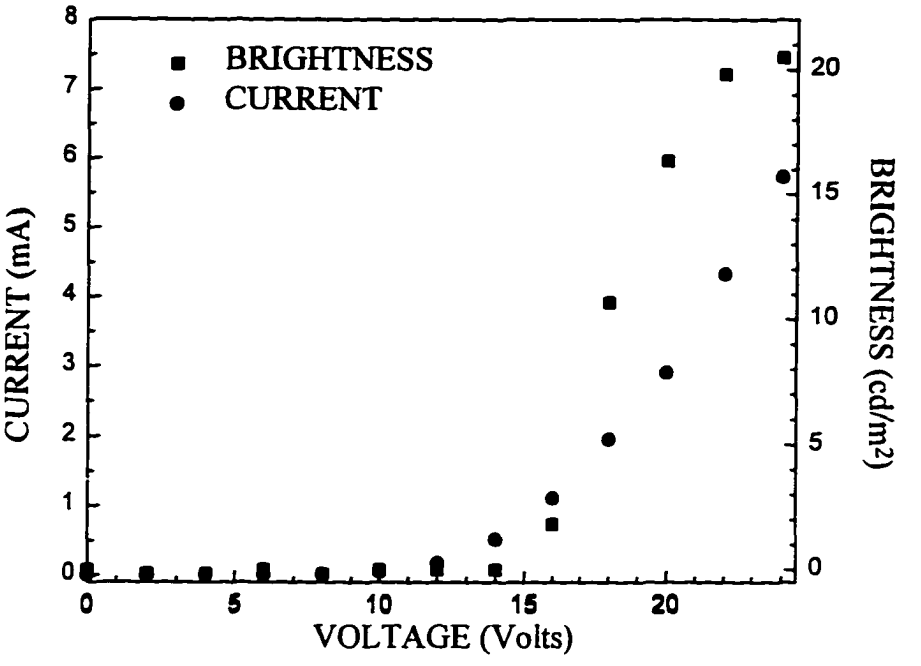

Figure 6-11. Current- and Brightness vs. Voltage for an ITO/PBP:PVK/Ca/Al LED Thickness of Organic Layer: 85 nm; Active layer: PBP:PVK doping is 1:3 by weight.

To improve the device performance, single layer LEDs were also fabricated with the ITO/PBP:PBD:PVK/Ca/Al configuration. The single layer devices with PBP, PBD and PVK showed EL spectra originating from the PBP molecules. No EL was observed from the PBD or PVK. Device performance was not significantly better than the single layer devices containing PBP-B and PVK in the active layer because charge injection and transport could not be fully optimized in the single layer structure.

To optimize injection of both carriers, multilayer devices were constructed.[26] The two layer devices had ITO/PBP:PVK/PBD:PMMA/Ca/Al cell structures. The

active layer of the double-layer devices contained a 1:1, 1:2, 1:3, 1:4 or 1:5 weight ratio of PBP to PVK. The electron transport layer was composed of butyl-PBD which has good electron transport properties and poly(methy methacrylate) (PMMA) to retard the crystallization of butyl-PBD. The electron transport layer had a composition of 3:1 weight ratio of PBD to PMMA. For all doping concentrations of the active layer, the corresponding EL spectra showed emission spectra corresponding to PBP photoluminescence. In general, the double layer devices operated longer and at higher currents. The maximum brightness values of 100 cd/m^2 were achieved with devices containing a doping concentration of 1:3 for PBP compared to PVK.[27]

Fig. 6-12 shows the EL spectrum of the double-layer LED. Blue EL was observed with a maximum at 446 nm. The EL spectra resembled the PL spectrum of a PBP film with a thickness of *ca.* 25 nm, (See Fig. 6-12). Thus, we conclude that recombination of electrons and holes eventually leads to the formation of PBP singlet excited states which then undergo radiative deactivation. As such, the origin of EL in PBP-B is markedly different from the benzophenone monomer which shows EL from the triplet excited states. As seen in Fig. 6-12, the EL spectrum is featureless, unlike the PL spectra. We have observed that photooxididation of a PBP film with UV light also leads to the loss of the vibronic structure in the PL spectrum (See Fig. 6-13). Therefore, we assign the shape of the EL spectrum to the effect of oxidation of PBP by the residual oxygen when LEDs are operated. However, it is also important to note that the high operating temperature of the LED could (to a lesser degree) also be responsible for the loss of vibronic structure in the EL spectrum.

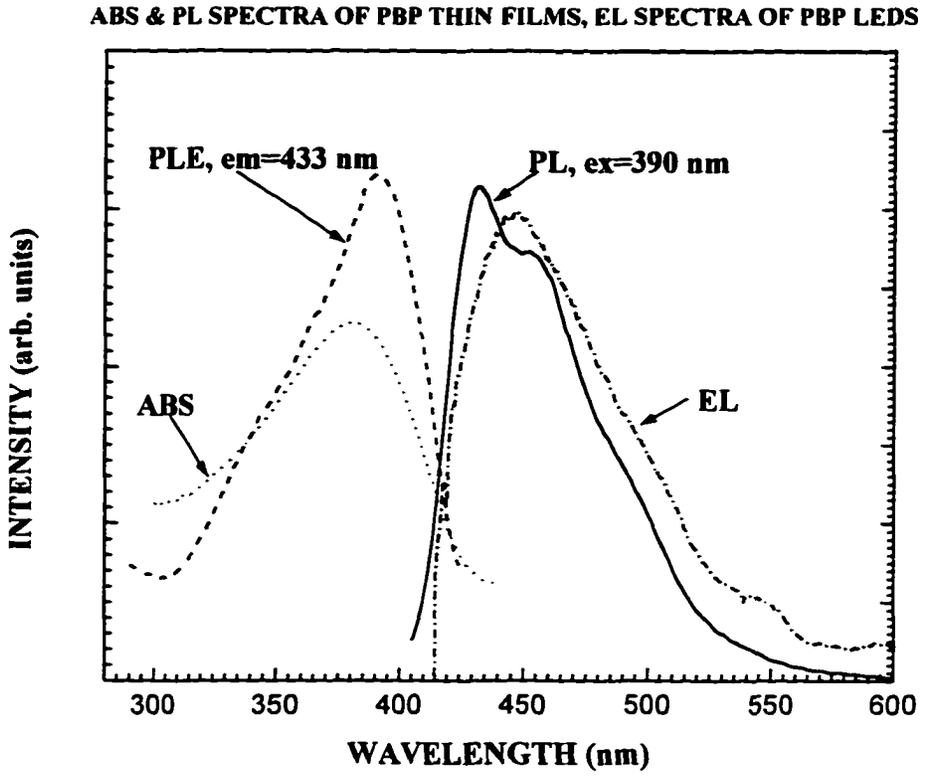

Figure 6-12. ABS & PL Spectra of PBP Films and EL Spectra of PBP LEDs

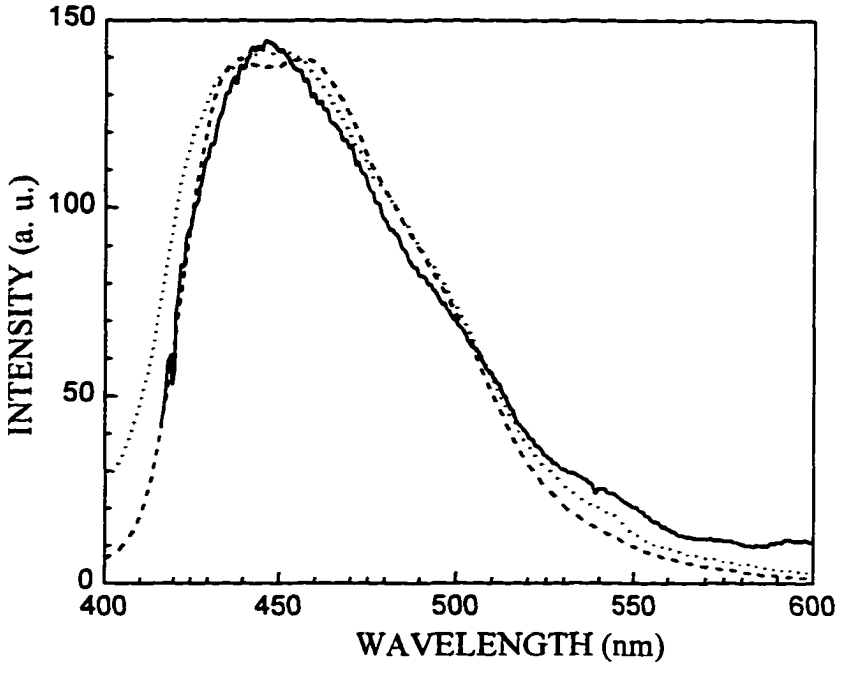

Figure 6-13. PL Spectra of Pristine & Photoxidized Films and EL Spectrum of LED

PL of Fresh Film: dashed line; PL of Photoxidized Film: dotted line; λ_{ex} = 390 nm for both films; Film Thickness: 25 nm; EL spectrum of the double-layer LED: solid line; All measurements were made at 300 K.

In Fig. 6-14 the current-voltage and brightness-voltage characteristics of a double- layer LED are shown. The maximum brightness of the LEDs was about 100 cd/m^2 and the external EL quantum efficiency was 0.17 % (photons/electron). The LEDs (thickness ≈ 80 nm) show turn-on voltages of about 12 V for current and EL. The turn-on voltage increases with the thickness of the device and, in contrast to inorganic LEDs, depends on the electric field strength. This implies a tunneling model for carrier injection in which the carriers are field-emitted through the barriers at the electrode/polymer interface.[28,29] However, a more detailed analysis of the I-V

characteristics is necessary to determine whether tunnelling or space-charge effects are the current-limiting processes in PBP-B.

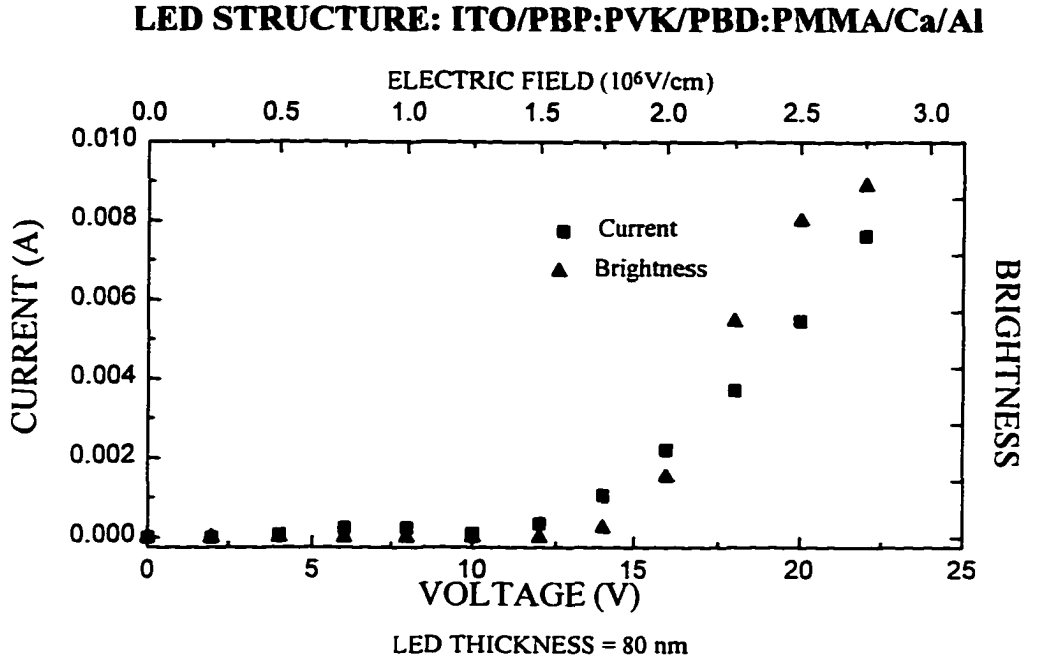

Figure 6-14. Current- and Brightness vs. Voltage Curves of Two-Layer PBP LEDs Current-voltage: (■); brightness-voltage: (σ); LED Structure: ITO/PBP-B:PVK/PBD:PMMA/Ca/Al; Thickness of device: 80 nm.

Three layer LEDs were also designed and constructed. The three layer devices with the ITO/PVK/PBP/PBD:PMMA/Ca/Al cell structure showed similar performance to the two layer LEDs. The EL originated from PBP-B and a maximum brightness of 100 cd/m^2 was observed.

6.5 Energy Transfer in PBP LEDs

The energy transfer processes occurring in the active layer of the two-layer PBP-B diodes, were investigated by analyzing the EL spectra of the LEDs and the PL spectra of films containing PBP-B, PVK or PBP-B and PVK in a 1:1 weight ratio. See Figure 6-15 for the PL spectra of the thin films and Figure 6-13 for the EL spectrum of the two layer LEDs with a PBP-B:PVK active layer. The ABS, PLE and PL spectra of PVK and PBP-B were discussed in earlier sections.

The PL spectrum of PVK overlaps with the absorption and excitation spectra of PBP-B. This allows for efficient energy transfer from PVK to PBP-B. In fact, when thin films containing PVK and PBP-B are photoexcited, the absorbed energy shows the profiles due to both compounds. For wavelengths below 350 nm, the absorption profile shows features of both polymers. Above 350 nm, the absorption profile reflects energy largely absorbed by PBP-B. When examining the excitation profile (for emission at 440 nm) of the composite film, the PLE spectrum resembles the absorption spectrum indicating that emission at 440 nm originates from the excitation of PVK and PBP-B. The corresponding emission spectrum shows a maximum at approximately 433 nm which is the emission peak for PBP-B. In general, the PL spectrum largely resembles the PL profile of PBP-B with a smaller contribution from PVK in the short wavelength tail of the emission spectrum.

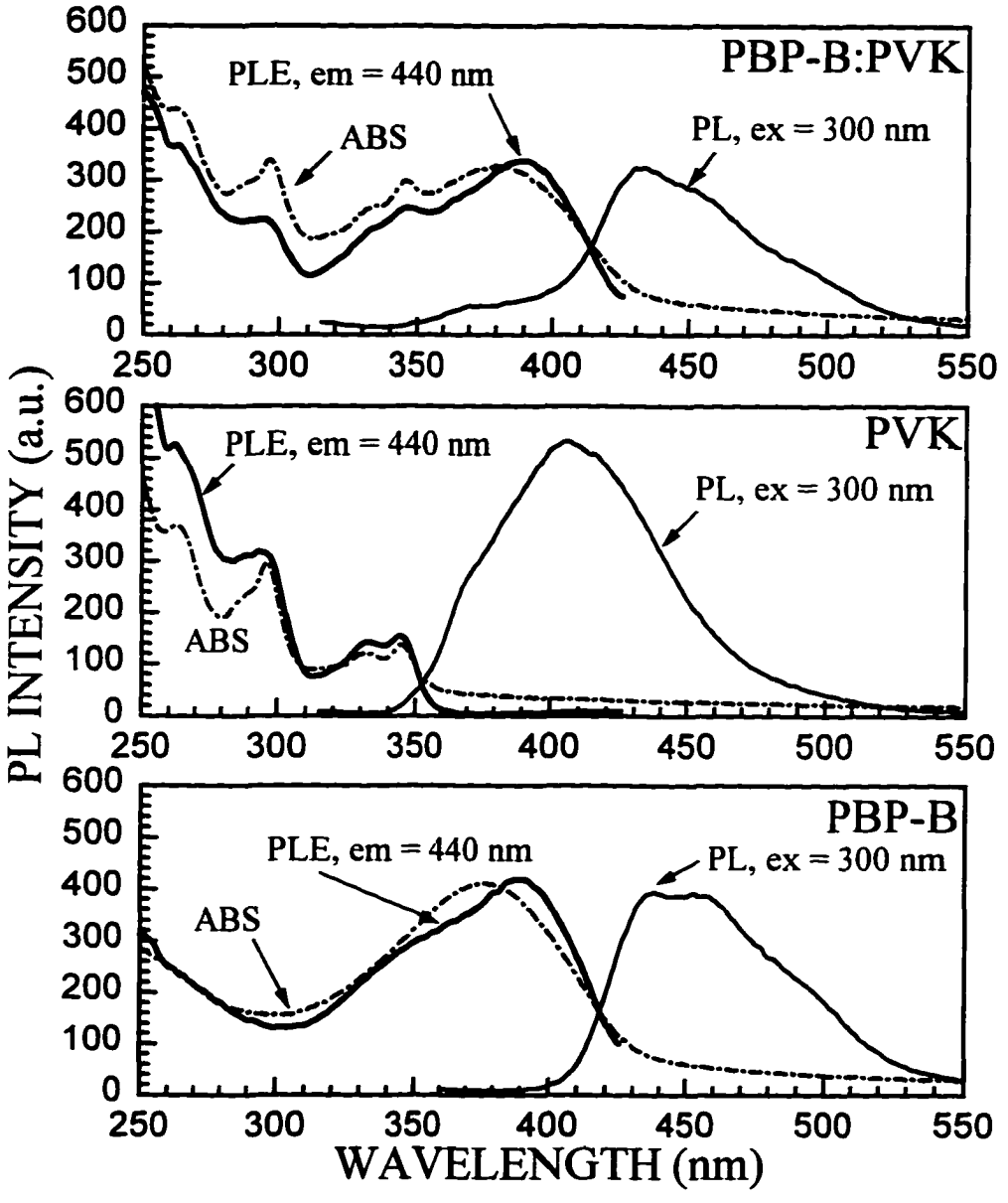

Figure 6-15. PL Spectra of PBP-B, PVK and PBP-B:PVK Films

Ratio of PBP-B to PVK: 1:1 by weight; Thickness of Films: ~ 30 nm

To fully determine the role of energy transfer processes in the composite film, the PL spectrum of the composite film was compared to the sum of the simulated PL of the individual films while normalizing for the energy absorbed by each compound. Based on our analysis, where roughly half of the energy is absorbed by each polymer, the emission is largely due to PBP-B. This indicates that there is energy transfer from PVK to PBP-B.

This energy transfer process should lead to an enhancement of the EL from PBP-B in the light emitting diodes. For carriers recombining on PBP-B, the EL originates from PBP-B. In addition, for carriers recombining on PVK, some of the energy is transferred (through radiative or non-radiative energy transfer processes) to PBP-B, thereby producing an increase in PBP-B electroluminescence. Figures 6-16 and 6-17 show this enhancement in the luminescence of PBP-B and the decrease in PVK contribution to photoluminescence.

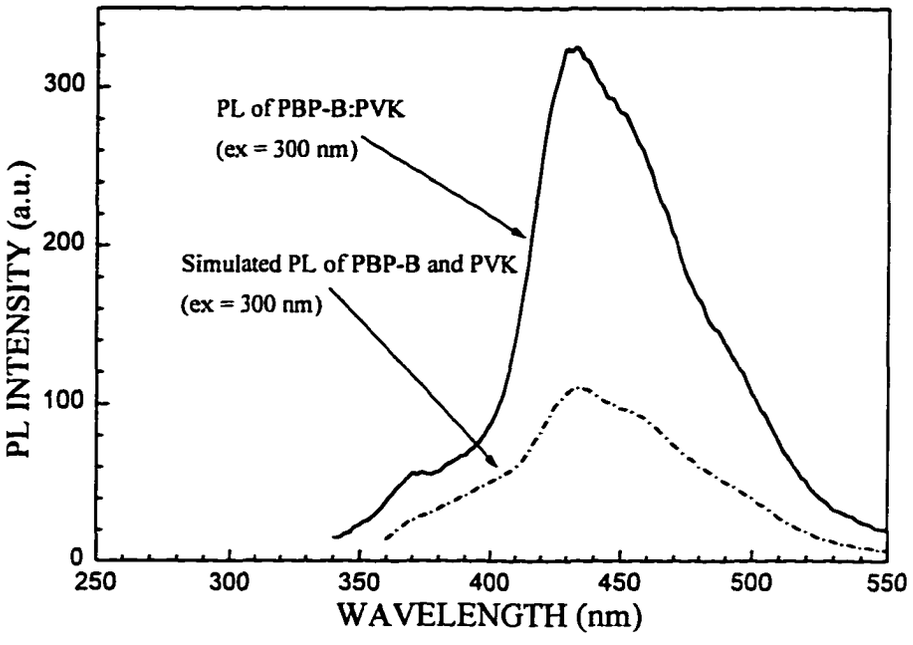

Figure 6-16. PL Spectrum of PBP-B:PVK and Simulated PL of PBP + PL of PVK

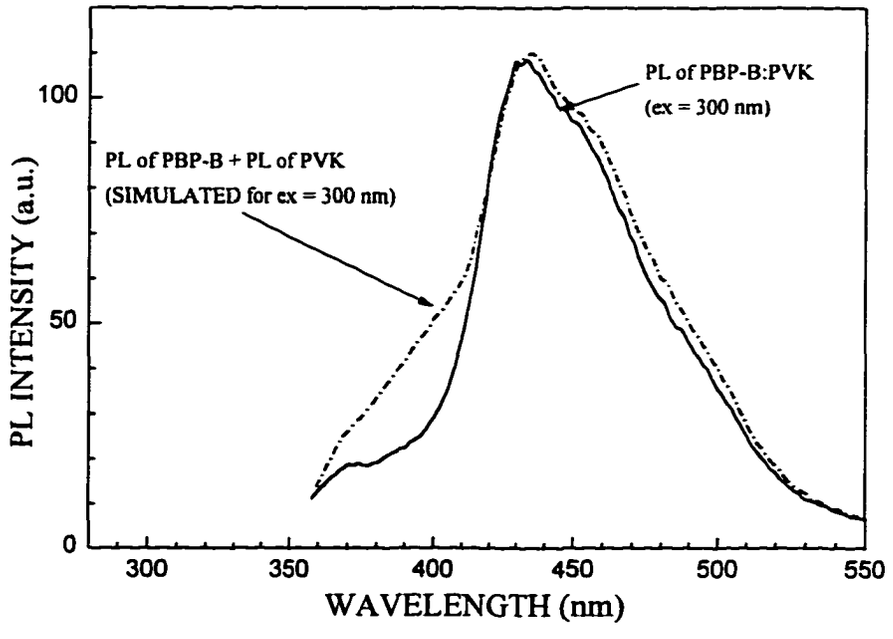

Figure 6-17. Normalized PL Spectra of PBP-B + PVK and PBP-B:PVK

6.6 Conclusions

In conclusion, blue LEDs have been successfully fabricated utilizing the novel emitter material PBP. The PL quantum yield in thin films of PBP is comparable to that of Alq_3, which is known to be a very efficient emitter material in organic LEDs. The peak wavelength of PL is 433 nm and the corresponding EL peak is 446 nm. The EL spectrum corresponds with the PL spectrum indicating that PL and EL originate from the same singlet excited state. Also energy transfer from PVK enhances the EL emission from PBP-B. The EL studies show devices with brightness values of about 100 cd/m^2, indicating that PBP-B is a promising material for electroluminescent display technology.

REFERENCES

1. J. H. Burroughes, D. D. C. Bradley, A. R. Brown, R. N. Marks, K. Mackay, R. H. Friend, P. L. Burns and A. B. Holmes, *Nature*, **347**, pp. 539 - 541, (1990).

2. P. L. Burn, A. B. Holmes, A. Kraft, D. D. Bradley, A. R. Brown, R. H. Friend and R. W. Gymer, *Nature*, **356** pp. 47 - 49, (1992).

3. C. Zhang, D. Braun and A. J. Heeger, *J. Appl. Phys.*, **73** No. 10, pp. 5177 - 5180, (1993).

4. M. Onoda, S. Morita, H. Nakayama and K. Yoshino, *Jpn. J. Appl. Phys.*, **32**, Pt. 2, No. 1A/B, pp. L82 - L85, (1993).

5. D. Braun , A. J. Heeger and H. Kroemer, *J. Elect. Mat.*, **20**, No. 11, pp. 945 -948, (1991).

6. G. Grem, G. Leditzky, B. Ullrich and G. Leising, *Adv. Mater.*, **4** No. 1, pp. 36 -37, (1992).

7. J. Grüner, P. J. Hamer, R. H. Friend, H. J. Huber, U. Scherf and A. B. Holmes, Adv. Mater. **6**, No. 10, pp. 748 - 752, (1994).

8. S. Tasch, A. Niko, G. Leising and U. Scherf, *Appl. Phys. Lett.* **68**, pp. 1090 -1092, (1996).

REFERENCES (Continued)

9. M. Uchida, Y. Ohmori, C. Morishima and K. Yoshino, *Synthetic Metals*, **55-57**, pp. pp. 4168 -4169, (1993).

10. D. D. Gebler, Y. Z. Wang, J. W. Blatchford, S. W. Jessen, L.-B. Lin, T. L. Gustafson, H. L. Wang, T. M. Swager, A. G. MacDiarmid and A. J. Epstein, *J. Appl. Phys.* **78** pp. 4264 - 4266, (1995).

11. J. Kido, K. Hongawa, K. Okuyama and K. Nagai, *Appl. Phys. Lett.* **63**, No. 19, pp. 2627 - 2629, (1993).

12. C. Zhang, H. V. Seggern, K. Pakbaz, B. Kraabel, H.-W. Schmidt and A. J. Heeger, *Synthetic. Metals*, **62** pp. 35 - 37, (1994).

13. B. Hu, Z. Yang and F. E. Karasz, *J. Appl. Phys.*, **76**, No. 4, pp. 2419 - 2422, (1994).

14. W. -X. Jing, A. Kraft, S. C. Moratti, J. Grüner, F. Cacialli, P. J. Hamer, A. B. Holmes and R. H. Friend, *Synthetic Metals*, **67**, pp. 161 - 163, (1994).

15. I. Sokolik, Z. Yang, F. E. Karasz and D. C. Morton, *J. Appl. Phys.* **74**, pp. 3584 - 3586, (1993).

16. R. W. Philips, V. V. Sheares, E. T. Samulski and J. M. Desimone, *Macromolecules*, **27** pp. 2354 -2356, (1994).

REFERENCES (Continued)

17. Y. Wang and R. P. Quirk, Macromolecules **28**, No. 10, pp. 3495 - 3501, (1995).

18. G. Leising, K. Pichler and F. Stelzer, Springer Series in Solid State Science **91** pp. 100, (1989).

19. J. L. Bredas, Springer Series in Solid State Sciences, **63**, pp. 166, (1985).

20. R. H. Friend, *J. Mol. Electronics*, **4**, pp. 37 - 38, (1988)

21. G. Louarn, L. Athouël, G. Froyer, J.P. Buisson and S. Lefrant, *Synth. Met.* **55-57**, pp. 4762 - 4763, (1993)

22. R. Kersting, U. Lemmer, R. F. Mahrt, K. Leo, H. Kurz, H. Bässler and E. O. Göbel, *Phys. Rev. Lett.* **70**, No. 24, pp. 3820 - 3823, (1993).

23. C. W. Tang, S. A. Van Slyke and C. H. Chen, *J. Appl. Phys.*, **65** pp. 3610 - 3616, (1989).

24. D. Z. Garbuzov, V. Bulovic, S. R. Forrest, *Chem. Phys. Lett.*, **249** pp. 433 - 435, (1996).

25. S. Hoshino and H. Suzuki, *Appl. Phys. Lett.*, **69** pp. 224 - 226, (1996).

26. A. Edwards, S. Blumstengel, I. Sokolik, R. Dorsinville, H. Yun, T. K. Kwei and Y. Okamoto, *Appl. Phys. Lett.*, **70**, No. 3, pp. 298 - 300, (1997).

REFERENCES (Continued)

27. A. Edwards, S. Blumstengel, I. Sokolik, H. Yun, Y. Okamoto and R. Dorsinville, *Synthetic Metals*, **84**, Nos. 1-3, pp. 639 - 640 (1997).

28. I. D. Parker, *J. Appl. Phys.* **75** No. 3, pp. 1656 - 1666, (1994).

29. D. Brown and A. J. Heeger, *Appl. Phys. Lett.*, **58** pp. 1982 - 1984, (1990).

CHAPTER SEVEN

7. CONCLUSIONS AND FUTURE DIRECTIONS

Chapter 7 summarizes the results of electroluminescence studies in the lanthanide-(benzoylbenzoate) organic complexes and the poly(2,5-benzophenone) polymers. This chapter also describes future experiments that may be performed to improve the performance of existing devices, and, suggests novel materials and device structures for future study. There is also a list of publications and presentations related to this thesis at the end of this chapter.

7.1 Conclusions of Electroluminescence Studies

This section summarizes the results of photoluminescent and electroluminescent studies reported in Chapters 5 and 6.

7.1.1 Lanthanide-(Benzoylbenzoate) Complexes

New thermally stable luminescent lanthanide complexes, terbium tris(4-methyl benzoylbenzoate) {$Tb(MeBB)_3$}, terbium tris(4-methoxy benzoylbenzoate) {$Tb(MeOBB)_3$} and europium tris(4-methoxy benzoylbenzoate) {$Eu(MeOBB)_3$} were synthesized. These lanthanide-(benzoylbenzoate) complexes show good thermal stability up the range of 320 - 340^0 C. The optical properties of these thermally stable metal-organic complexes were studied and reported in Chapter 5. The PL quantum efficiencies of the lanthanide-(methoxy benzoylbenzoate) complexes were higher with Φ = 27 % for

$Tb(MeOBB)_3$ and with Φ = 16 % for $Eu(MeOBB)_3$, both in methylene chloride solution. The chemical structure of one of the lanthanide complexess, $Eu(MeOBB)_3$, is shown in Figure 7-1.

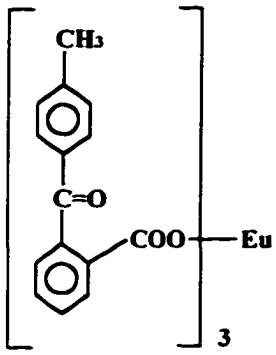

Figure 7-1. Chemical Structure of $Eu(MeOBB)_3$

Organic light emitting diodes were developed to study electroluminescence in the lanthanide complexes. Single layer LEDs were fabricated from the Tb and Eu complexes combined with PVK and butyl-PBD, and these devices showed EL spectra that are attributed to emission from the Tb^{3+} or Eu^{3+} ions. The single layer devices had the ITO/$La(MeOBB)_3$:PBD:PVK/Ca/Al structure. Two layer LEDs fabricated from the lanthanide-(methoxy benzoylbenzoate) complexes showed improved brightness compared to single layer devices. The two layer devices had the ITO/$La(MeOBB)_3$:PVK/PBD:PMMA/Ca/Al structure. The $Tb(MeOBB)_3$-based devices showed a maximum brightness of 45 cd/m^2 at an operating voltage of 24 volts. The two layer $Eu(MeOBB)_3$ LEDs also showed better light output compared to the single-layer devices based on the Eu complex but brightness readings were less than 10 cd/m^2. The higher brightness values of the $Tb(MeOBB)_3$ devices compared to $Eu(MeOBB)_3$ LEDs is

due to the higher PL quantum efficiency of the Tb complex and the higher luminous efficiency of the eye in the green region of the spectrum.

PL and EL studies show that the $La(MeOBB)_3$ molecules act as charge traps and recombination centers for charge carriers within the doped PVK layer. However, while PVK aids in charge transport, the possible lack of radiative and nonradiative energy transfer from the PVK molecules to the La complexes may limit the overall brightness of the LEDs. In the future, other transport materials may be used to enhance the energy transfer from the conducting materials to the luminescent centers. Increased energy transfer to the lanthanide centers should result in brighter EL intensities.

7.1.2 Poly(2,5-Benzophenone) Polymers

Poly(benzoyl-1,4-phenylene) (PBP), a novel thermally stable organic compound, was synthesized. This poly(2,5-benzophenone) polymer has two isomers which are thermally stable up to 500^0 C. The chemical structures of the PBP isomers (head-to-head and head-to-tail configurations) are shown in Figure 7-2. The photoluminescence quantum efficiency of the head-to-tail isomer in dilute chloroform solution is 15 %. On the other hand, the PL quantum efficiency of the head-to-head isomer is less than 0.5 % in dilute chloroform solution. The PL quantum yield in thin films of PBP (head-to-tail configuartion) is comparable to that of Alq_3, which is known to be a very efficient light emitting material and electron transport material in organic LEDs. The head-to-head isomer shows very weak PL in the solid state.

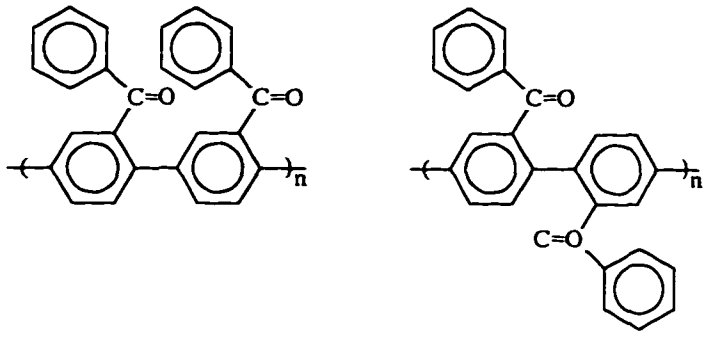

head-to-tail head-to-head

Figure 7-2. Chemical Structures of Poly(2,5-benzophenone) Isomers

Blue emitting LEDs have been successfully fabricated utilizing the head-to-tail PBP isomer. Based on two- and three- layer cell configurations, these LEDs produced brightness values of up to 100 cd/m^2. The peak wavelength of electroluminescence is 446 nm and the spectrum overlaps with the PL emission spectrum thereby indicating that PL and EL originate from the same excited state. We have also shown that the EL of PBP may due to photooxidized PBP molecules. Residual or atmospheric oxygen has been shown to severely degrade device performance and operating lifetime. Therefore, PBP-based may need to be encapsulated to improve device performance. Also, residual oxygen should be removed from all chemicals used for processing. Our results show that PBP is a promising material for optoelectronic applications.

7.2 Future Directions

This section describes future experiments to be performed for improving the brightness of organic light emitting devices. This section also describes novel materials to be studied for the development of organic LEDs.

7.2.1 Lanthanide-Organic Complexes

The lanthanide-organic complexes exhibit very sharp line-like photoluminescence spectra that originate from the radiative decay of the excited lanthanide ions.[1-3] Based on these emission characteristics, several researchers have developed electroluminescent devices that emit with the same characteristic spectral lines of the lanthanide ions.[4-7] The following paragraphs will outline several design techniques that may be used to enhance the electroluminescent radiation from the lanthanide ions.

The cell structure of the light emitting device is important for improving the brightness output of the LEDs. In particular, multilayer – instead of single layer – cell structures have been used to improve carrier injection into the emitting layer and the subsequent radiative output of the devices. Many researchers have used an electron transporting layer (ETL), located between the cathode and the emitting layer (EML), and/or a hole transporting layer (HTL), inserted between the anode and the EML, to improve the operation of their devices. In all cases the individual layer thicknesses are selected so that the EML encompasses the recombination zone for charge carriers.

Several research groups have used LB film deposition techniques to produce LEDs with monolayer film structures inside the device. In this case the emitting layers consist of several monolayers of organic material instead of one continuous layer. The layers used to separate the emitting dipoles within the lanthanide complex layer may be composed of inert spacers, charge transporting agents or materials that transfer their energy to the emitting LB layers. Figure 7-3 illustrates one possible structure of a

multilayer LB-film device that can be optimized to transfer energy to the lanthanide complexes.

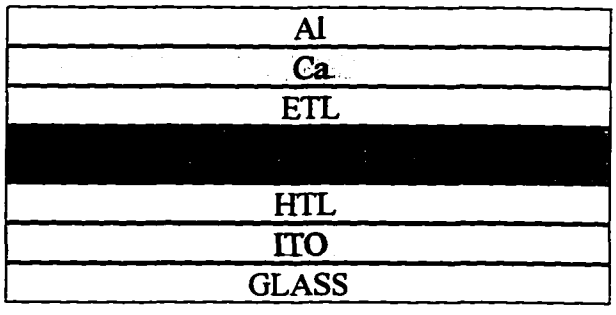

Figure 7-3. A Microcavity LED Optimized for Lanthanide Ion Emission

The MeOBB ligand is one candidate material that may be used as a spacer within the light emitting cell. We have studied the energy transfer processes between MeOBB and $TbCl_3$ and found that when a MeOBB layer is photoexcited, it will transfer its energy to an underlying $TbCl_3$ layer to produce emission from the Tb^{3+}ion. This suggests that in a multilayer device, an MeOBB layer may act as a spacer that will transfer its energy (due to carrier recombination) to the lanthanide layer. A more detailed study of the morphological, chemical and physical properties of the MeOBB or $TbCl_3$ films, and the MeOBB/$TbCl_3$ interface is necessary to determine if these layers may be used in LED structures. Figure 7-4 shows the PL and PLE spectra of MeOBB/$TbCl_3$ films.

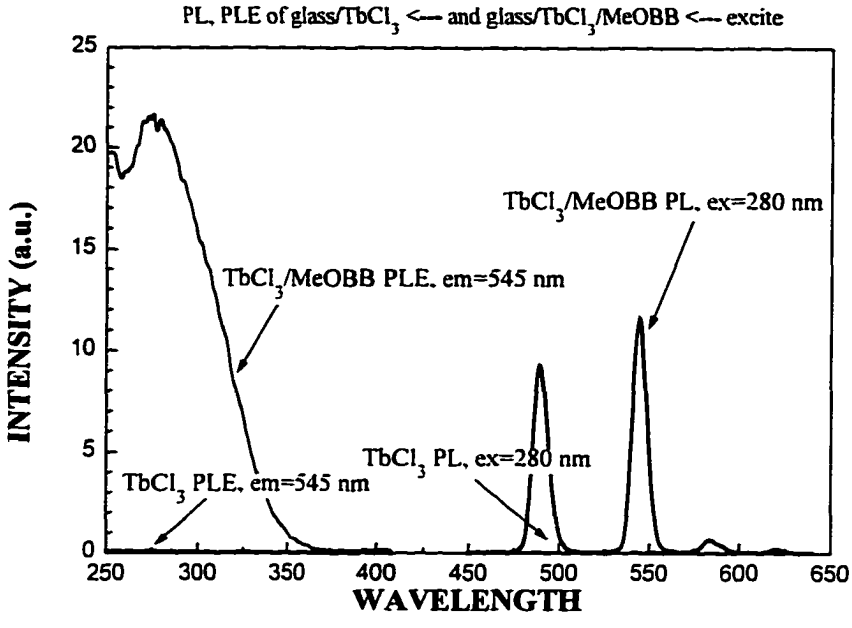

Figure 7-4. PL and PLE Spectrum of Glass/$TbCl_3$ and Glass/$TbCl_3$/MeOBB Films

The energy level of the components located within the emitting layer can be adjusted to improve the brightness of the devices. The degree of matching between the triplet level of the ligand and the lanthanide ion's energy levels determines the efficiency of energy transfer to the upper resonance levels of the metal ion. Several groups have already studied the effect of the ligand's triplet level on the emission from the La ions.[8] However, current devices have not been optimized for radiative or Forster-type energy transfer from the other molecular components to the lanthanide complexes. Consequently, the lanthanide ions may be doped into polymer matrices that emit within the absorption band of the ligand. Alternatively, novel ligands can be designed to have absorption bands overlapping the emission spectrum of the existing polymer materials such as poly(n,vinylcarbazole) (PVK). Figure 7-4 shows the PLE and PL spectra of bilayer films composed of $TbCl_3$ (spin coated from water) and the ligand MeOBB (spin cast from

chloroform). When exciting the absorption band of the ligand (280 nm), we have observed emission from the Tb^{3+} ion. This suggests that there may be energy transfer from MeOBB to $TbCl_3$. However, a more detailed study is necessary to fully determine the energy transfer mechanisms.

Latva and coworkers have shown that the luminescence of europium chelates in solution can be enhanced by the addition of ligands to the polymeric structure of the compound.[9] These additional ligands are attached within a polymeric structure that includes both the emitting Eu(III) ions and Y(III) ions (which help to link the ligands together within the polymer matrix). In this configuration, there is an excess concentration of energy donors (ligands) compared to acceptors (Eu^{3+}) ions. Therefore, the europium ion luminescence intensity can be adjusted by the concentration of ligands.

Similarly, the output of LEDs may be adjusted by the synthesis of novel polymeric networks containing energy donating sites attached to a polymer structure. Also, device brightness may be tailored by simply doping more ligand-type molecules into the emitting layer of the LED. Of course, a more thorough investigation should be undertaken to determine the effect of doping additional ligand-type molecules into the emitting layer.

The organic LEDs' performance depends on our ability to deposit multilayer optical quality thin films. These multilayer structures consist of separate charge transport or luminescent layers that may deposited by spincasting from solution or by thermal evaporation techniques. The terbium tris(2,2,5,5-tetramethylheptadionate) $Tb(THD)_3$ and

europium tris(2,2,5,5-tetramethylheptadionate) $Eu(THD)_3$ complexes were synthesized by researchers at Polytechnic university.[10] These lanthanide complexes are sublimable and form uniform optical quality thin films. These novel lanthanide-organic complexes may be used as the active layers in organic LEDs. The chemical structure of $Tb(THD)_3$ is shown in Figure 7-5.

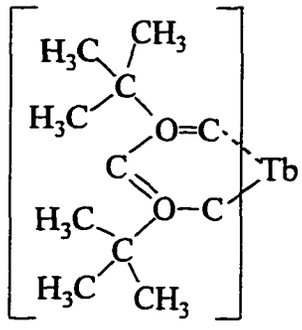

Figure 7-5. Chemical Structure of $Tb(THD)_3$

7.2.2 *Poly(2,5-benzophenone) Polymers*

Several research groups have shown that the electroluminescence spectrum of organic materials may be tuned by doping the active layers with highly fluorescent dyes. In addition, the brightness output of the LEDs can be increased by doping the active layer. Poly(Benzoyl-1,4-Phenylene) may also be doped with highly fluorescent dyes to shift the emitted spectrum to the green, yellow or red regions of the spectrum. By selectively processing localized regions of the emitting layer, multicolored and/or patterned emission may also be realized.

The PL and EL quantum efficiency of organic materials is enhanced by the efficiency of radiative decay and is conversely limited by the presence of nonradiative processes within the emitting layer. In molecules with high degrees of freedom, these nonradiative processes may be due to C-C bond-stretching vibrations, bond-stretching vibrations between phenyl rings along the carbon backbone or rotational modes of the phenylene rings along the polymer backbone. To reduce rotational loss mechanisms, ladder-type polymers have been used by some research groups. Another approach is to use more planar polymer structures.

One novel polymer, poly(dibenzoyl-1,4-phenylene) (PDBP) was recently synthesized by Yun and coworkers at Polytechnic University. The chemical structure of PDBP is shown in Figure 7-6. This compound has benzoyl side-groups attached to the phenyl rings located along the phenylene backbone of the polymer. These sidegroups make this compound soluble in common organic solvents which allows easy processing from solution. The placement of these benzoyl side-groups should lead to a smaller torsional angle (compared to PBP) between phenyl rings along the phenylene backbone. Consequently, the reduced degree of freedom may lead to reduced losses and increase the PL and EL efficiency of this compound compared to PBP. However, more detailed studies are necessary to fully understand the PL, EL and energy transfer processes occurring in PDBP.

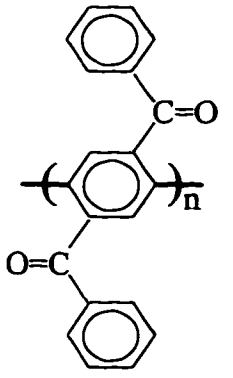

Figure 7-6. Chemical Structure of PDBP

The photoluminescence of PDBP thin films, spin cast from chloroform solution, was studied. Preliminary studies have shown that PDBP forms optical quality thin films when spin casted from solution. These films showed bright blue-green photoluminescence in the solid state. The peak of photluminescence is located at 470 nm when exciting at 400 nm. The maximum absorbance and peak of the PL excitation (for emission at 470 nm) are located at approximately 400 nm. This material also shows good thermal stability and should be a promising candidate for optoelectronic applications.

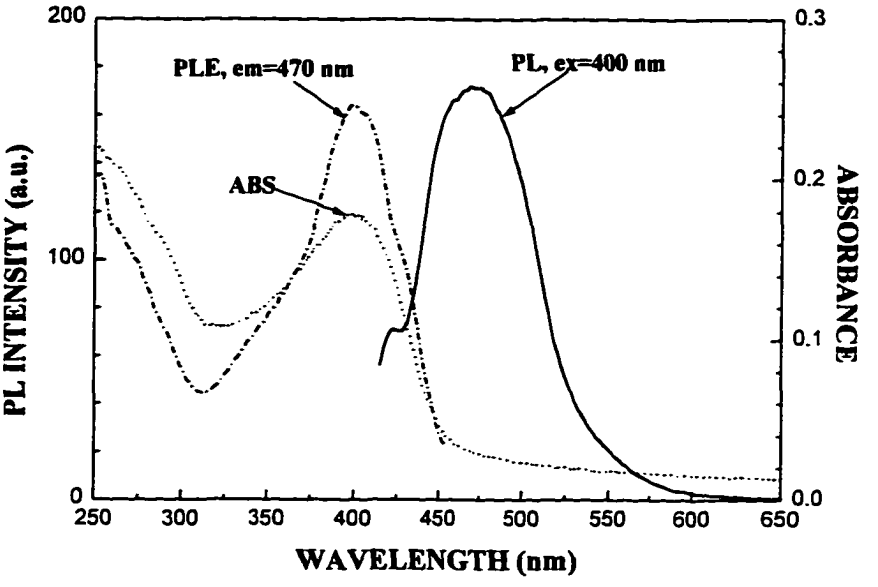

Figure 7-7. PL of PDBP Thin Films

7.3 List of Publications and Presentations Related to this Thesis

Scientific Publications

A. Edwards, S. Blumstengel, I. Sokolik, R. Dorsinville, H. Yun, T. K. Kwei and Y. Okamoto, "Blue Photo- and Electroluminescence from Poly(Benzoyl-1,4-Phenylene)", *Applied Physics Letters*", **70**, No. 3, pp. 298 - 300, (1997).

A. Edwards, I. Sokolik, R. Dorsinville, C. Claude, T. Y. Chu and Y. Okamoto, "Photoluminescence and Electroluminescence of New Lanthanide-(Methoxybenzoyl)benzoate Complexes", *Journal of Applied Physics*, Accepted for Publication (1997).

A. Edwards, T. Y. Chu, C. Claude, I. Sokolik, Y. Okamoto, and R. Dorsinville, "Synthesis and Characterization of Organo-Lanthanide(III) Complexes", *Synthetic Metals*, **84**, Nos. 1-3, pp. 433 - 434, (1997).

A. Edwards, S. Blumstengel, I. Sokolik, H. Yun, Y. Okamoto and R. Dorsinville, "Photoluminescence and Electroluminescence of a Soluble PPP-type Polymer", 1997 *Synthetic Metals*, **84**, Nos. 1-3, pp. 639 - 640, (1997).

Conference Presentations

A. Edwards, T. Y. Chu, C. Claude, I. Sokolik, Y. Okamoto and R. Dorsinville, "Photo- and Electroluminescence of New Lanthanide(III) Organic Complexes", Fall 1996 Materials Research Society Conference, (Oral Presentation).

S. Blumstengel, H. Yun, A. Edwards, T. K. Kwei, I. Sokolik, Y. Okamoto and R. Dorsinville, "Blue Photo- and Electroluminescence from a Soluble PPP-type Polymer", Fall 1996 Materials Research Society Conference, (Poster Presentation).

A. Edwards, T. Y. Chu, C. Claude, I. Sokolik, Y. Okamoto, and R. Dorsinville, "Synthesis and Characterization of Electroluminescent Organo-Lanthanide(III) Complexes", 1996 International Conference on the Science and Technology of Synthetic Metals, (Poster Presentation).

A. Edwards, S. Blumstengel, I. Sokolik, H. Yun, Y. Okamoto and R. Dorsinville, "Photoluminescence and Electroluminescence of a Soluble PPP-type Polymer", 1996 International Conference on the Science and Technology of Synthetic Metals, (Poster Presentation).

A. Edwards, S. Blumstengel, I. Sokolik and R. Dorsinville, H. Yun, T. K. Kwei and Y. Okamoto, "Photo- and Electroluminescence Properties of Phenyl-substituted Poly(p-phenyl)s", Symposium on Molecular Aggregates: Photochemistry, Photophysics, Spectroscopy and Nonlinear Optics, Sponsored by the Center for Analysis of Structures and Interfaces at CCNY, April 11, 1997 (Poster Presentation).

REFERENCES

1. R. G. Charles and R. C. Ohlmann, *J. Inorg. Nucl. Chem.*, **27** pp. 119 - 127, (1965).

2. R. Heller and E. Wasserman, *J. Chem. Phys.*, **42**, No. 3, pp. 949 - 955, (1965).

3. W. R. Dawson, J. L. Kropp and M. W. Windsor, *J. of Chem. Phys.*, **45** No. 7, pp. 2410 -2418, (1966).

4. A. Edwards, T. Y. Chu, C. Claude, I. Sokolik, Y. Okamoto and R. Dorsinville, *Synthetic Metals*, **84**, Nos. 1-3 (1997).

5. J. Kido, K. Nagai and Y. Okamoto, *J. Alloys and Compounds*, **192** pp. 30 - 33, (1993).

6. N. Takada, T. Tsutsui and S. Saito, *Jpn. J. Appl. Phys.*, **33** Part 2, No. 6B, pp. L863 - L866, (1994).

7. T. Sano, M. Fujita, T. Fujii, Y. Hamada, K. Shibata and K. Kuroki, Jpn. J. Appl. Phys., **34** Part 1, No. 4A, pp. 1883 - 1887, (1995).

8. S. Sato and M. Wada, *Bull. of the Chem. Soc. of Jpn.*, **43** pp. 1955 - 1962 (1970).

9. M. Latva, H. Takalo, K. Simberg and J. Kankare, *J. Chem. Soc. Perkin. Trans.* **2** pp. 1990 - 1994, (1995).

10. C. Claude, Ph.D. Dissertation, Polytechnic University, (1996).

BIBLIOGRAPHY

Abe, Y., K Onisawa, S. Aratani and M. Hanazono, *J. Electrochem. Soc.*, **139**, No. 3, pp. 641 - 642 (1992).

Atkins, P., *Physical Chemistry (Fifth Ed.)*, W. H. Freeman and Co., New York, pp. 451 - 456, (1994).

Baker, B. C., and D. T. Sawyer, *Analytical Chem.*, **40** No. 13, pp. 1945 - 1951, (1968).

Bassler, H., G. Schonherr, M. Abkowitz and D. M. Pai, *Phys. Rev. B*, **26** pp. 3105 - 3106 (1982).

Bhaumik, M. L., and C. L. Telk, *Opt. Soc. Am.* **54,** No. 10, pp. 1211 - 1215, (1964).

Bhaumik, M. L., and M. A. El-Sayed, *J. Chem. Phys.* **42**, pp. 787 - 788, (1965).

Birks, J. B., *Photophysics of Aromatic Molecules*, pp. 98, John Wiley & Sons Ltd., New York, (1969).

Braun, D., A. J. Heeger and H. Kroemer, *J. Elect. Mat.*, **20**, No. 11, pp. 945 -948, (1991).

Braun, D., and A. J. Heeger, *Thin Solid Films*, **216** pp. 96 - 98, (1992).

Bredas, J. L., *Springer Series in Solid State Sciences*, **63**, pp. 166, (1985).

Brown, D., and A. J. Heeger, *Appl. Phys. Lett.*, **58** pp. 1982 - 1984, (1990).

Buono-Core, G. E., H. Li and B. Marciniak, *Coord. Chem. Rev.* **99**, pp. 55 - 87, (1990).

Burn, P. L., A. B. Holmes, A. Kraft, D. D. Bradley, A. R. Brown, R. H. Friend and R. W. Gymer, *Nature*, **356** pp. 47 - 49, (1992).

Burroughes, J. H., D. D. C. Bradley, A. R. Brown, R. N. Marks, K. Mackay, R. H. Friend, P. L. Burns and A. B. Holmes, *Nature*, **347**, pp. 539 - 541, (1990).

Burrows, P. E., and S. F. Forrest, *Appl. Phys. Lett.*, **64** No. 17, pp. 2285 - 2287, (1994).

Burrows, P. E., L. S. Sapochak, D. M. McCarty, S. R. Forrest and M. E. Thompson, *Appl. Phys. Lett.*, **64** No. 20, pp. 2718 - 2720, (1994).

Burrows, P. E., V. Bulovic, S. R. Forrest, L. S. Sapochak, D. M. McCarty and M. E. Thompson, *Appl. Phys. Lett.*, **65** No. 23, pp. 2922 - 2924, (1994).

Burrows, P. E., Z. Shen, V. Bulovic, D. M. McCarty and S. R. Forrest, *J. Appl. Phys.*, **79** No. 10, pp. 7991 - 7995 (1996).

Cao, Y., G. M. Treacy, P. Smith and A. J. Heeger, Appl. *Phys. Lett.*, **60** No. 22, pp. 2711 - 2713, (1992).

Charles, R. G., and R. C. Ohlmann, *J. Inorg. Nucl. Chem.*, **27** pp. 119 - 127, (1965).

Claude, C., Ph.D. Dissertation, Polytechnic University, (1996).

Dawson, W. R., J. L. Kropp and M. W. Windsor, *J. of Chem. Phys.*, **45** No. 7, pp. 2410 -2418, (1966).

Dieke, G. H., *Spectra and Energy Levels of Rare Earth Ions in Crystals*, Interscience Publishers, New York, pp. 243 - 261, (1968).

Edwards, A., I. Sokolik, R. Dorsinville, C. Claude, T. Y. Chu and Y. Okamoto, *J. Appl. Phys.*, Accepted for Publication (1997).

Edwards, A., S. Blumstengel, I. Sokolik, H. Yun, Y. Okamoto and R. Dorsinville, *Synthetic Metals*, **84**, Nos. 1-3, pp. 639 - 640 (1997).

Edwards, A., S. Blumstengel, I. Sokolik, R. Dorsinville, H. Yun, T. K. Kwei and Y. Okamoto, *Appl. Phys. Lett.*, **70**, No. 3, pp. 298 - 300, (1997).

Edwards, A., T. Y. Chu, C. Claude, I. Sokolik, Y. Okamoto, and R. Dorsinville, *Synthetic Metals*, **84**, Nos. 1-3, pp. 433 - 434 (1997).

Fowler, R. H., and L. Nordheim, *Proc. R. Soc. (London)*, Ser. A, **119** pp. 173 - 181, (1928).

Friend, R. H., *J. Mol. Electronics*, **4**, pp. 37 - 38, (1988)

Garbuzov, D. Z., V. Bulovic, P. E. Burrows and S. R. Forrest, *Chem. Phys. Lett.* **249** pp. 433 - 437, (1996).

Gebler, D. D., Y. Z. Wang, J. W. Blatchford, S. W. Jessen, L.-B. Lin, T. L. Gustafson, H. L. Wang, T. M. Swager, A. G. MacDiarmid and A. J. Epstein, *J. Appl. Phys.* **78** pp. 4264 - 4266, (1995).

Grem, G., G. Leditzky, B. Ullrich and G. Leising, *Adv. Mater.*, **4** No. 1, pp. 36 - 37, (1992).

Grüner, J., P. J. Hamer, R. H. Friend, H. J. Huber, U. Scherf and A. B. Holmes, Adv. Mater. **6**, No. 10, pp. 748 - 752, (1994).

Gudmundsen, R., O. Marsh, and E. Matovich, *J. Chem. Phys.* **39**, No. 2, pp. 272 -274, (1963).

Gustafsson, G., Y. Cao, G. M. Treacy, F. Klavetter, N. Colaneri and A. J. Heeger, *Nature*, **357** pp. 477 - 479, (1992).

Hamada, Y., T. Sano, M. Fujita, T. Fujii, Y. Nishio and K. Shibata, *Jpn. J. Appl. Phys.*, **32** pp. L514 - L515, (1993).

Hayes, A. V., and H. G. Drickamer, *J. Chem. Phys.* **76** pp. 114 - 115, (1982).

Heeger, A. J., I. D. Parker and Y. Yang, *Synthetic Metals*, **67** pp. 23 - 29, (1994).

Heller, A., and E. Wasserman, *J. Chem. Phys.*, **42**, No. 3, pp. 949 - 955, (1965).

Herzberg, G., *Atomic Spectra and Atomic Structure*, Prentice-Hall, New York, pp. 198 (1937).

Hoshino, S., and H. Suzuki, *Appl. Phys. Lett.*, **69** pp. 224 - 226, (1996).

Hu, B., Z. Yang and F. E. Karasz, *J. Appl. Phys.*, **76** No. 4, pp. 2419 - 2422, (1994).

Jing, W. -X., A. Kraft, S. C. Moratti, J. Grüner, F. Cacialli, P. J. Hamer, A. B. Holmes and R. H. Friend, *Synthetic Metals*, **67**, pp. 161 - 163, (1994).

Kersting, R., U. Lemmer, R. F. Mahrt, K. Leo, H. Kurz, H. Bässler and E. O. Göbel, *Phys. Rev. Lett.* **70**, No. 24, pp. 3820 - 3823, (1993).

Kido, J., and K. Nagai, *J. Alloys and Compounds*, **192** pp. 30 - 33, (1993).

Kido, J., C. Ohtaki, K. Hongawa, K. Okuyama and K. Nagai, *Jpn., J. Appl. Phys*, **32** pp. L917 - L920, (1993).

Kido, J., H. Hayase, K. Hongawa, K. Nagai and K. Okuyama, *Appl. Phys. Lett..*, **65** No. 17, pp. 2124 - 2126, (1994).

Kido, J., K. Hongawa, K. Okuyama and K. Nagai, *Appl. Phys. Lett.* **63**, No. 19, pp. 2627 - 2629, (1993).

Kido, J., K. Nagai and Y. Okamoto, *J. Alloys and Compounds*, **192** pp. 30 - 33, (1993).

Kido, J., K. Nagai, Y. Okamoto and T. Skotheim, *Chem. Lett.*, pp. 1267 - 1268 (1991).

Kido, J., W. Ikeda, M. Kimura and K. Nagai, *Jpn. J. Appl. Phys.* **35**, Pt. 2, No. 3B, pp. L394 - L396, (1996).

Kubesh, R. J., *Am. J. Phys.*, **60**, No. 10, pp. 919 - 923, (1992).

Latva, M., H. Takalo, K. Simberg and J. Kankare, *J. Chem. Soc. Perkin. Trans.* **2** pp. 1990 - 1994, (1995).

Leising, G., K. Pichler and F. Stelzer, *Springer Series in Solid State Sciences*, **91** pp. 100, (1989).

Louarn, G., L. Athouël, G. Froyer, J.P. Buisson and S. Lefrant, *Synth. Met.* **55-57**, pp. 4762 - 4763, (1993)

Mark, P., and W. Helfrich, *J. of Appl. Phys.*, **33** No. 1, pp. 205 - 215, (1962).

Meggers, W. F., C. H. Corliss and B. F. Scribner, *Tables of Spectral-Line Intensities Part I*, National Bureau of Standards Monograph 32-Part I, pp. 3, (1961).

Mori, T., K. Miyachi, T. Kichimi and T. Mizutani, *Jpn. J. Appl. Phys.*, Part 1 No. 12, pp. 6594 - 6595, (1994).

Neudeck, G. W., G. W. Neudeck and R. F. Pierret Eds., *The PN Junction Diode*, Modular Series on Solid State Devices, Vol. II, 2nd Ed., Addison-Wesley, New York, pp. 56, (1989).

Ohnesorge, W. E., and L. B. Rogers, *Spectrochimica Acta*, pp. 27 - 31, (1959).

Ohnesorge, W. E. and L. B. Rogers, *Spectrochimica Acta*, pp. 41 - 48, (1959).

Onoda, M., S. Morita, H. Nakayama and K. Yoshino, *Jpn. J. Appl. Phys.*, **32**, Part 2, No. 1A/B, pp. L82 - L85, (1993).

Pai, D. M., J. F. Yanus and M. Stolka, *J. Phys. Chem.*, **88** pp. 4714 - 4717, (1984).

Parker, I. D., *J. Appl. Phys.* **75** No. 3, pp. 1656 - 1666, (1994).

Pei, Q., G. Yu, C. Zhang, Y. Yang, and A. J. Heeger, *Science*, **269** pp. 1086 - 1088, (1995).

Phillips, R. W., V. V. Sheares, E. T. Samulski and J. M. Desimone, *Macromolecules*, **27** pp. 2354 - 2356, (1994).

Pope, M., and C. E. Swenberg, *Electronic Processes in Organic Crystals*, Oxford University Press, New York, pp. 704 - 706, (1982).

Pope, M., H. P. Kallman and P. Magnante, *J. Chem. Phys.*, **38,** pp. 2042 - 2043, (1963).

Priestley, R., I. Sokolik, A. D. Walser, C. W. Tang and R. Dorsinville, *Synthetic Metals*, **84** Nos. 1-3, pp. 915 - 916, (1997).

Radel, S. R., and M. H. Navidi, Chemistry (2nd Ed.), West Publishing Co., pp. 311, (1994).

Samelson, H., A. Lempicki and C. Brecher, *J. Chem. Phys.*, **40** No. 9, pp. 2553 -2558, (1964).

Sano, M., M. Pope and H. Kallman, *J. Chem. Phys.*, **43,** pp. 2920 - 2921, (1965).

Sano, T., M. Fujita, T. Fujii, Y. Hamada, K. Shibata and K. Kuroki, *Jpn. J. Appl. Phys.* **34** Part 1, No. 4A, pp. 1883 - 1887, (1995).

Sato, S., and M. Wada, *Bull. of the Chem. Soc. of Jpn.*, **43** pp. 1955 - 1962 (1970).

Shen, Z., P. E. Burrows, V. Bulovic, D. M. McCarty, M. E. Thompson and S. R. Forrest, *Jpn. J. Appl. Phys.*, **35**, Part 2, No. 3B, pp. L401 - L404, (1996).

Sokolik, I., A. D. Walser, R. Priestley, R. Dorsinville and C. W. Tang, *Materials Research Society Symposium Proceedings*, **413** pp. 65, (1996).

Sokolik, I., Z. Yang, F. E. Karasz and D. C. Morton, *J. Appl. Phys.* **74**, pp. 3584 -3586, (1993).

Steger, H. F., and A. Corsini, *J. Inorg. Nucl. Chem.*, **35** pp. 1621- 1636, (1973).

Steger, H. F., and A. Corsini, *J. Inorg. Nucl. Chem.*, **35** pp. 1637 - 1643, (1973).

Sugiyama, K., D. Yoshimura, E. Ito, T. Miyazaki, Y. Ouchi and K. Seki, *Mol. Cryst. Liq. Cryst.*, To be published.

Takada, N., T. Tsutsui and S. Saito, *Jpn. J. Appl. Phys.* **33** Part 2, No. 6B, pp. L863 - L866, (1994).

Takada, N., T. Tsutsui and S. Saito, *Jpn. J. Appl. Phys.*, **33** pp. L863 - L866, (1994).

Tang, C. W., and S. A. Van Slyke, *Appl. Phys. Lett.* **51**, No. 12, pp. 913 - 915, (1987).

Tang, C. W., S. A. VanSlyke and C. H. Chen, *J. Appl. Phys.*, **65** No. 9, pp. 3610 -3616, (1989).

Tasch, S., A. Niko, G. Leising and U. Scherf, *Appl. Phys. Lett.* **68**, pp. 1090 -1092, (1996).

Tokuhisa, H., M. Era, T. Tsutsui and S. Saito, *Appl. Phys. Lett.*, **66**, No. 25, pp. 3433 - 3435, (1995).

Uchida, M., Y. Ohmori, C. Morishima and K. Yoshino, *Synthetic Metals*, **55-57**, pp. 4168 -4169, (1993).

Verdeyen, J. T., *Laser Electronics (2nd Ed.)*, Prentice-Hall, pp. 137, (1989).

Wang, Y., and R. P. Quirk, *Macromolecules*, **28**, No. 10, pp. 3495 - 3501, (1995).

Whan, R. E., and G. A. Crosby, *J. Mol. Spectr.* **8** pp. 315 - 327, (1962).

Wicks, G. W., *Compound Semiconductor*, July/Aug, pp. 39 - 40, (1995).

Yang, E. S., *Fundamentals of Semiconductor Devices*, McGraw-Hill, New York, pp. 5 - 9, (1978).

Yang, Y., E. Westerweele, C. Zhang, P. Smith and A. J. Heeger, *J. Appl. Phys.*, **77** No. 2, pp. 694 - 698, (1995).

Zhang, C., D. Braun and A. J. Heeger, *J. Appl. Phys.*, **73** No. 10, pp. 5177 - 5180, (1993).

Zhang, C., H. V. Seggern, K. Pakbaz, B. Kraabel, H.-W. Schmidt and A. J. Heeger, *Synthetic. Metals*, **62** pp. 35 - 37, (1994).